Title

I. THE FARADAY EFFECT IN ORGANIC MOLECULES AND COMPLEXES. II. CONFORMATIONS OF CELLULOSE TRIACETATE

Author

Thome, James Meyers.

Publication Date

1966-08-01

UCRL-17100

University of California

Ernest O. Lawrence Radiation Laboratory

I. THE FARADAY EFFECT IN ORGANIC MOLECULES AND COMPLEXES
II. CONFORMATIONS OF CELLULOSE TRIACETATE

Berkeley, California

DISCLAIMER

UCRL-17100

UNIVERSITY OF CALIFORNIA
Lawrence Radiation Laboratory
Berkeley, California

AEC Contract No. W-7405-eng-48

I. THE FARADAY EFFECT IN ORGANIC MOLECULES AND COMPLEXES
II. CONFORMATIONS OF CELLULOSE TRIACETATE

James Meyers Thorne

(Ph. D. Thesis)

August 1966

I. THE FARADAY EFFECT IN ORGANIC MOLECULES AND COMPLEXES

II. CONFORMATIONS OF CELLULOSE TRIACETATE

Contents

II. CONFORMATIONS OF CELLULOSE TRIACETATE

ACKNOWLEDGMENTS

I wish to express my sincere gratitude to Professor Melvin Calvin for guidance and support throughout the course of this research. His deep involvement in things scientific has been a source of constant stimulation to me in my own scientific endeavors.

I am greatly indebted to Dr. Ignacio Tinoco, Dr. Melvin Klein, and Dr. Kenneth Sauer for their valuable help during certain phases of this research. Discussions with them have been of great help to me in clarifying certain concepts and judging the advisability of proposed courses of action. Much the same can be said of the influence of my fellow graduate students. I am particularly grateful to Mr. Edward Dratz and Mr. David Downie for the close and scientifically fruitful association we have had.

I would also like to thank Dr. J. J. Duffield of Applied Physics Corp. for his time and comments and the use of his MORD apparatus for purposes of comparison with the instrument used here.

I am grateful to Dr. W. E. Skiens and Dr. T. Davis, both of the Dow Chemical Research Center in Walnut Creek, Calif., for the cellulose triacetate powder and films used in this work. I am also indebted to them for a number of helpful and enlightening discussions regarding CTA.

The patience and skill of Mrs. Johanna Onffroy and Mrs. Evelyn Litton in preparing the manuscript at a time when their work load was heavy and demanding, is particularly appreciated.

I am especially grateful to my wife, Kaye, for her unfailing support and encouragement throughout our stay here at Berkeley. Without her assistance and understanding it would have been extremely difficult,

if not impossible, to continue this research.

This work was supported, in part, by the U. S. Atomic Energy Commission.

I. INTRODUCTION

In 1845 Michael Faraday discovered that transparent materials placed in a magnetic field would rotate the plane of polarized light.[1] In his experiment, light from an Argand lamp was plane polarized by reflection from a glass surface. A Nicol prism was used to determine the plane of polarization (the image of the lamp was extinguished at the proper angular position of the prism). Figure 1 shows the arrangement of his apparatus. Inserting a piece of glass in the beam ahead of the Nicol prism had no effect on the plane of polarization, but if a magnetic field permeated the glass it was found that the image of the lamp reappeared through the prism. However, a new angular position of the prism could be found where the image was once again extinguished. This demonstrated that the magnetic field had simply rotated the plane of polarization of the light beam. Faraday found that the amount of rotation was unique for each of the transparent substances he investigated (except for a few where his crude instrument was not sensitive enough to detect the small rotation produced). It is now accepted that all material will show a characteristic magneto-optical rotation, although in certain cases the effect is extremely small. This optical rotation induced by magnetic fields came to be called the Faraday Effect.

Only a moderate amount of work has been done on the Faraday effect although it attracted the consideration of some of the most able scientists of the late nineteenth and early twentieth centuries. Aside from measurements taken only at the sodium D line, only a relatively few materials have been studied, and most of these have been

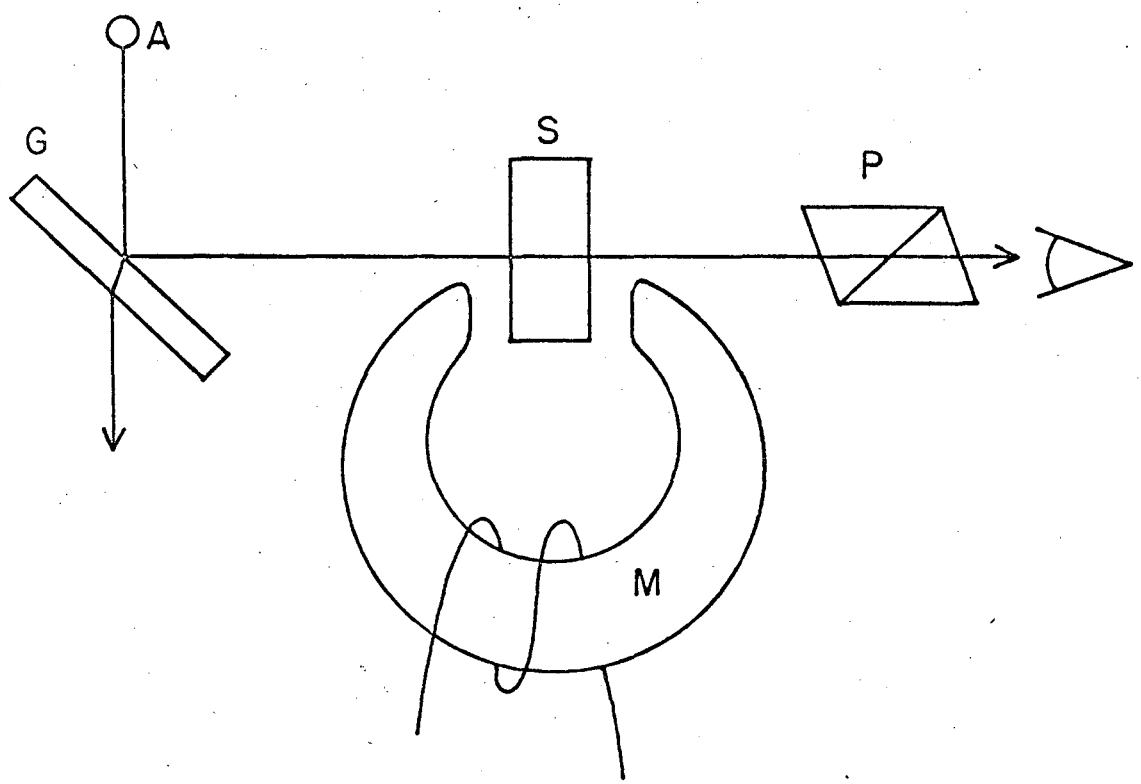

MUB-11457

Fig. 1. Faraday's apparatus for the detection of magneto-optical rotation. A is an Argand lamp, G a glass plate, S the sample, P a Nicol prism, and M is soft iron wound with a coil carrying current to produce a magnetic field.

investigated only in the visible portion of the spectrum. However, the Faraday effect has been observed in the microwave region,[2] in the infrared,[3] and in the ultraviolet.[4] Solids,[1] liquids,[1] and gases[5] all produce magneto-optical rotation.

The closely related phenomenon of optical rotatory dispersion (ORD) has received far more attention than magneto-optical rotatory dispersion (MORD). This is not really surprising since MORD is generally considered a special case of ORD. In addition, ORD is more easily measured and in the past has returned far more useful scientific information than MORD. For example, natural optical rotation has been used extensively to characterize disymmetric molecules,[6] to determine concentrations of reactants during certain reactions,[7] and to elucidate the stereochemistry of organic molecules[8] and transition metal complexes.[9] In addition, ORD has found wide application in biochemistry, particularly in the study of proteins and nucleic acids.[10]

Nevertheless, ORD has certain limitations that the Faraday effect may not have. For instance, only a small fraction of known compounds are optically active, but in principle all should show Faraday activity. One might reason that anything ORD will reveal about an optically active molecule, the Faraday effect will reveal about any molecule. Even a cursory study of the two phenomena will show that this is not entirely true (as will be pointed out in more detail later). But at the time this work was begun the limitations and potentialities of the Faraday effect had not been established. The possibility that MORD could yield information not obtainable from ORD, but of a similar nature and value,

provided strong motivation for this investigation. Specifically, we wanted to investigate singlet-triplet transitions because of their possible importance in biological processes.[11] It also appeared possible that the Faraday effect would be sensitive to the local environment of a molecule, thus providing a method for detection of molecular aggregation, conformation changes (especially of macromolecules), and chelation. In addition, it seemed highly likely that electronic absorption bands that are masked by stronger, nearby bands could show relatively strong Faraday rotation, and thus be detected and studied. It must be admitted at the outset that these properties of the Faraday effect have not proven as fruitful in practice as we had hoped. But this does not mean that the Faraday effect is not presently of value in chemistry, nor that it will not become useful in the future for the types of investigations mentioned.

II. PHENOMENOLOGY OF THE FARADAY EFFECT

A. Circular Birefringent Nature

The rotation of the plane of polarization in optical rotation and the Faraday effect actually arises from circular birefringence--that is, the index of refraction for right circularly polarized light is not the same as that for left circularly polarized light. A quantitative description of this fact will be given later, but it can be visualized qualitatively as follows:

The electric vector in right circularly polarized light appears to rotate clockwise when the observer looks toward the light source. A vector rotating counterclockwise results in left circularly polarized light. For two coincident beams the effective electric field is the vector sum of the two instantaneous fields. In the special case where the two beams have the same frequency and intensity, but opposite handedness, the effective electric field will appear to be plane polarized (i.e., electric vector directed parallel or anti-parallel to a single line with magnitude oscillating sinusoidally at the frequency of the light).

Figure 2 depicts this relationship as one would see it upon looking toward the light source. E_L, the electric vector of the left circularly polarized light, rotates counterclockwise at the same speed as E_R rotates clockwise. The resultant of E_L and E_R is always parallel or anti-parallel to E, and the magnitude of E varies sinusoidally in time. This resultant vector is then identical with the electric vector of plane polarized light, both in time and space.

Since the resultant vector bisects the angle between E_L and E_R, it will be rotated if either circularly polarized vector is retarded in

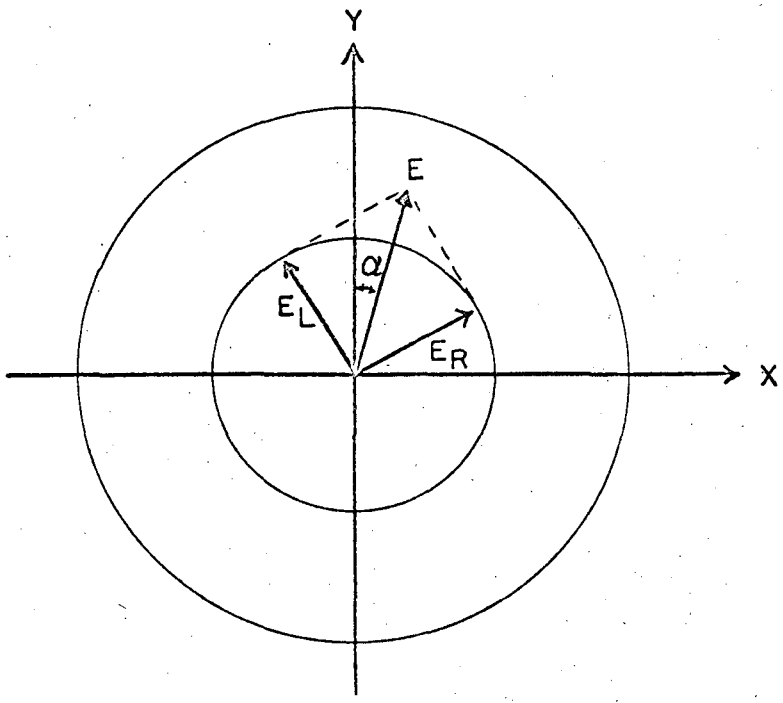

Figure 2. Addition of electric vectors of left circularly polarized light, E_L, and right circularly polarized light, E_R, to give plane polarized light, E. Outer circle shows maximum amplitude of E which is achieved when both E_L and E_R are parallel to the vector E shown.

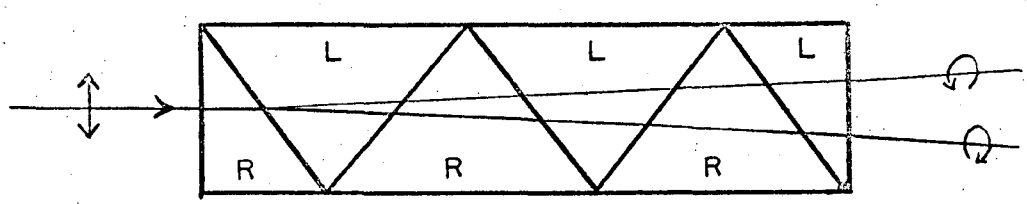

MUB-11218

Figure 3. Fresnel's Experiment.[12] Left- and right-handed quartz prisms split plane polarized light into two beams of circularly polarized light.

time with respect to the other. This is exactly what happens when the index of refraction for each of the circularly polarized waves is different. Thus, optical rotation of a plane polarized light arises from the non-equality of the indices of refraction of left and right circularly polarized light.

The fact that it is not just a mental construct was shown by Fresnel[12] with several prisms made of optically active quartz. In Figure 3 a plane polarized light beam enters the series of prisms from the left. The beam is refracted and split into two circularly polarized components at the surface between the first two prisms, L and R. This happens only if the two prisms are made of types of quartz that have opposite optical rotations (e.g., L for left rotating quartz and R for right). In this case, a left circularly polarized beam will experience one index of refraction in an L prism and a different index in an R prism. A right circularly polarized beam will see the opposite change in refractive index in crossing the same interface, and so the two circularly polarized components of the plane polarized light will be refracted in slightly different directions. The remaining interfaces are inclined so as to increase the angular separation of the two beams. The observed result is that two divergent beams of opposite circular polarity emerge from the prism, thus proving that optical rotation is really circular birefringence.

A similar experiment was conducted by Brace for magnetically induced rotation in a series of dense glass prisms. He placed a half-wave ($\lambda/2$) retardation plate between the prism to reverse the sense of the circular polarization so that angular separation would occur between prisms whose

rotation was in the same direction in the magnetic field. The calculated angular separation was less than 3 sec. of arc, which was too small to be seen. He later[14] succeeded in separating the two rays with the prisms in the arrangement shown in Figure 4. Plane polarized light enters the system through the auxiliary prism P_3 and is internally reflected several times, forming a sort of spiral. It finally emerges from auxiliary prism P_4. The emerging beam shows a single image of the slit until the magnetic field is turned on--then the image clearly doubles. To explain this, Brace reasoned that the plane polarized entering ray was split into two circularly polarized rays at A. These rays have different angles of reflection from the silver surface because they see different indices of refraction along the direction of the magnetic field. The angular separation is increased at C_1 and C_2 only if the polarization of each beam is changed by the quarter wave plate between the prisms. The form of the polarization in each region of the device is complicated by the metallic reflection at the surfaces so some effort is required to verify that it is really circular birefringence that is caused by the magnetic field. In fact, the emergent light is observed to be nearly plane polarized. The interested reader is referred to the account of the experiment given by Wood[15] for further details and interpretation.

Mills[16] performed a more elegant and instructive experiment demonstrating that the Faraday effect is magnetically induced circular birefringence. He used a Michelson interferometer with a solenoid in one of the two arms. The solenoid was wired differentially with four terminals so that a certain set of connections permitted current to

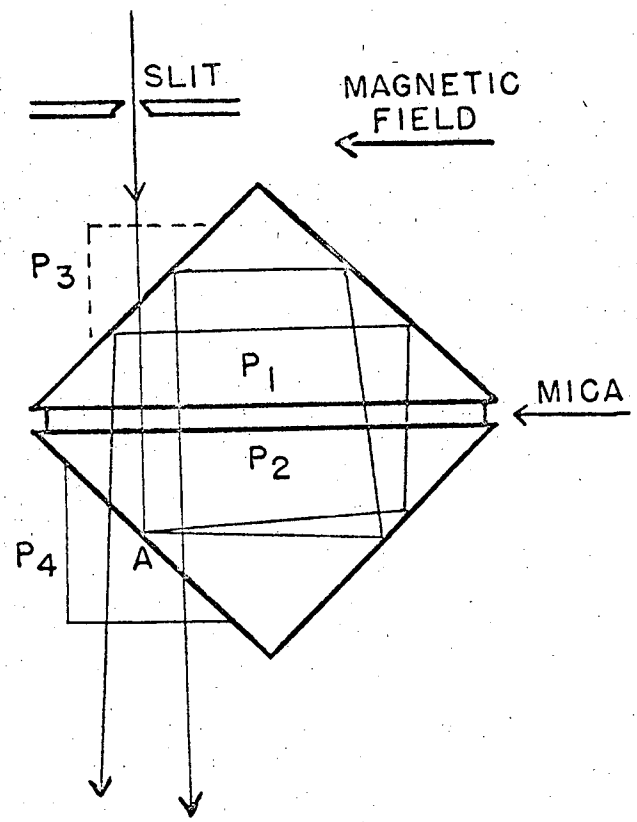

MUB-11216

Figure 4. Brace's Experiment.[14] Plane polarized light split into two beams by glass prisms, P_1 and P_2, and mica in a magnetic field. P_3 and P_4 are auxiliary prisms for the entrance and exit of the light beam.

flow thrugh it without producing a magnetic field. Inside the solenoid he placed a long tube filled with carbon disulfide. The light passed through a Brevais double plate before entering the interferometer, thus illuminating half the field with right circularly polarized light, the other half with left. The interference fringes crossing the field were at right angles to the line dividing the two types of polarization at the eyepiece. When the magnetic field was turned on the fringes in one-half of the field were observed to shift with respect to those in the other half. Experimental artifacts were ruled out by checking the effects of mechanical disturbances and by putting current through the magnet when it was wired to produce no magnetic field. This experiment clearly demonstrated the effectiveness of a magnetic field in changing the indices of refraction of left and right circularly polarized light in opposite directions. It might be mentioned that a shift of one full fringe width is equivalent to an angular rotation of the plane of polarization of 180°. Shifts of up to four fringe widths were achieved in this experiment.

B. Conditions Affecting Faraday Rotation

Faraday[1] discovered that the magneto-optical rotation was largest when the magnetic lines of force were parallel to the rays of light in the material under investigation. The rotation dropped to zero when the two were perpendicular. He also stated that the magnitude of the rotation appeared to be directly proportional to the strength of the magnetic field and the length of the material through which the light passed. Verdet[17] confirmed these observations and expressed them in

quantitative form:

$$\phi = V_{\lambda,T} \ell H \cos \zeta \qquad (1)$$

where ϕ is the observed rotation, ℓ the length of the light path in the sample, H the magnetic field strength, and ζ the angle between the magnetic lines of force and the light path. $V_{\lambda,T}$ is the so called Verdet constant which is a function of the wavelength of the light used, λ, and of the temperature, T. More will be said about the λ and T dependences of the Faraday effect later.

For gases, equation (1) must be modified to include the density, ρ:

$$\phi = \rho V_{\lambda,T} \ell H \cos \zeta$$

Similarly, if we are dealing with the MOR of a solute we must include its concentration, c:

$$\phi = c V_{\lambda,T} \ell H \cos \zeta$$

The last equation assumes that the Verdet constant of a mixture is the sum of the Verdet constants of the components. This was shown to be the case for several systems by Verdet.[17] This behavior can be described by saying that each component of a mixture behaves as if it alone were present in the total volume of the mixture (Verdet's rule). Schonrock[18] and Chuckerbutti[19] showed that if there is a change in total volume upon mixing, the Faraday rotation reflects this change. Schuner[20] found a number of systems for which Verdet's rule does not hold.

Faraday[1] and others observed that MOR is additive to natural optical rotation--that is, if a material is observed to produce optical rotation α in the absence of a magnetic field, the rotation in a magnetic field will be $\alpha + \phi$, where ϕ is given by the appropriate one of the preceding three equations. What may appear surprising to those

unfamiliar with the Faraday effect is that φ is the same for enantiomers of a given compound (e.g., d- and l-camphor), indicating that the Faraday effect is completely insensitive to the non-superimposable mirror image type symmetry which gives rise to optical rotation. In fact, no well accepted experimental correlation has been established between any type of symmetry and any characteristic of the Faraday effect.

Since 1870, serious efforts have been made to demonstrate and classify relationships between chemical constitution and the MOR measured at one or a very few wavelengths. De la Rive[21] pointed out the great differences that could exist between the observed Faraday rotations of constitutional isomers such as actaldehyde (I) and ethylene oxide (II). This led him to state "the mode of combination, and particularly the mode

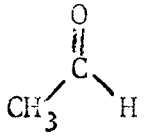

I

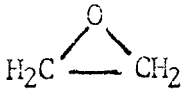

II

of grouping of the atoms, consequently the atomic volume, has, independently even of the nature of the atoms, a great influence upon the intensity of the magneto-rotatory power".[22] The same considerations led Sir G. G. Stokes[23] to make a similar statement regarding the potential usefulness of the Faraday effect. With reference to Perkin's measurements of the Faraday effect in structural isomers, Sir G. G. Stokes in 1892 said: "It appears therefore that the rotation of the plane of polarization produced by the action of magnetism on bodies across which light is proceeding, like the natural rotation belonging to such bodies as sirup of sugar, etc. is capable of laying hold of

and revealing delicate differences of molecular grouping." Beginning in 1882, Perkin[24] devoted 30 years to the investigation of chemical applications of the Faraday effect with some success. Practically all of his measurements were made at the sodium D line only, but he did demonstrate a fairly reliable mathematic expression of the Faraday rotation for members of a homologous series of compounds. He defined a "relative molar magnetic roticity", [RM]:

$$[RM] = \frac{M_1 \alpha_1 \rho_2}{M_2 \alpha_2 \rho_1}$$

where M is the molecular weight, α is the angle of rotation, ρ is the density and subscripts 1 and 2 refer to the compound being investigated and water respectively. From his measurements on 222 compounds he formulated the following empirical equation for a given homologous series:

$$[RM] = 1.023\ n + s$$

where n is the number of $-CH_2$ groups and s is an empirical constant. A few typical values of s are 0.508 for n-paraffins, 0.261 for aldehydes and 0.375 for ketones. Actual values of [RM] were found to deviate as much as 11% from the calculated values, and the smallest member of a series often does not fit the pattern. Even with these handicaps, Perkin's work proved to be of value in establishing the furanose structure of sugars in solution.[25] His measurements were also instrumental in establishing that the two double bonds were conjugated in a sample of Δ-p-menthadiene, (III), but they were not conjugated in dipentene (dl-limonene, IV).[26] Perkin put the Faraday effect to several other uses of a similar nature.[24]

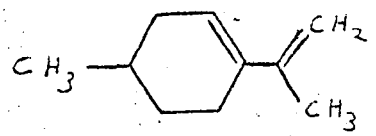

III

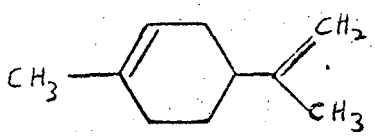

IV

This empirical method of using the Faraday effect for classifying compounds as members of one or another series has been continued by Gallais[27] for certain organic compounds, and by Labbauf, Nutt and Garner[28] for some compounds of interest in the refining of petroleum.

In contrast to natural optical rotation, Faraday rotation is independent of the direction the light is traveling through the sample. A curious device based on this fact is the Rayleigh "light trap".[29] Figure 5 is a schematic diagram of its optical elements. The two Nicol prisms have their transmitting axes inclined at 45° to one another. The magnetic field causes 45° rotation of the plane polarized light passing through it. So, with reference to the diagram, light will be transmitted from A to B, but not from B to A. Such a "light trap" is truly a one-way window. This device has found application in microwave circuitry as an isolator. Wave guides replace the two Nicol prisms in Figure 5, and the sample is a ferrite rod in the field of an electromagnet. When this field is adjusted to the strength that produces 45° rotation in the ferrite rod microwaves can travel only one way through the system, thus preventing any reflected power from being transmitted into the input wave guide.

Qualitative reasons for this behavior will be given here, although quantitative descriptions are available from recent quantum mechanical derivations of the Faraday effect. Consider now a plane polarized light beam passing through a sample and being reflected so that it traverses the sample once more. If the sample is in a magnetic field, the rotation of the emergent light will be twice that for one traversal of the cell. But if the sample is only optically active, the emergent light will have the same plane of polarization as the incident light. This behavior is to be expected from the nature of circularly polarized light and from the circular birefringent nature of the two phenomena as discussed above. First we must visualize what happens to circularly polarized light upon reflection. The electric vector of left circularly polarized light rotates clockwise when the observer faces the oncoming ray. But if the

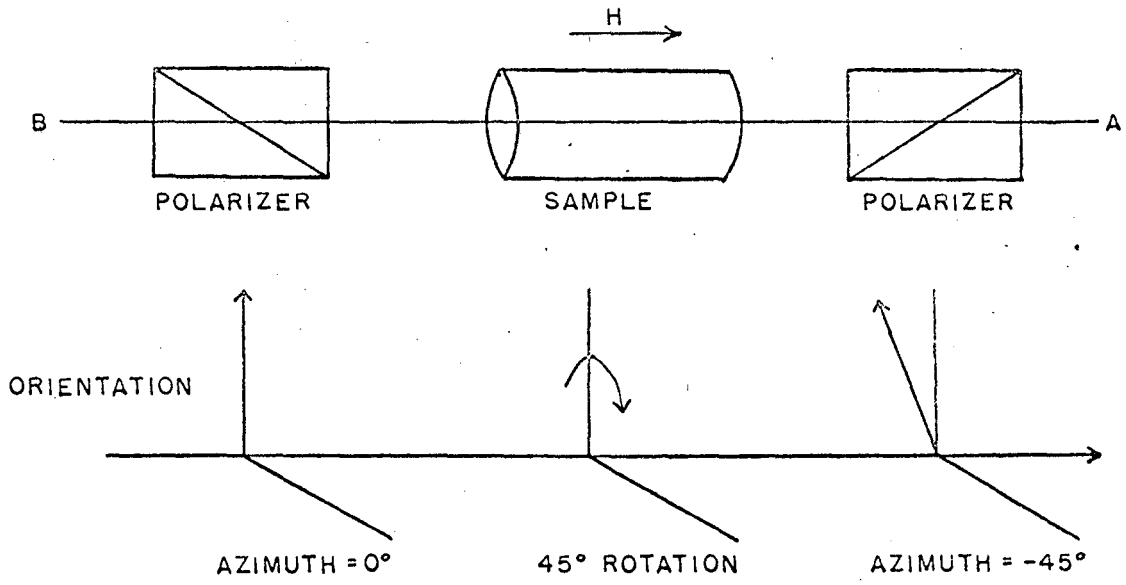

Figure 5. Rayleigh Light Trap.[29] Top line shows the optical elements. Bottom line shows their relative azimuthal orientations of the polarizers and the direction of the Faraday rotation caused by the sample.

observer is situated at the face of the cell and watches the rotation of this vector as it strikes the back of the cell, it will appear to be rotating in a counterclockwise direction. This is a purely geometrical consideration--a clock's hands appear to rotate counterclockwise when viewed in a mirror. The result of reflection is seen to be conversion of left to right circularly polarized light, and conversely. In optical terms it is stated that reflection reverses the phase of a beam.

In a sample exhibiting natural optical rotation, the left circular component of the incident light experiences index of refraction n_l before reflection, and n_r after. The opposite is true for the right circular compenent. By the time they emerge, both components have had the same total optical path length (distance times refractive index), and their phases are identical. Consequently, no optical rotation is observed.

Consider now the Faraday rotation of a non-optically active material. The same reversal of the circular polarizations occurs, but the relative direction of the magnetic field is also reversed for the reflected light. The optical path lengths and rotation are therefore twice as large as those observed for one traversal of the sample.

This aspect of the Faraday effect has several experimental implications. Multiple reflections in a Faraday rotation cell will increase the observed rotation in proportion to the number of times the light beam traverses the sample when total reflection occurs.[30] The "effective" length of the sample can thus be increased for the Faraday effect just as it is in other types of spectroscopy. An odd number of reflections causes the cancellation of any natural optical rotation the sample might have imposed on the light beam. If, however, only partial reflection occurs at the sample surface, the observed rotation will have some value greater than that for one

transversal. If the sample is thin enough and flat enough to act like an interference filter, the observed rotation will vary periodically with the wavelength of the incident beam. Such effects have been observed for a thin sample of PbS at wavelengths between 3 and 30 μ.[31] The results were explained mathematically and the corrected Faraday rotation used to obtain the concentration of the charge carrier electrons and the relaxation time in the sample.

Unwanted multiple reflections can cause spurious rotations in the visible and ultraviolet regions of the spectrum (in MORD but not ORD). In most polarimeters the reflected light will miss the detection system if the sample is mounted so that it is not quite perpendicular to the light beam.

An increase of temperature usually decreases the Faraday rotation of a sample, but the effect is usually not very pronounced. Several factors could cause such behavior. As a sample expands because of rising temperature, there will be fewer molecules in the light path if the length of the light path remains fixed. This is approximately what happens to a liquid in a glass or quartz cell. One would therefore expect the Faraday rotation to be proportional to the density of the liquid. Rodger and Watson[32] found this to be nearly true for carbon disulphide, but the temperature coefficient for the Verdet constant was larger than the temperature coefficient for the density.

For thin films of ferromagnetic materials, the Verdet constant has very nearly the same value until the material is heated to the point where it loses its magnetic properties.[33] In this case the number of molecules in the light path does not change on heating, and the Faraday rotation is proportional to the magnetization of the metal, so the result is not too surprising. However, the natural optical rotation of crystalline quartz is much more sensitive to temperature than is the Faraday

rotation.[34] This might be explained by noting that this natural optical rotation arises from the dissymmetry of the crystal structure, not the constituent molecules. Lattice vibrations induced by heating would thus be expected to influence the optical rotation. But the Faraday effect apparently depends only upon the molecules (or atoms) and not their arrangement, since the magneto-optical rotation does not change markedly even at the quartz transition temperature (575°C).[35] The natural rotation shows a large discontinuity at this temperature.

Temperature changes may also affect Faraday rotation by changing the equilibrium concentrations of ions in solution. For example, De la Rive[36] found the ratios of the Faraday rotations and densities of alcohol and of ethyliodide were equal when measured at two temperatures. But the Faraday rotation of water and of sulfuric acid decreased much faster than their densities.

From the foregoing it is seen that the Faraday effect has been of some use to chemists interested in molecular structure, and more recently to those studying conduction in semiconductors. It has also proven valuable in microwave technology, but a statement on the Faraday effect made by John Tyndall[37] was nearly as applicable in 1960 as it was in 1873: "The experiment, however, long remained rather a scientific curiosity than a fruitful germ. That it would bear fruit of the highest importance, Faraday felt profoundly convinced, and recent researches are on the way to verify his conviction."

III. THEORY

In this section we show how optical rotation and magnetic optical rotation arise from the inequality of the indices of refraction for right and left circularly polarized light. Two classical theories based on different models are presented to indicate how this difference of index of refraction comes about through the action of a magnetic field on the electrons in the material. Finally, a recently published theory of the Faraday effect is discussed with emphasis on the predictions it makes regarding the characteristics of the magneto-optical rotation to be expected from different types of compounds.

These theories will not be presented in great detail, but those parts of them that bear intimately on the experimental results of this work will be given special attention. An effort will also be made to give the reader a qualitative, reasonably tangible picture of the origins of the Faraday effect as proposed by each of these theories. The rigorous mathematical descriptions of these theories (especially the quantum theory) are rather long and involved, and the reader is referred to the original papers for their complete development.

A. Macroscopic Equations

Fresnel[38] established the circularly birefringent nature of optical rotation in 1822. In its quantitative form this relationship is known as Fresnel's Formula (equation 1), and holds for

$$\alpha = \frac{\pi}{\lambda}(n_\ell - n_r) \tag{1}$$

magneto-optical rotation as well as for natural optical rotation. Here α is the observed rotation, λ is the vacuum wavelength of the light, n is the refractive index, and the subscripts ℓ and r refer to right- and left circularly polarized light.

Fresnel's Formula and a similar formula for circular dichroism can be derived with the aid of the complex index of refraction, $\hat{n}$, in the electromagnetic description of light.[39] $\hat{n} = n' - in''$ where n' and n'' are the real and imaginary parts of the index of refraction. An elliptically polarized light wave propagating in the + z direction through a material will have its electric vector $\underline{E}(z,t)$ given by

$$\underline{E}(z,t) = \underline{E}_o e^{-n''rz/c}\left[\cos\omega\left(t-n'_r\frac{z}{c}\right)\underline{i} - \sin\omega\left(t-n'_r\frac{z}{c}\right)\underline{j}\right]$$
$$+ \underline{E}_o e^{-n''rz/c}\left[\cos\left(t-n'_\ell\frac{z}{c}\right)\underline{i} - \sin\left(t-n'_\ell\frac{z}{c}\right)\underline{j}\right] \tag{2}$$

if the major axis of the ellipse is polarized in the xz plane at z = 0. Unit vectors $\underline{i}$ and $\underline{j}$ are directed in the x and y directions respectively. (See Figure 6). As the light passes through the medium, the angle of rotation of the major axis of the ellipse is denoted by ϕ, which is measured from the x axis toward the negative y axis. The ellipticity, θ, is given by

$$\theta = \tan^{-1}\frac{a_1}{a_2} \tag{3}$$

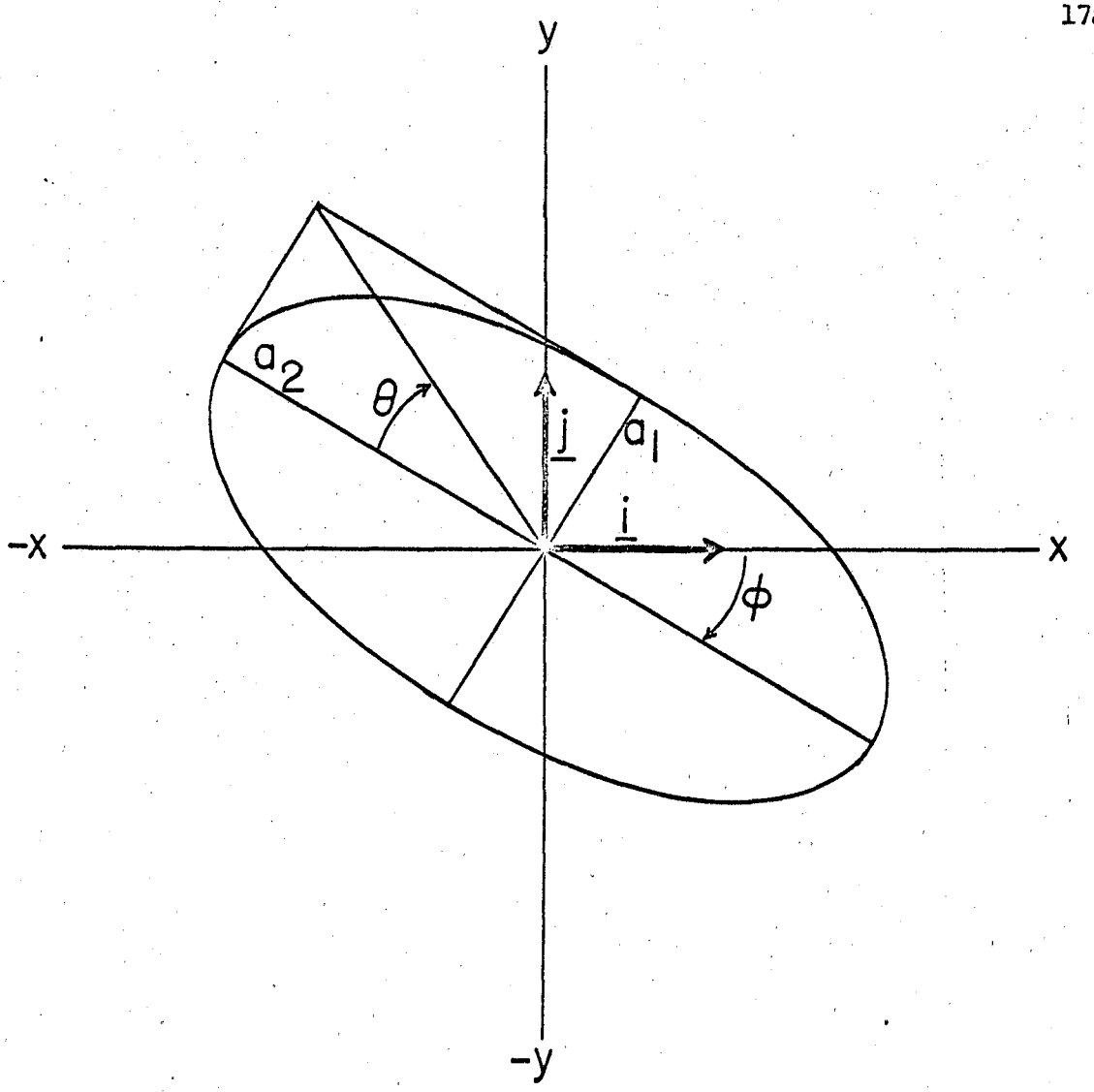

MUB-11633

Fig. 6. Diagram showing the components of elliptically polarized light. a_1 and a_2 are the minor and major axes of the ellipse, ϕ the optical rotation, and $\underline{i}$ and $\underline{j}$ are unit vectors.

where a_1 and a_2 are the minor and major axes of the ellipse traced out by the tip of the electric vector of the light. This vector makes one revolution in $2\pi/\omega$ seconds, or in terms of distance along the z axis, $n'_r z/c$ or $n'_\ell z/c$, which is the wavelength of the light of that polarization in the material. This describes elliptically polarized light. Two limiting cases are: 1) when $a_1 = 0$, the light is plane polarized, and 2) when $a_1 = a_2$, the light is circularly polarized.

We may now obtain expressions for ϕ, the optical rotation, and for θ, the ellipticity in terms of ω, z, and the components of n by noting that

$$|E(z,t)| = \left[E_x(z,t)^2 + E_y(z,t)^2\right]^{1/2} .$$

So

$$|E(z,t)| = E_o \left[e^{-2\omega n''_r z/c} + e^{-2\omega n'' z/c} + 2e^{-\omega(n''_r + n''_\ell)z/c} \cos 2\omega[t-(n'_\ell + n'_\ell)z/2c] \right]^{1/2} . \qquad (4)$$

We can now write the maximum and minimum values of the amplitude of the electric vector as

$$|E(z)|_{max} = E_o \left[e^{-\omega n''_r z/c} + e^{-2\omega n''_\ell z/c} \right] \qquad (5)$$

which occurs at $t = (n'_\ell + n'_r)z/2c + \pi k/\omega$, and

$$|E(z)|_{min} = E_o \left[e^{-\omega n''_\ell z/c} - e^{-\omega n''_\ell z/c} \right] \qquad (6)$$

which occurs at $t = (n'_\ell + n'_r)z/2c + \frac{\pi(1+2k)}{2\omega}$. k is an integer.

It can be seen from Figure 6 that

$$\phi_{(z)} = \tan^{-1}\left(\frac{-E_y(z)}{E_x(z)}\right) \qquad (7)$$

evaluated where $|E(z)| = |E(z)|_{max}$,

so
$$\phi_{(z)} = \tan^{-1}\left[\frac{e^{-\omega n''_r z/c}\sin\omega(n'_\ell - n'_r)z/2c - e^{-\omega n''_\ell z/c}\sin(n'_r - n'_\ell)z/2c}{e^{-\omega n''_r z/c}\cos\omega(n'_\ell - n'_r)z/2c + e^{-\omega n''_\ell z/c}\cos\omega(n'_r - n'_\ell)z/2c}\right] \tag{8}$$

$$\phi_{(z)} = \omega(n'_\ell - n'_r)z/2c = \pi/\lambda\,(n'_\ell - n'_r)\,, \tag{9}$$

which is Fresnel's Formula.

A similar equation for the ellipticity can be derived by noting that

$$\theta_{(z)} = \tan^{-1}\left(\frac{|E_{(z)}|_{min}}{|E_{(z)}|_{max}}\right) = \tan^{-1}\left(\frac{1-e^{-\omega(n''_\ell - n''_r)z/c}}{1+e^{-\omega(n''_\ell - n''_r)z/c}}\right) \tag{10}$$

$$\theta_{(z)} \cong \tan^{-1}\left[\omega(n''_\ell - n''_r)z/c\right], \tag{11}$$

upon expanding to first order since $\omega(n''_\ell - n''_r)z/c \ll 1$ for commonly used experimental path lengths. Also, in MORD, the observed values of θ are small enough to permit setting $\tan\theta = \theta$, so

$$\theta = \omega(n''_\ell - n''_r)z/2c = \pi/\lambda\,(n''_\ell - n''_r)\,. \tag{12}$$

n'', the imaginary part of the complex index of refraction, is identified with the molar extinction coefficient, ε, by the equation

$$n'' = \frac{2.303\,\varepsilon c}{\ell} \tag{13}$$

where c is molar concentration, and ℓ is the length of the medium through which the light travels.

Equation (12) can then be written

$$\theta = 3300\,(\varepsilon_\ell - \varepsilon_r) \tag{14}$$

if the constants are evaluated in cgs units.

Equations (9) and (12) show that ellipticity bears the same relationship to the extinction coefficients of right and left circularly polarized light that optical rotation does to the corresponding real indices of refraction. But there is an even more fundamental relationship between ellipticity and rotation which is expressed by the Kronig-Kramer Relations.[40] These mathematical relationships are independent of the model chosen to represent the interaction of light with matter; in fact, they have found application in such unrelated areas as calculating strain as the effect of stress and calculating the output of a radiation detector or an amplifier in response to an input signal. In the field of optics they link the absorption of a material to its dispersion over the whole electromagnetic spectrum. This includes energies as high as those of nuclear particles, where they relate nuclear scattering and the probability of particle capture.

The derivation is based on the assumptions that: 1) the system is linear--that is, the system will show response a+b to cause A+B if its response to A is a and to B is b when applied individually; 2) the system is causal--that is, it does not respond before it receives a stimulus.

Equations relating the real and imaginary parts of the dielectric constant, ϵ_d, can be derived fairly easily if certain other equations from the electromagnetic theory of light are used.[41] This derivation illustrates the important aspects of the Kronig-Kramers equations without going into excessive detail or becoming too complicated. The equations upon which the derivation is based are: $P = (\epsilon_d - 1)E$; $D = \epsilon_d E$

and

$$\hat{n}^2 = \epsilon_d = \epsilon(\omega) + \epsilon_\infty$$

where P is the electric polarization, and D is the electric displacement, $\hat{n}$ is the complex refractive index, and ϵ_∞ is the value of ϵ_d at $\omega = \infty$ where $\epsilon(\omega)$ will be equal to zero. Now let $\epsilon(\omega) = F(\omega) - i\,G(\omega)$, so

$$D = \epsilon_\infty E + \sqrt{2/\pi}\,\mathcal{R}\int_0^\infty \epsilon(\omega)\, e^{i\omega t}\, d\omega \qquad (15)$$

for a very short electrical pulse where the Fourier transform is a uniform energy spectrum so that

$$D = \sqrt{2/\pi}\,\mathcal{R}\int_0^\infty \epsilon_d e^{i\omega t}\, d\omega\ . \qquad (16)$$

$\mathcal{R}$ means "take the real part of". Before the electrical pulse at $t = 0$, both E and D were zero, so equation (16) becomes

$$\mathcal{R}\int_0^\infty \epsilon(\omega)\, e^{i\omega t}\, d\omega = 0\ . \qquad (17)$$

Since the exponential term may be expanded as

$$e^{i\omega t} = \cos \omega t + i \sin \omega t\ , \text{ for } t > 0, \qquad (18)$$

and

$$e^{i\omega t'} = \cos \omega t' - i \sin \omega t'\ , \text{ for } t < 0 \text{ where } t' = -t, \qquad (19)$$

we may write

$$\int_0^\infty F(\omega) \cos \omega t'\, d\omega t + \int_0^\infty G(\omega) \sin \omega t'\, d\omega = 0 \qquad (20)$$

for $t < 0$, and

$$\int_0^\infty F(\omega) \cos \omega t - \int_0^\infty G(\omega) \sin \omega t\, d\omega = 0 \qquad (21)$$

for $t > 0$. We now define

$$m(t) = \sqrt{2/\pi}\int_0^\infty F(\omega) \cos \omega t\, d\omega = \sqrt{2/\pi}\int_0^\infty G(\omega) \cos \omega t\, d\omega \qquad (22)$$

from equation (21), so we can write

$$F(\omega) = \sqrt{2/\pi} \int_0^\infty m(t) \cos \omega t \, dt \, . \tag{23}$$

We now substitute for m(t) from equation (22),

$$F(\omega)\ 2/\pi \int_0^\infty G(\omega') \sin \omega' t \cos \omega t \, d\omega' \, dt \tag{24}$$

where ω' indicates which part is to be integrated. Equation (24) can be integrated by contour integration to give

$$F(\omega) = 2/\pi \, \mathcal{P} \int_0^\infty \frac{\omega' \, G(\omega') \, d\omega'}{\omega'^2 - \omega^2} \tag{25}$$

where $\mathcal{P}$ indicates the principle value is to be taken.

The equation

$$G(\omega) = 2/\pi \, \omega \mathcal{P} \int_0^\infty \frac{F(\omega') \, d\omega'}{\omega'^2 - \omega^2} \tag{26}$$

can be derived in a similar fashion.

The last two equations establish the relationship between the real and imaginary parts of the frequency dependent dielectric constant for a homogeneous material. They show that if there is dispersion (i.e., $F(\omega) \neq 0$), then there must be absorption ($G(\omega) \neq 0$) for at least some part of the spectrum $0 \leq \omega \leq \infty$. But to obtain $F(\omega)$ at a given frequency, one must integrate a function of $G(\omega)$ over all frequencies, ω', and likewise, $G(\omega)$ requires that $F(\omega)$ be integrated from $\omega' = 0$ to $\omega' = \infty$

The foregoing relationships can be extended to connect the real and imaginary parts of the index of refraction (i.e., normal dispersion and absorption). This was accomplished independently by Kronig[42] and Kramers.[43] The equations have been adapted to relate optical rotation

an ellipticity or circular dichroism. A notably simple form of these equations has been given by Moffitt and Moscowitz:[44]

$$\phi_k(\lambda) = 2/\pi \int_0^\infty \frac{\theta_k(\lambda')\ \lambda'}{\lambda^2 - \lambda'^2}\ d\lambda' \qquad (29)$$

$$\theta_k(\lambda) = -2/\pi\lambda \int_0^\infty \frac{\phi_k(\lambda')\ \lambda^2}{\lambda^2 - \lambda'^2}\ d\lambda' \qquad (30)$$

The subscript k refers to a particular absorption band. It should be noted that the Kronig-Kramer relationships apply to the sums of the absorption and dispersion curves as well as individually to the component bands. Also, in deriving the last two equations, it was assumed by Moffitt and Moscowitz that 1) the optical rotation and ellipticity of a solution are strictly proportional to the concentration of the optically active material; and 2) that the electromagnetic field of the light in the material has the same magnitude as it does in free space. The first assumption is valid in all but a few cases where certain types of interaction take place (for example, dimerization of solute molecules). The second assumption is never valid, but corrections are small except near optical absorption bands.

In practice it is seldom easy to apply equations (29) and (30) to ORD and CD or MORD and MCD data. One must integrate numerically or find a suitable mathematical expression for the curves that is integrable. The latter is possible and has been done for CD and MCD curves which have Gaussian or Lorentzian shapes.[46] But conversion of optical rotation data is much more difficult because the rotation associated with a given optical absorption band cannot be easily distinguished from that

associated with other bands. However, a computer program utilizing numerical integration has been written[47] and appears to convert rotation to dichroism accurately if the rotational spectrum is known well enough at wavelengths remote from the band of interest. Errors in the optical rotation data are magnified during the conversion, but the program is of great value in interpreting ORD and MORD spectra. Circular dichroism can be converted to optical rotation by the program somewhat more accurately.

It should be emphasized once again that the Kronig-Kramers equations are extremely general, and relate circular dichroism and optical rotation regardless of the physical factors giving rise to these optical phenomena. If molecular dissymmetry, magnetic fields, or mechanical strain produce optical rotation, they also produce circular dichroism, and the two will have a definite and fixed relationship to one another. Examples of some forms of the relationship will be given a little later.

B. Classical Theories

The two main classical theories of the Faraday effect are presented by Drude[48] in Theory of Optics. A much more lucid discussion of the classical theory of the Faraday effect for non-conductors has been given by Dratz,[46] who also develops the theory in more detail and gives applications. We will discuss only the qualitative aspects of the classical theories here, since it will be shown later that they are not useful in understanding the details of the MORD of the molecules studied here. They do help one to understand, in a qualitative way, how magneto-optical rotation comes about, however.

The hypothesis of molecular currents is the designation given to

one of the classical theories of the Faraday effect. It assumes that an external magnetic field brings into existence microscopic currents which are maintained without the expenditure of energy. For definiteness, let us consider each current to be an electron in a circular orbit. Each such molecular current is elastically bound to a particle (say, the nucleus of an atom) which cannot oscillate nearly as fast as the electron or a light wave. The center of rotation of the molecular current can be caused to oscillate about the nucleus by the electric field in a light wave, however. Neither the shape nor the size of the current is changed by the light wave, only its position with respect to the nucleus.

Consider one such current brought into existence by a magnetic field along the z axis of a right-handed coordinate system. The current will lie in the xy plane and its center of rotation will oscillate along the y axis if the electric vector of the light is polarized in the y direction. But the current creates a magnetic field along the z axis, just as a solenoid would. This "solenoid" then moves up and down the y axis at the frequency of the light wave. This causes a weak transverse magnetic wave to propagate in the direction the light beam is traveling (similar radiating dipoles nearby will interfere destructively with waves traveling in other directions, according to classical theory). Now the original light beam had an oscillating magnetic wave polarized in the x direction. This is perpendicular to the wave being radiated by the molecular currents. Since both waves have the same frequency, their resultant will be a magnetic wave whose polarization has been rotated slightly from that of the original light. The plane of

polarization of the electric part of the wave suffers the same rotation, according to a similar argument, and thus optical rotation occurs.

The other theory of MORD is designated the hypothesis of the Hall effect, because it is based on the same interaction of moving electrons with a magnetic field that gives rise to the Hall effect. The interaction is expressed quantitatively as

$$\underline{F} = e\underline{V} \times \underline{B} \tag{31}$$

where e is the electronic charge, $\underline{V}$ the directed velocity of the electron, $\underline{B}$ the magnetic field, and $\underline{F}$ is the force this interaction exerts on the electron. $\underline{F}$ is perpendicular to the plane containing $\underline{V}$ and $\underline{B}$, so for a field in the +z direction an electron moving in the +x direction will feel a force tending to move it in the +y direction. In a conductor the electrons moving in the +x direction will therefore tend to accumulate on the +y side of the conductor in a +z magnetic field. This is the Hall effect.

Equation (31) also holds for an oscillating electron that is elastically bound to a fixed position. We note that for motion in the +y direction, the force is in the -x direction, as can be seen from equation (31) and the definition of the vector cross product. But +x motion yields +y force. Thus a handedness is established by the magnetic field. Another way to express this is to say that any motion of the electron away from the origin of coordinates (except along the z axis) will force the electron to move in a clockwise curve rather than a straight line. Motions toward the origin result in a counter-clockwise curve. If we consider only the electronic motion induced by the electric field of plane polarized light, we see that the static magnetic field has perturbed this motion by

introducing oscillations perpendicular to those from the light wave. Because of this, the radiation emitted by the oscillating electron will have its plane of polarization rotated slightly away from the plane of the incident light wave. For the quantitative aspects of this argument, the reader is referred to Dratz[46] or Drude.[48]

Drude's calculations involve the dielectric constant which can be set equal to the square root of the index of refraction. If one then assumes dispersion for the index of refraction, dispersion of the Faraday effect will also be obtained. The two theories of the Faraday effect give different types of dispersion for the same classical wavelength dependence of the index of refraction, however. For the molecular currents,

$$V \propto \left(n \ \frac{a'}{\lambda^2} + \frac{b'}{\lambda^2 - \lambda_h^2} \right) \tag{32}$$

and for the Hall effect,

$$V \propto \left(1/n \ \frac{a'}{\lambda^2} + \frac{b'\lambda^2}{(\lambda^2 - \lambda_h^2)^2} \right) \tag{33}$$

where λ is the wavelength of the light, and a' and b' are constants of the motion of the electrons from a harmonic oscillator description of their binding, λ_h is a constant which may be thought of as the effective wavelength of absorption of the molecule, and n is the index of refraction. It is seen from the equations that the Verdet constant will have opposite signs on the two sides of an absorption band for molecular currents, but will be symmetric in sign about a Hall effect type absorption band. (This assumes a' is smaller, or not much larger, than 6', which is the case for the systems Drude considers.)

Until recently, the MORD of very few compounds had been measured through absorption bands, but examples of both equations (32) and (33)

had been found. For example, Cotton's[49b] measurement of the MORD of $CoCl_2$ (Figure 7) shows inversion of the sign in passing through the absorption band. Wood's[49a] values for the MORD are nearly symmetrical about the absorption band, as equation (33) would predict. The MORD remote from absorption bands could sometimes be fit equally well by either equation. Carbon disulfide provides one such case.[48]

In conclusion, the classical theories provided very little information about molecular or atomic structure. The parameters used in these theories were mostly empirical, and their values indicated the tightness of electronic binding in a rather indefinite manner.

It is not claimed here that any other theory explains MORD accurately in every detail, but the quantum mechanical theory presented in the next section makes considerable progress in this direction and certainly holds more promise than any other current approach to the problem.

It should also be said that the MORD of certain systems lends itself to a classical or semi-classical analysis. As mentioned previously, Dratz has extended the Hall effect theory and applied it to molecules

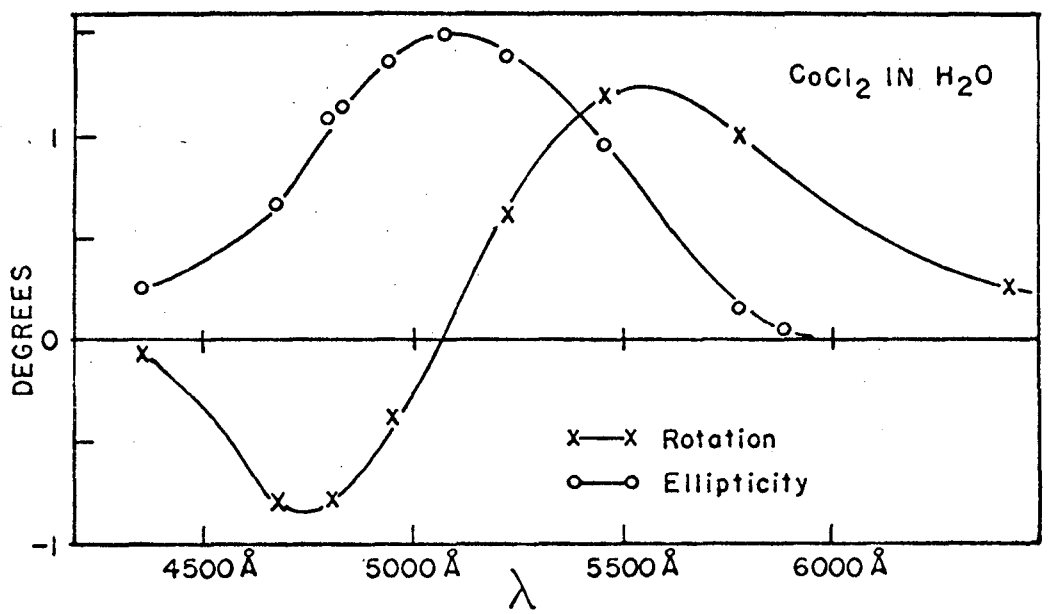

MUB-11215

Fig. 7. MORD and MCD (ellipticity) of $CoCl_2$ in water as measured by Cotton.[49b]

and complexes that have degenerate electronic states which can be split by a static magnetic field. The MORD, and especially the MCD, then prove to be of considerable value in understanding the electronic states and also interactions between molecules and transition metal ions, etc.

C. Quantum Mechanical Theory

In 1929 Rosenfeld[50] developed a quantum mechanical theory of the Faraday effect in atoms. A year later Kramers[51] treated paramagnetic crystals, and in 1937 Serber[52] extended the theory to molecules. Tinoco and Bush[53] have given an equation for the Faraday effect of diamagnetic molecules of low symmetry. Groenewege[54] also treats such molecules, but in somewhat more detail. The most detailed and complete treatment of the Faraday effect in polyatomic molecules is that of Stephens[55] and Buckingham and Stephens.[56] All of the treatments of molecules are extensions and modifications of Serber's work.

A brief discussion of Stephens' derivation and results will be given here to permit comparison of the quantum mechanical predictions with experimental results in the next section.

Stephens (and also others previous to him) shows how Fresnel's relation and the analogous relationship for circular dichroism arise from the induced electric and magnetic moments in the molecule. This is basically the same as in the classical theories. The divergence between the classical and the quantum theories comes in the next step where the induced moments are calculated. The classical description of molecules not only lacked accuracy, but was simply not detailed enough (in any tractable form) to explain the structure of observed MORD spectra.

Quantum mechanically, the electrons of a molecule are presumed to occupy a set of mathematically well defined orbitals, each with its own

quantized energy. (If two orbitals have the same energy, they are said to be degenerate.) Both the energy and shape of the orbitals are functions of several parameters, the most important of which for our purposes is the location of the atomic nuclei relative to one another. The absorption of a light quantum causes an electron to jump to a vacant orbital where it will have higher energy. The dipole moment of a molecule of low symmetry will be different in this excited state than it was in the ground state. For a given type of electronic transition the change in the dipole moment will always point in a certain direction with respect to the framework of the molecule, and it is found that no (or very little) absorption occurs when the electric vector of the light is perpendicular to this direction. Maximum absorption occurs when the electric vector is parallel to the molecule's transition dipole moment. Magnetic transition dipole moments also exist and are described analogously. The orbitals have certain symmetries with respect to the molecular framework, as do the transition moments, even in certain cases involving molecules of high symmetry where no net dipole is observed in either the ground or excited state. It is possible to tell by group theoretical methods whether the transition moment between two given orbitals is zero. The transition is termed forbidden if the moment is zero, and it is found that such transitions have no, or very low, absorbance.

The orbital electrons of a molecule are perturbed by magnetic and/or electric fields according to the Lorentz relation

$$\underline{F} = e\underline{E} + e\underline{V} \times \underline{B} \qquad (35)$$

where the terms and notation have been defined previously. In fact, the absorption intensity can be calculated from a knowledge of the orbitals and the perturbations caused by the electromagnetic fields of light waves. A static magnetic field causes other types of perturbations. For example,

if the electrons have well defined orbital angular momentum, the field will cause normally degenerate states to have different energies (Zeeman effect). The implication of this effect is discussed by Dratz[49] but will not concern us here because the molecules to be considered do not have well defined orbital angular momentum.

Stephens treats molecules whose orbital electrons are perturbed both by light and a static magnetic field. First order perturbation theory[57] is used to calculate the induced moments. In this formulation, a perturbed orbital ψ_a', is expressed as a sum over all the unperturbed orbitals ψ_b,

$$\psi_a' = \sum_b c_b \psi_b \qquad (34)$$

where the coefficients c_b are less than or equal to one. Such sums enter the final formulation of the expression for Faraday rotation. The c_i's are determined by the nature of the perturbation (many are zero or negligible), and the functions ψ_b are obtained from solving the Schrödinger equation for the unperturbed system.

Qualitatively, equation (34) says that the shape of an orbital distorted by a field can be described by adding the proper amounts of the shapes of certain unperturbed orbitals of the set. In practice, it is found that orbitals with energies near that of ψ_a are used to a greater extent. This fact enters as an energy denominator (i.e., $1/(E_b - E_a)$) in the final expression for the Faraday rotation. It should be mentioned that Stephens is careful to take the Zeeman effect energy of each orbital wherever it applies. If the ground state is split, there will be a Boltzman distribution of the electrons among the low lying orbitals, which is significant in the calculation of Faraday rotation and gives rise to a temperature dependence not found for unsplit ground states.

In each of the quantum mechanical treatments of the Faraday effect certain terms are dropped from the derivation on the grounds that they are small compared to the terms retained, or that they do not apply to the Faraday effect. Stephens keeps more terms than other authors but still drops terms that are higher than first order in the magnetic field (since the Faraday effect depends on the first power of the field strength). He also drops quadrapole and higher order interactions with the electromagnetic field of the light. He assumes that there are no conduction electrons in the system under consideration, so his results do not apply to metals and semiconductors. He also ignores the magnetic perturbation of natural optical activity, but his derivation is still more general than others in that it includes electron spin, applies to molecules of any symmetry, and is not limited to regions outside absorption bands.

Stephens gives the expressions for the frequency independent factors of Faraday rotation as

$$A_{oa} = 1/6\ \mathrm{Im}[\underline{m}_{aa} - \underline{m}_{oo}] \cdot [\underline{\mu}_{oa} \times \underline{\mu}_{ao}] \tag{36}$$

$$B_{oa} = 1/3\ \mathrm{Im}\left[\sum_{b\neq o} \frac{\underline{m}_{bo}}{\omega_{bo}} \cdot \underline{\mu}_{oa} \times \underline{\mu}_{ab} + \sum_{b\neq a} \frac{\underline{m}_{ab}}{\omega_{ab}} \cdot \underline{\mu}_{oa} \times \underline{\mu}_{bo}\right] \tag{37}$$

$$C_{oa} = 1/6\ \mathrm{Im}\ \underline{m}_{oo} \cdot [\underline{\mu}_{oa} \times \underline{\mu}_{ao}] \tag{38}$$

where μ is the electric dipole transition moment, m is the magnetic dipole transition moment, the subscripts o, a, and b designate the ground state and two excited electronic states, and Im means take the imaginary part of.

The A term is non-zero only for molecules with degenerate energy levels. Molecules with three-fold or higher symmetry axes have degenerate states; those with lower symmetry do not. The C term is

non-zero for molecules having two or more energy levels with different non-zero electronic populations in the ground state. Since the populations depend on temperature, so will the rotation arising from the C term. Zeeman splitting of the ground state results in two or more energy levels which are accessible thermally. The B term arises from perturbation of the wave-functions by the magnetic field. It is non-zero for all molecules and is independent of temperature. Stephens[55] indicates that for most cases where the A or C term exists, the B term will be 10 to 25 times smaller than either. For most of the molecules studied in this work, only the B term is non-zero.

Stephens takes the vector potential of the light to be

$$\underline{A} = 1/2[A_o\, e^{i\omega(t-\delta)} + A_o^*\, e^{-i\omega(t-\delta)}] \qquad (39)$$

as is common, where A_o is the maximum amplitude of the vector potential and the asterisk denotes its complex conjugate. ω is the circular frequency of the light, and δ is a phase factor. The vector potential enters into the perturbation calculation and confers a frequency dependence on the final result. But the expression does not take the finite bandwidth of the transition into account, and so a bandwidth factor, Γ, is added ad hoc to the expression. The justification for this is that the area under the dichroism and optical rotatory dispersion curves is not changed and Γ simply accounts for the environmental perturbations (solvent effects, etc.) that we are not presently able to calculate with sufficient accuracy. The ORD frequency dependence of A is found to be

$$\frac{2\,\omega_{oa}\,\omega^2[\omega^2\,\Gamma_{oa}^2 - (\omega_{oa}^2 - \omega^2)^2]}{[(\omega_{oa}^2 - \omega^2)^2 + \omega^2\,\Gamma_{oa}^2]^2} \qquad (40)$$

For B and C the frequency dependence is

$$\frac{\omega^2(\omega_{oa}^2 - \omega^2)}{(\omega_{oa}^2 - \omega^2) - \omega^2\,\Gamma_{oa}^2} \qquad (41)$$

Figure 8 shows these functions graphically along with those of the associated dichroism bands. These graphs show pictorially how the Kronig-Kramers equations would transform MCD to MORD and vice versa. Upper curves are MCD and the lower ones the associated MORD.

$\Gamma_{1/e}$ is the width of the band at where its amplitude is $1/e$ (i.e., about 37%) of the maximum amplitude. It can be seen from the figure that the MCD is nearly zero at frequencies not far from the center of the band, but the associated MORD curve still has considerable amplitude at these frequencies. Thus, for a closely spaced set of bands, the MORD tails may overlap considerably and lead to a very complicated spectrum. The MCD will not overlap to as great an extent for the same bands, and will therefore be more easily resolved and interpreted. However, for bands in frequency regions that are instrumentally inaccessible, no MCD can be observed but the MORD tail may extend to frequencies where measurements can be made. There is some doubt as to the reliability of the information provided by MORD tails, since in practice they are the superposition of the tails of several bands, whose contributions might not be resolvable. For these reasons MCD is presumed to be the most valuable of the two measurements. At present, MORD can be measured with more precision and at higher frequencies than MCD--factors which are of importance in the study of the aromatic hydrocarbons considered in this work. MORD was chosen over MCD for these reasons.

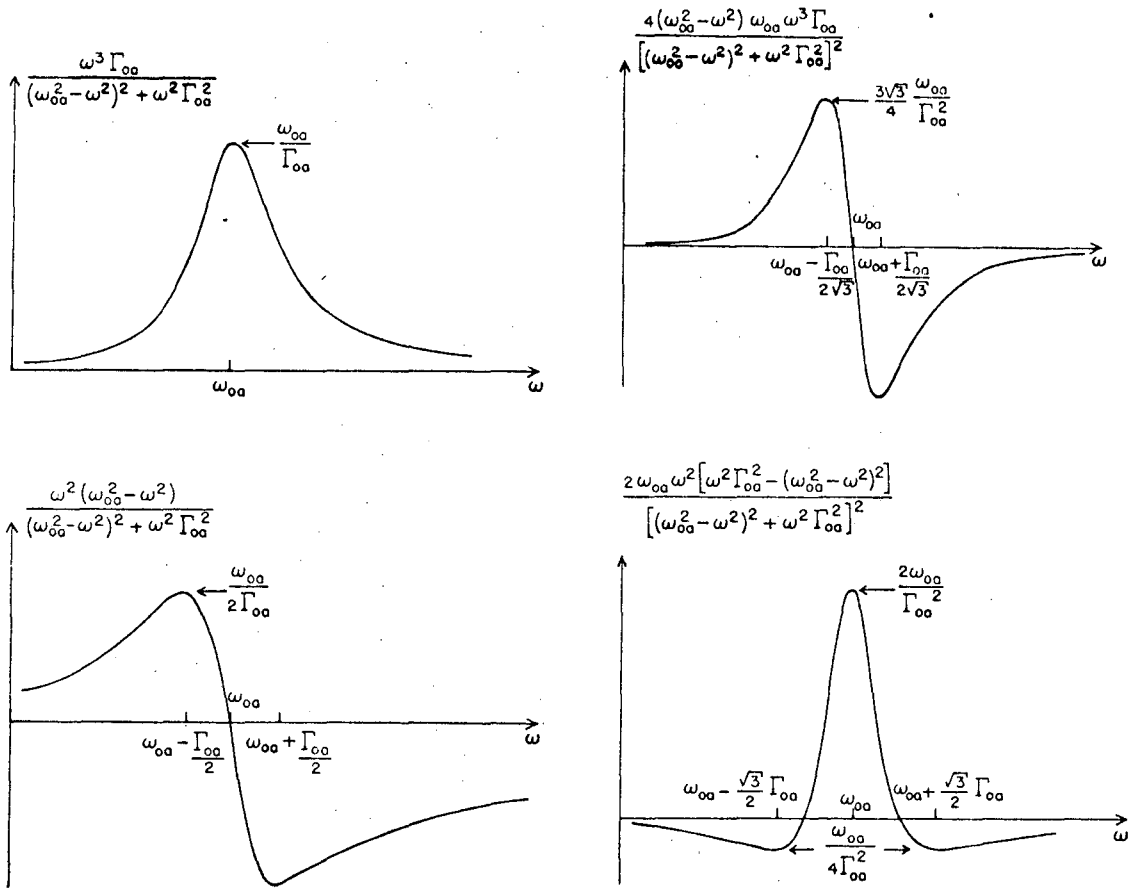

MUB-11219

Fig. 8. Frequency dependences of MCD and MORD.[55] The upper left graph shows the form of the MCD of a damped oscillator absorption band; the upper right curve results when the transition's excited state is split by the magnetic field. Each lower curve shows the form of the MORD associated with the MCD curve directly above. The ordinate is the value of the function written at the top of each graph. The scale for ω is the same for each curve.

III INSTRUMENTATION AND METHODS

In this section we discuss the design and construction of a magnet assembly that permits the measurement of MORD with a commercial polarimeter. This is presented in detail to show that the MORD measurements to be given later are accurate and reliable. This was considered necessary because certain published MORD curves have been shown to contain instrumental artifacts, and there is still some disagreement in the literature regarding the MORD of a few compounds, particularly small ketones.

We also discuss experimental methods and conditions, and show how data reduction by a digital computer can be achieved.

1) Apparatus for Measuring Magneto-optical Rotation

It is possible to measure magneto-optical rotation (MOR) with a commercial spectropolarimeter if a sufficiently intense magnetic field can be imposed upon the sample without disrupting the normal operation of the instrument. This has been accomplished by placing a suitably designed permanent magnet in the sample compartment of a Cary Model 60 spectropolarimeter.

Figure 8b is a photograph of one of the permanent magnet assemblies used in the instrument. The Alnico V horseshoe magnet can be seen in the upper half of the assembly. Directly below it are the two soft iron pole pieces, which are tapered toward the air gap. The magnet and pole pieces are in good thermal contact with the brass cooling block which can be seen supporting them. The tubes on the upper right permit coolant to be circulated through the cooling block. The screw at the left edge of the assembly is one of two which allow the gap length to be changed by sliding the left pole piece laterally. A sample cell can be placed in the gap between the pole pieces. The hole passing lengthwise through both pole pieces allows the instrument light beam to travel through the gap parallel to the magnetic field.

Even when covered with styrofoam for thermal insulation, this assembly fits into the sample compartment of the polarimeter. Others[58] have used a set of electromagnets in the same polarimeter position to measure MOR. Permanent magnets have certain advantages such as simplicity, reliability, and excellent magnetic field stability. The control of temperature over wide ranges is relatively easy and precise,

58. J. J. Ruffield, personal communication.

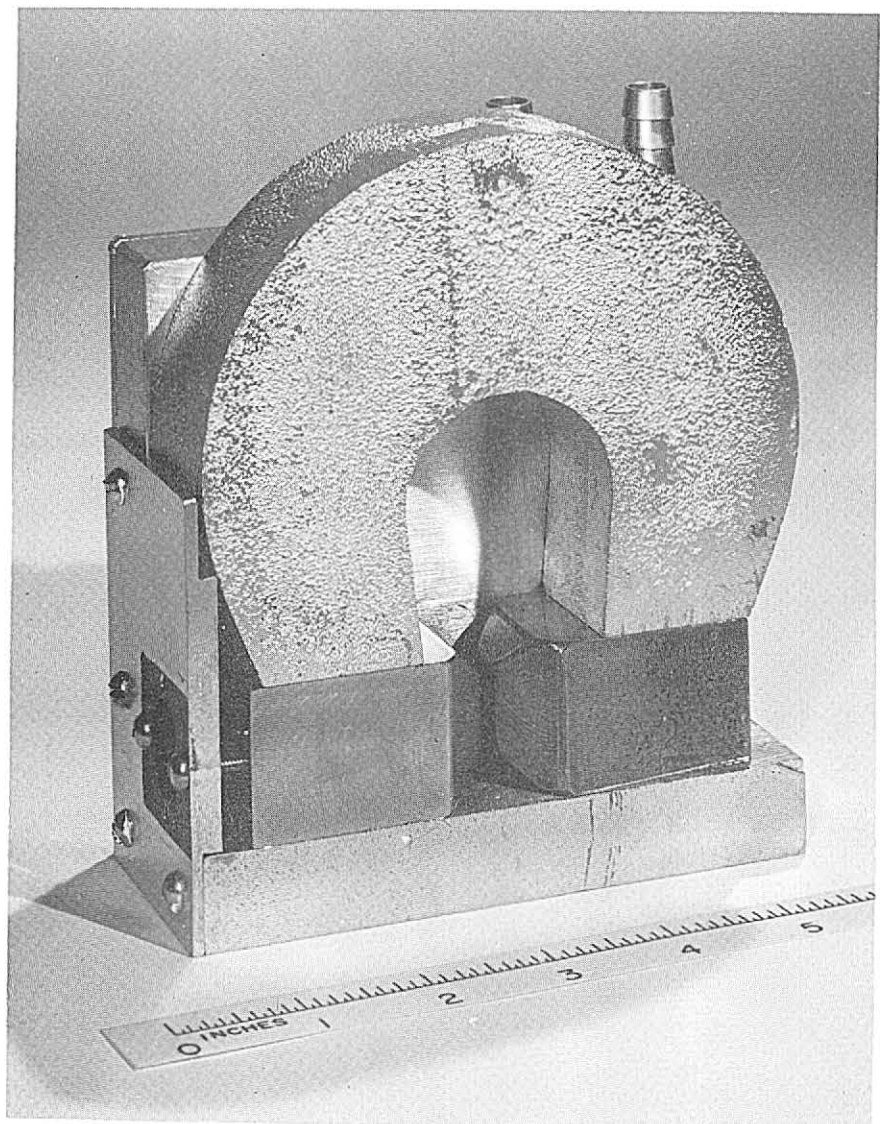

ZN-5767

Fig. 8b. Photograph of one of the permanent magnet assemblies used in connection with the Cary 60 Spectropolarimeter for the measurement of magneto-optical rotatory dispersion.

and maintenance is a very simple matter. Unfortunately, there are also disadvantages. These will be enumerated when sufficient background has been given to show they impose no serious handicap upon most Faraday rotation experiments. It should be mentioned that nearly the same magnetic field strengths have been obtained for both electro- and permanent magnets, but superconducting magnets are expected to give considerably higher useful fields.

Figure 9 shows a cross section of the magnet pole pieces, indicating the form of the longitudinal hole and the approximate configuration of the magnetic lines of force in the gap (dashed lines). It can be seen that the magnetic field in the light path is only a fringing field. Its strength can be optimized by properly designing the pole pieces.

At this point it seems desirable to set forth the criteria by which the design is to be judged, to describe the design procedure, and to establish how nearly the magnet assembly approaches the theoretical maximum performance.

The optimum pole piece geometry is that which gives the highest signal-to-noise ratio. The signal is the magnitude of the Faraday rotation, and the noise is the root-mean-square error in finding the correct polarimeter null. The design parameters affecting noise will be discussed later. The problem to be considered now is the magnet design that will maximize the signal by giving the most intense magnetic field.

It is impossible to predict accurately what pole piece geometry will give the highest field with a given permanent magnet. There are a few equations which can be used as guidelines, however, and the usual procedure is to calculate the best configuration as nearly as possible,

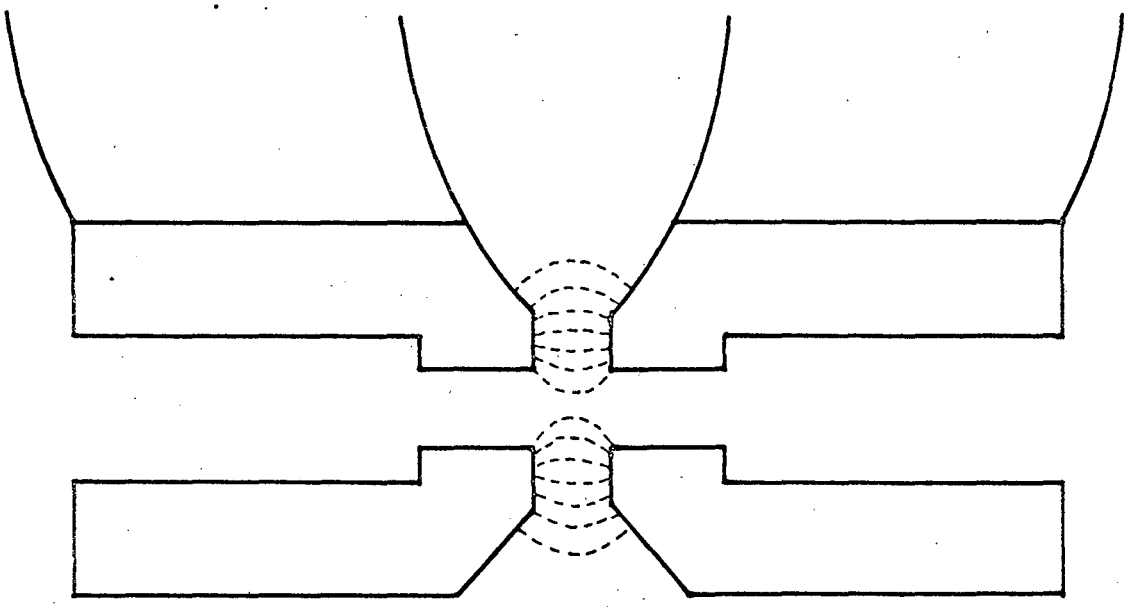

MUB-10542

Fig. 9. Cross-section of magnet pole pieces showing the approximate paths of the magnetic field lines (dotted lines).

construct a magnet according to the calculation, measure its field, and redesign using the measured field strength in the equations. This method was used, and has proven satisfactory.

The design equations were derived for simple magnetic circuits such as the one shown in Figure 10. Assuming the magnetic flux density is uniform over the cross sectional area of the magnet, A_m, and over the area of the gap, A_g, and that there is no leakage of flux, we can write

$$B_g A_g = B_m A_m \qquad a)$$

where B_g and B_m are the magnetic induction in the gap and in the magnet respectively. The equation holds because of the conservation of flux.

Since air has magnetic permeability, μ, very nearly equal to 1 (in e.m.u.), we may set $B_g = H_g$ because $B_g \equiv \mu H_g$. Thus, Faraday rotation will be proportional to B_g, and it becomes advantageous to increase B_g. For a given gap length and magnet cross sectional area, B_g can be increased by reducing A_g, the area of the gap.

An equation similar to a) holds for the length of the gap l_g, and the length of the magnet, l_m.

$$B_g l_g = H_m l_m \qquad b)$$

H_m is the magnetic field inside the magnet and is not equal to B_m. This equation is seen to be valid by considering the energy required to move a unit magnetic pole completely around the magnetic circuit shown in Figure 10. By conservation of energy, the work done in moving through the magnet must equal the negative of the work done in moving across the gap. Equation b) is the integrated form of this relationship and is only valid when H_m and B_g are constant over their respective lengths.

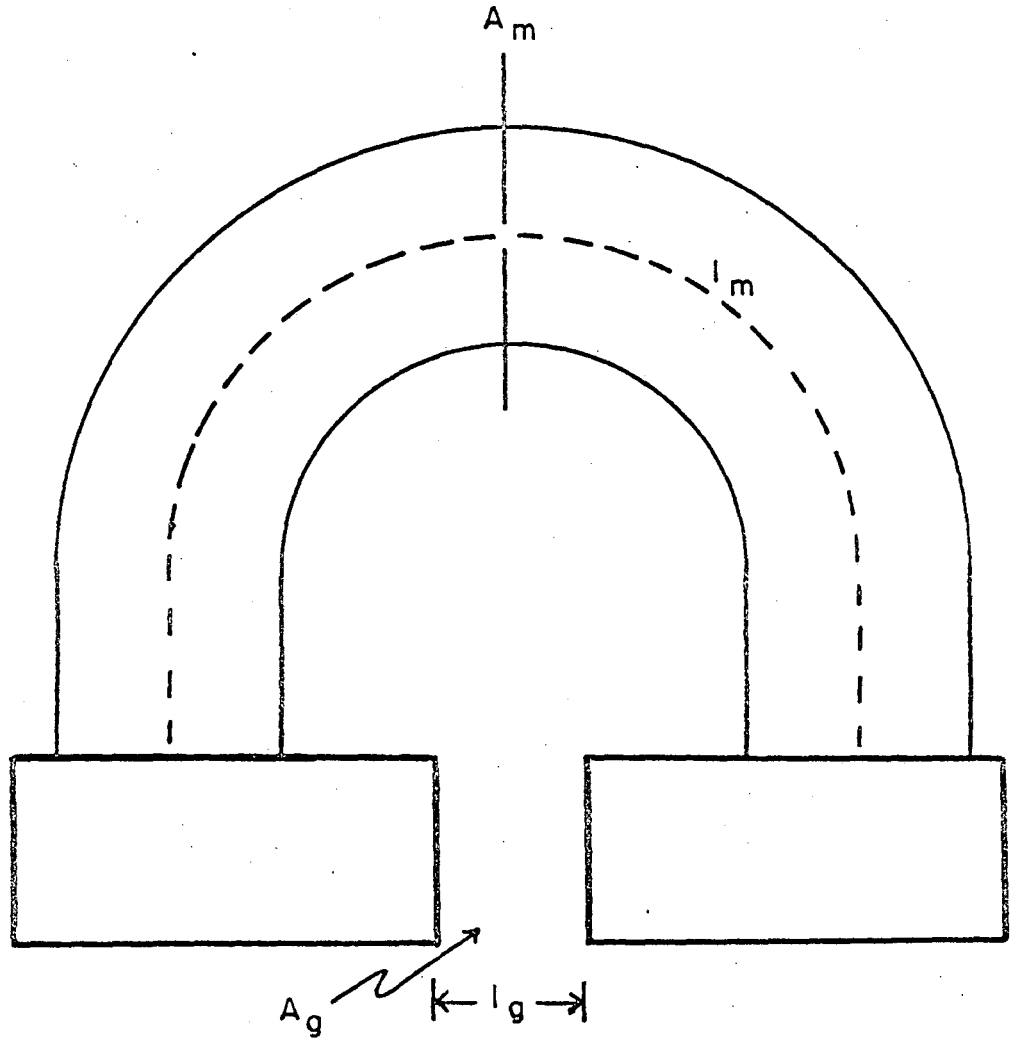

MUB-10546

Fig. 10. Simple magnetic circuit. A_m is the cross-sectional area of the magnet, A_g that of the gap. l_m is the length of the magnet, and l_g that of the gap.

Combining equations a) and b) we have

$$B_g^2 = \frac{A_m l_m}{A_g l_g} B_m H_m \qquad c)$$

For a given gap length and magnet, only the gap area can be varied by the design. But this may have a profound effect on the $B_m H_m$ product, whose maximum value is 5.5×10^6 gauss-oersteds for the Alnico V used in this system. To maximize B_g we must therefore understand the relationship between $B_m H_m$ and the gap dimensions. The relationship is best described by comparing the magnetic circuit to an electrical circuit (see Figure 11).

Obtaining the maximum magnetic energy product, $B_m H_m$, is analogous to getting maximum power dissipated in the load resistor, Ω_L, in Figure 11. Ω_L corresponds to the magnet gap reluctance which is proportional to l_g/A_g. The battery has an internal resistance, Ω_i, just as the magnet has a certain reluctance. In the electrical circuit, the power flowing through Ω_L is

$$P = \frac{V^2}{\Omega_L + \Omega_i} \qquad d)$$

P is maximum when $\Omega_i = \Omega_L$ if voltage V is fixed. Similarly, the energy stored in the gap is maximum when the reluctance of the gap equals the reluctance of the magnet. The desired gap reluctance can be obtained by adjusting A_g to the value specified by the equation

$$A_g = \frac{B_m l_g}{H_m l_m} A_m \qquad e)$$

which is obtained by elimination of B_g between equations a) and b). The ratio of B_m to H_m is 20 when the magnetic energy product is maximum. This value is obtained from the demagnetization curve for Alnico V (Figure 12).

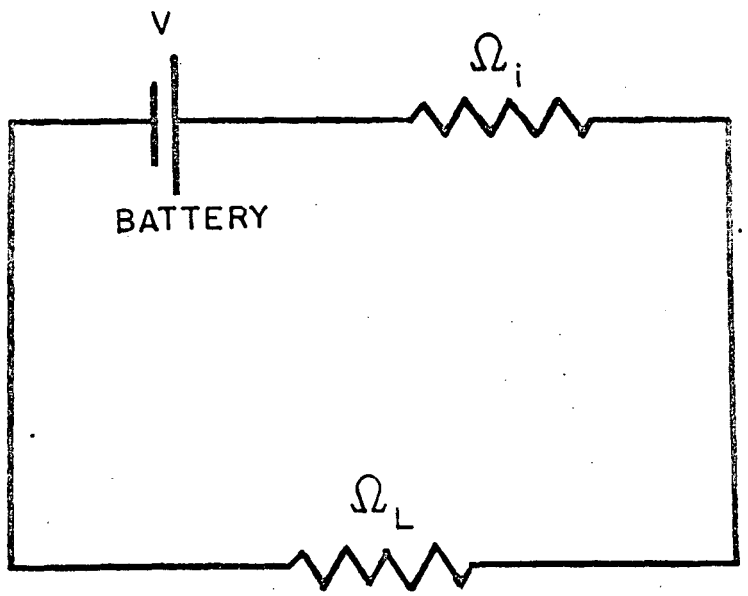

MUB-10545

Fig. 11. Electrical circuit analog of the simple magnetic circuit. Ω_i is the internal resistance and Ω_L is the load resistance.

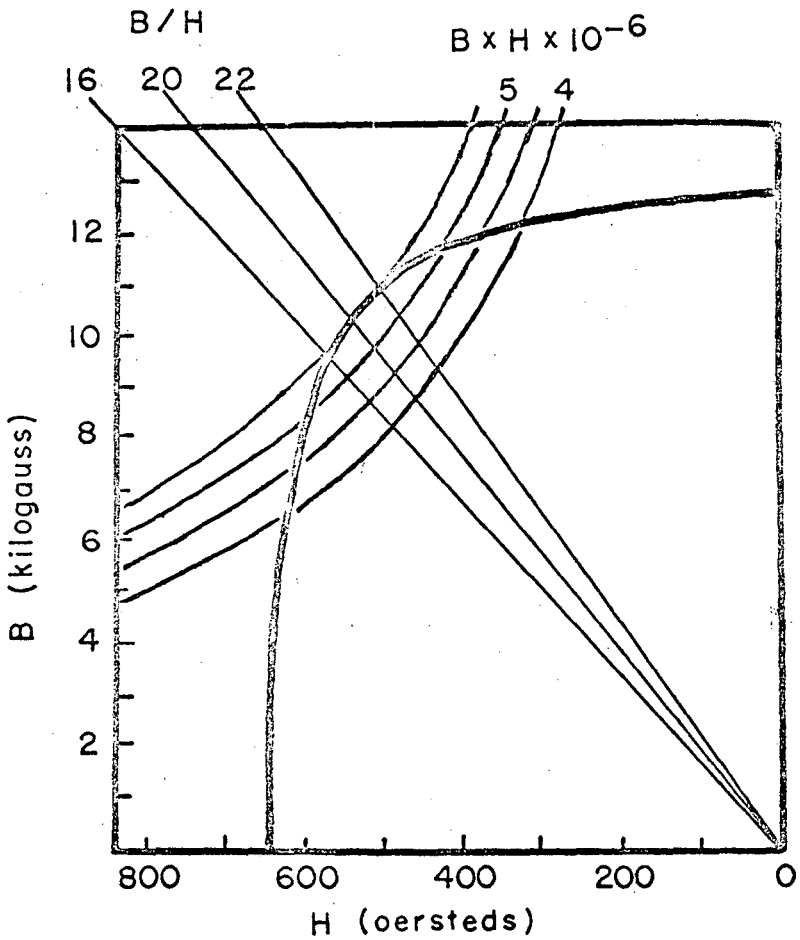

Fig. 12. Demagnetization and energy product curves for Alnico V.

A design based on the foregoing considerations would probably be far from optimum in reality because of the drastic assumptions that have been made. To avoid gross errors we must take into account flux leakage, inhomogeneity of the field in the magnet, and circuit shapes that differ from that shown in Figure 10.

Calculation of flux leakage is a very tedious and often inaccurate process. In addition, the final magnet circuit configuration must be known for the calculation. Since we do not yet know this configuration, we must estimate the effects of flux leakage. This can be done by the following empirical method: 1) Replace A_g by FA_g, and l_g by fl_g in all of the preceding equations. 2) Assign a value of 1.35 to f and find the value of F from a leakage factor monograph.[59] For the proposed circuit, F

59. Permanent Magnet Handbook, Crucible Steel Co. (1957).

is estimated to be approximately 2.8, but could be as high as 4.0.

Variations in the magnetic field over the length of the magnet are very difficult to estimate accurately. Their effects are at least partially contained in the empirical factors, f and F, so no further correction will be made for field inhomogeneity in the magnet.

The shape of the horseshoe magnet (see Figure 8b) causes some ambiguity in the values to be used for its length, l_m, and its cross sectional area, A_m, as compared with the simple circuit shown in Figure 10. The values used here were approximately the mean values for A_m and l_m. Estimation of the effective area and length of the gap was complicated because the pole tips were tapered. Such pole pieces give higher fields at the center of the gap than do those with rectangular ends, since the

reluctance in each pole piece is low except near the gap, and since tapering leads to a smaller effective gap volume. (The advantage of small gap volume can be seen from equation c).)

We digress at this point to explain how the pole piece shape was chosen. A series of experiments was done using pole pieces with various taper angles in an electromagnet. All pole pieces had longitudinal holes and circular cross section. It was found that a 45° taper gave maximum field at the center of the gap, but the field was still above 98% of its maximum value for any taper between 37° and 55°. The pole tip diameter (d in Figure 13) was optimum when it was 33% of the total pole piece diameter, but 98% of the maximum field was retained for pole tips between 28% and 42% of the overall diameter. The longitudinal hole was 1/6 the diameter of the pole pieces, as was the gap when the other dimensions were optimized. The magnetic field obtained in this case was about 10 kiloguass. For different field strengths, these relative dimensions were not optimum.

For pole pieces with the same geometry, but with all dimensions scaled down by some factor, S, we can expect the same field (10 kiloguass) if the magnetomotive force is reduced by the factor S. Within acceptable limits, this situation existed in going from the electro- to the permanent magnet, so the relative dimensions given above were nearly optimum. However, the shape of the permanent magnet pole pieces was rectangular rather than circular, and some small corrections may be needed to optimize the angles and relative areas in this case.

Now that the approximate shape of the pole pieces has been established, we have all the infonmation necessary to solve equation e), which will give us the value of A_g expected to maximize the magnetic

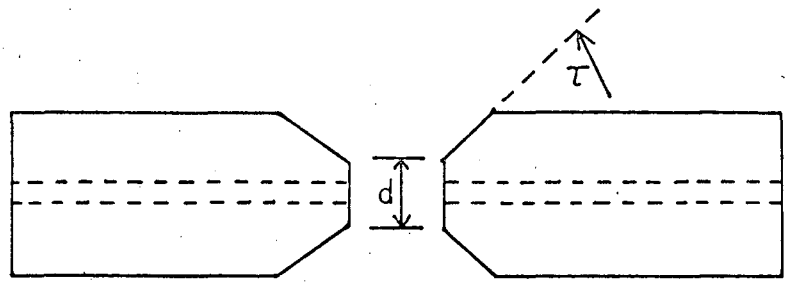

MUB-10541

Fig. 13. Shape of magnet pole tips. d is the tip diameter, and τ is the angle of taper.

field in the gap. Remembering the modifications required by flux leakage, equation e) becomes

$$A_g = \frac{B_m l_g}{H_m f l_m} F A_m \qquad f)$$

Using the values obtained previously and the estimated values l_g = 0.2 cm, A_m = 11 cm^2, and l_m = 15 cm, we find A_g = 6.1 cm^2. This is the proposed "effective" gap area, and is expected to be larger than the actual pole tip area because of the proximity of the tapered sections to the gap. The optimum pole tip area derived from the electromagnet relative dimensions experiments is 1.02 cm^2 for pole pieces with 10.1 cm^2 overall cross sectional area. As a compromise between the two values proposed for A_g, 2.5 cm^2 was chosen for the pole tip area of the first magnet assembly built.

This magnet assembly gave a maximum field of 12.8 kilogauss between solid portions of the pole tips when the gap was 3 mm. The effective field for material in a 1 mm path length cell inserted in this gap was found to be 8.3 kilogauss. B_m and H_m can be obtained from equations a) and b), if flux leakage is taken into account, and if we use 12.8 kilogauss for B_g. It was found* that B_m was 11.6 kilogauss and H_m was 345 oersteds. Referring to Figure 16, it can be seen that B_m is too large and H_m is too small to give the maximum $B_m H_m$ product. Decreasing the area of the pole tips appeared to be the correct remedy for this situation. The field in the gap may be increased by up to 14% by causing the circuit to operate at $(B_m H_m)_{max}$. At this stage of the design procedure, we must also consider several other factors which will affect the signal-to-noise ratio developed by the proposed magnet assembly.

*Actual measured dimensions of l_g and A_g were used in this calculation. It was found that F must be 4.0 to have the magnet operating point lie on the demagnetization curve.

The width of the longitudinal hole is the key parameter throughout the remainder of the design procedure. Together with the pole tip area, it determines the reluctance of the gap, and therefore the important value of B_m/H_m. Only the shape of the longitudinal hole determines the fraction of the maximum gap field that will be effective in producing Faraday rotation. In addition, the transmittance of the system is dependent entirely on the size and shape of the hole. We will express the signal-to-noise ratio, S/N, as a function of the hole size and maximize this ratio to determine the final dimensions of the pole pieces.

The Faraday rotation signal is proportional to the magnetic field, B_g, where sample concentration and cell path length are constant. The noise, N, is inversely proportional to the square root of the light transmitted by the system.[61] We may therefore write

$$S/N = kHT^{-1/2} \qquad g)$$

where k is constant with respect to changes in the size of the pole piece hole. OD_p, the effective optical density of the hole, is related to T by

$$T = e^{-OD_p} \qquad h)$$

so we can write

$$S/N = kHe^{-1/2\ OD_p} \qquad i)$$

We now require the functional dependence of OD_p on the hole width. This was measured by inserting an opaque plate with a narrow slit in it into the polarimeter light beam, and noting the resulting photomultiplier dynode voltage. This voltage rises as the effective optical density in the cell compartment increases. Figure 14 shows the results of a series of such measurements using different hole widths. Figure 15 is the calibration curve that relates optical density to dynode voltage. Neutral

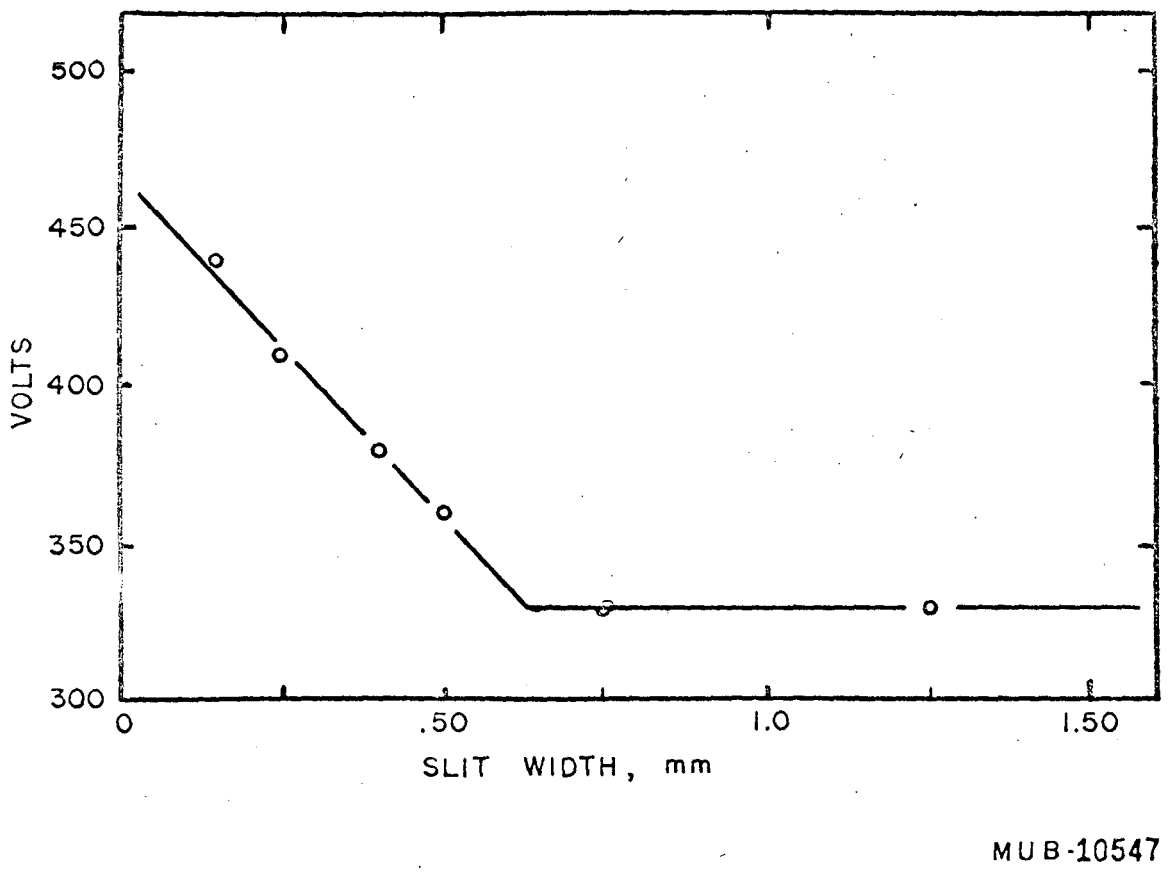

Fig. 14. Photomultiplier dynode voltage versus width of a slit inserted in the sample compartment of the spectropolarimeter.

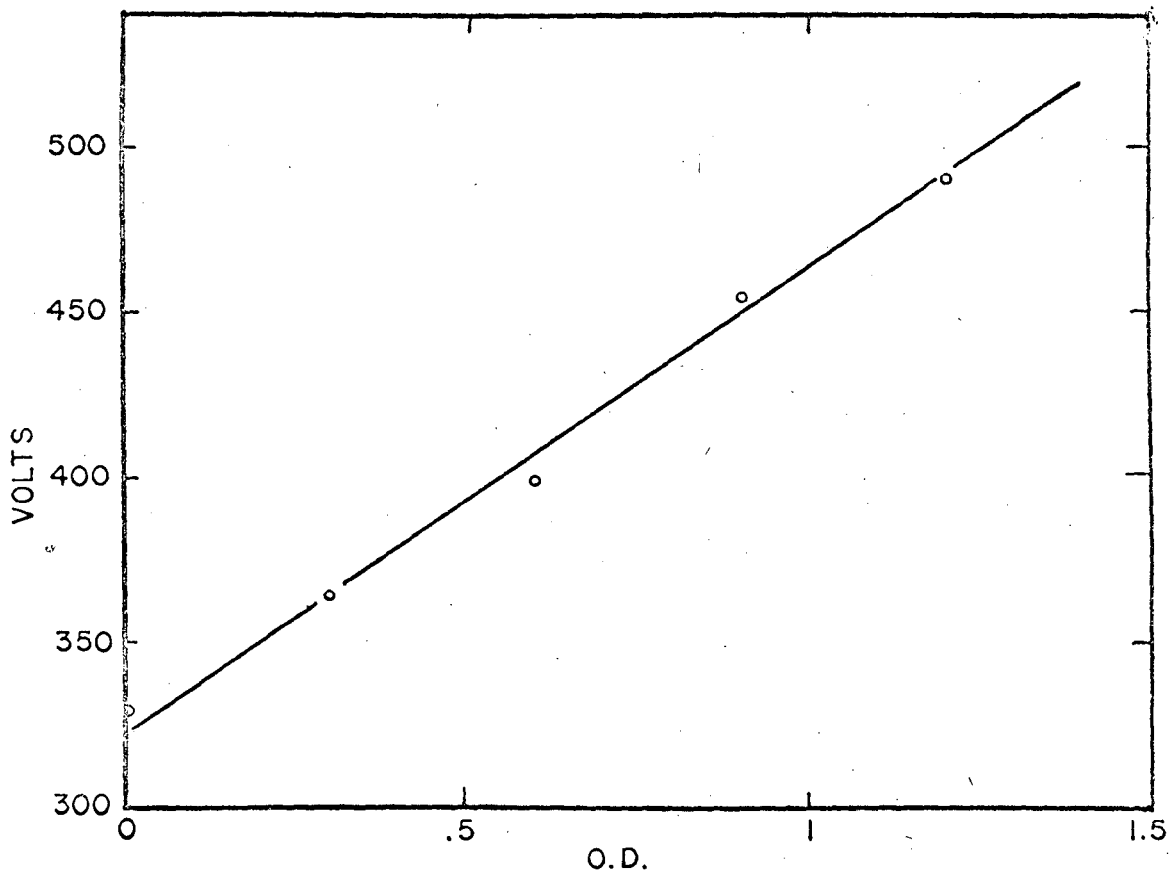

Fig. 15. Dynode voltage as a function of the optical density in the sample compartment of the spectropolarimeter.

density filters were used to obtain this curve. Both of these curves were taken at 4000 Å with the polarimeter slits adjusted to 0.11 mm (equivalent to a 10 Å spectral slit width).

From Figure 14 it can be seen that all the light was transmitted until the hole was less than 0.65 mm wide. For more narrow holes the curve fits the function

$$V_{pm} = -230W + 475 \qquad j)$$

where V_{pm} is the dynode voltage and W is the hole width (in mm). The curve in Figure 15 fits the equation

$$V_{pm} = 1.39(OD_p) + 330 \qquad k)$$

Eliminating V_{pm} from these two equations gives

$$OD_p = -165W + 104 \qquad l)$$

for W less than 0.65 mm. Equation i) can now be written:

$$S/N = kHe^{82.5W_c - 52} \qquad m)$$

We must now find the dependence of H on the hole width, W. H represents the field effective in producing Faraday rotation. It is a complicated function of the pole piece geometry, the light intensity distribution over the hole area, and the direction of the magnetic field at each point. It was therefore decided not to try to calculate H, but only to determine its limits and their effect on the signal-to-noise ratio. It will be shown that this procedure gives adequate results.

For a small light beam just grazing the edge of the hole, the effective field is somewhat independent of the hole width. That is, the major portion of the effective field is contributed by the iron which is in very close proximity to the light beam, not the iron across the hole. Therefore, as one limiting case, let us consider the effective field to be independent

of the hole width. It can easily be seen that maximum signal-to-noise in this case is achieved for any hole width which is larger than the light beam in the instrument.

As the other limiting case, we choose the effective field to have maximum dependence on the hole width--for example, the same dependence as the magnetic field at the center of the gap, H_c. A good estimate of H_c between shaped pole pieces can be made from considering equivalent surface poles.[60] The equation for rectangular pole tips is

$$H = \frac{2M}{\pi} \tan^{-1} \left[\frac{(\tan x)(\tan y)}{(1 + \tan^2 x + \tan^2 y)^{1/2}} \right] \qquad \text{n)}$$

60. D. B. Montgomery, in High Magnetic Fields,

where M is the magnetization (M was 12,800 gauss for the magnet mentioned previously). Figure 15a shows the geometry of angles x and y. Equation n) applies to solid pole tips, but by the principle of magnetic superposition we may obtain the field at the center of the gap between axial hole pole tips from the equation

$$H_c = \frac{2M}{\pi} \tan^{-1} \left[\frac{(\tan x)(\tan y)}{(1 + \tan^2 x + \tan^2 y)^{1/2}} \right] - \frac{2M}{\pi} \tan^{-1} \left[\frac{(\tan x')(\tan y')}{(1 + \tan^2 x' + \tan^2 y')} \right] \qquad \text{o)}$$

where x' and y' apply to the hole and are defined in analogy with Figure I10. The term involving x and y in equation o) is independent of gap width and is estimated to be about 14,000 gauss. (Its exact value is of no importance provided it is greater than 8,300 gauss, as will be seen later.) This term will be referred to as H*.

For the 3 mm gap required to accommodate a 1 mm path length cell, tan x' becomes W/3. The hole must be more than 12.5 mm high to transmit

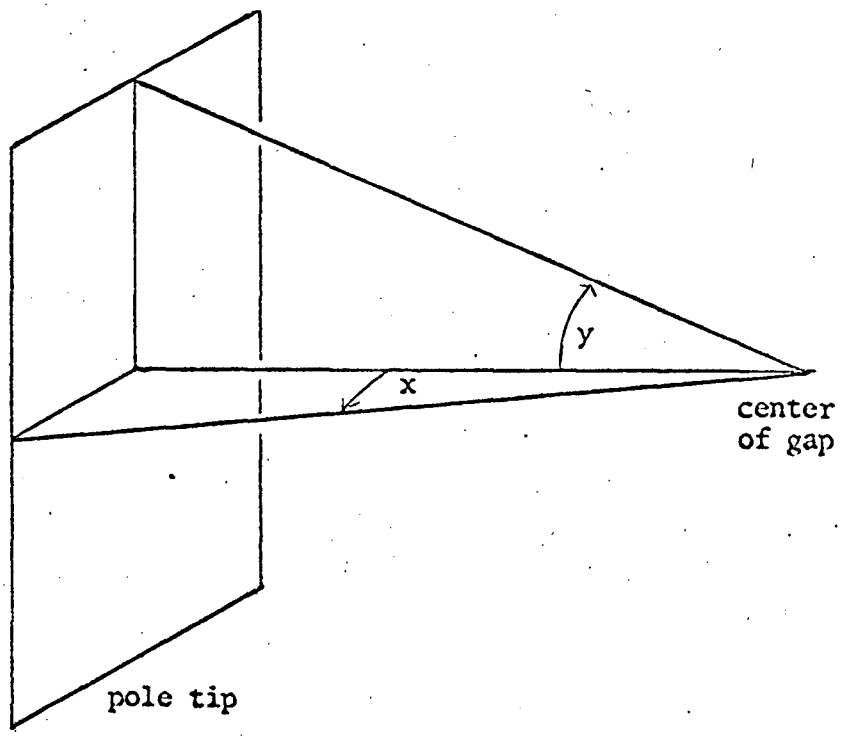

Fig. 15a. Diagram showing angles used to calculate magnetic field at center of gap.

all of the instrument light beam. Moderately shorter holes do not contribute appreciably to H_c and only serve to block off part of the light beam. We therefore set tan y' = 12.5/3 = 4.17. We will use the value 21,400 gauss for M. This is appropriate for saturated iron and will give the greatest dependence of H_c on hole width, which is what we require for this limiting case calculation.

Using the foregoing values, we can write

$$H_c = H^* - 13{,}600 \tan^{-1} \left[\frac{(W/3)(4.17)}{(1 + W^2/9 + 17.2)^{1/2}} \right] \qquad p)$$

Substituting this into equation m) gives

$$S/N = k(14{,}000 - 13{,}600 \tan^{-1} \left[\frac{12.5\ W}{(164 + W^2)^{1/2}} \right] e^{82.5W}\, e^{-52} \qquad q)$$

We now assume W is less than 0.65 mm, making W^2 small compared to 164 in the denominator of the $\tan^{-1}$ term in equation q). The limit on the size of W is reasonable because larger widths do not increase the magnetic field (equation q)), nor do they allow more light to be transmitted (Figure 18), so nothing is gained by wider holes. It is not clear from equation q) that narrower holes would improve the signal-to-noise ratio, but this can be determined by differentiating q), setting d(S/N)/dW = 0, and solving for W. This procedure shows S/N is maximum when W = H*/13,200. H* is certain to be greater than 8,600 gauss, which means W is optimum for values greater than 0.65 mm according to equation q), and when Figure 18 is considered, W is optimum when it is exactly the width of the light beam. This is true for light beams up to about 1 mm wide, at which point it may be advantageous to block off part of the light beam in order to increase the magnetic field strength.

The next magnet assembly built had an effective field of 12,600 gauss--a substantial increase over the previous assembly. This was achieved by reducing the pole tip area to 1.1 cm^2 and narrowing the hole to 0.125 cm. For a 10 Å spectral slit width the hole is wider than necessary at 4000 Å, but is near optimum in the UV at about 2200 Å. The measurement of the effective field was made on a 1 mm path length of water, in a gap 3 mm long. The maximum field between the pole pieces was 13,900 gauss, indicating that the magnet assembly was operating relatively near the point of maximum BH product.

The magnetic saturation of the iron pole pieces limits the field attainable with such a magnet assembly if the total bulk of the system can be large. This limit is 21,400 gauss for soft iron. It is higher for certain alloys such as Hyperco, but these alloys would be degraded to the same status as soft iron by the machining required to make them suitable for this application. We may therefore say we have reached 65% of the bulk-unlimited maximum field. Magnets small enough to fit the polarimeter cannot develop the magneto-motive force required to give 21,400 gauss in a gap large enough to accommodate a sample cell of reasonable size. The values of the maximum fields for small magnets are not readily available; however, the author knows of one magnet used for gauss meter calibration which has a field of 14,100 gauss. This magnet is approximately the same size as that used in the measurement of MOR, and it has approximately the same gap length. If we assume its design is optimum, then the MOR magnet is developing 98.5% of the maximum field attainable under the size limit imposed upon it. Efforts to increase the effective field by further design refinements were deemed unprofitable, since it would be possible to increase the field 35% at most, and it is very likely that less than 10% increase could be

obtained with the present gap and hole dimensions.

A brief description of how the polarimeter operates will now be given to facilitate the understanding of the magnet assembly's influence on the instrument. More detailed information has been given by Cary, et al.[61]

61. H. Cary, et al., Applied Optics 3, 329 (1964).

Figure 16 is an optical diagram of the polarimeter taken from the Operation Manual for the instrument. Light is generated by a xenon arc, A, and passes through a double monochromator (all elements between S_1 and S_3). It then passes through the adjustable slit labeled S_3, and is focused by lenses I so that an image of a monochromator slit stop is formed at the position of the sample cell, SC. A Sénarmont polarized, LP, is positioned ahead of the sample cell, and only light with approximately horizontal polarization is allowed to pass through the sample cell. F is the Faraday modulator--a slug of fused silica wrapped with a coil of wire carrying 120 watts of 60 cycle AC power. The magnetic field generated in the silica imposes a sinusoidal oscillation on the plane of polarization of the emerging light beam. LA is an analyzer which permits only the vertical component of the light to pass. If the plane of polarization is horizontal at LA, the output signal generated at the photomultiplier tube, PM, will look like a 60 cycle voltage which has been full-wave rectified. If the polarization is not horizontal, neighboring peaks of the signal will have different amplitudes. This condition activates a servo mechanism which rotates LP to restore balance. Thus, sample optical rotation α causes LP angular rotation $-\alpha$, which can be sensed and recorded by the instrument.

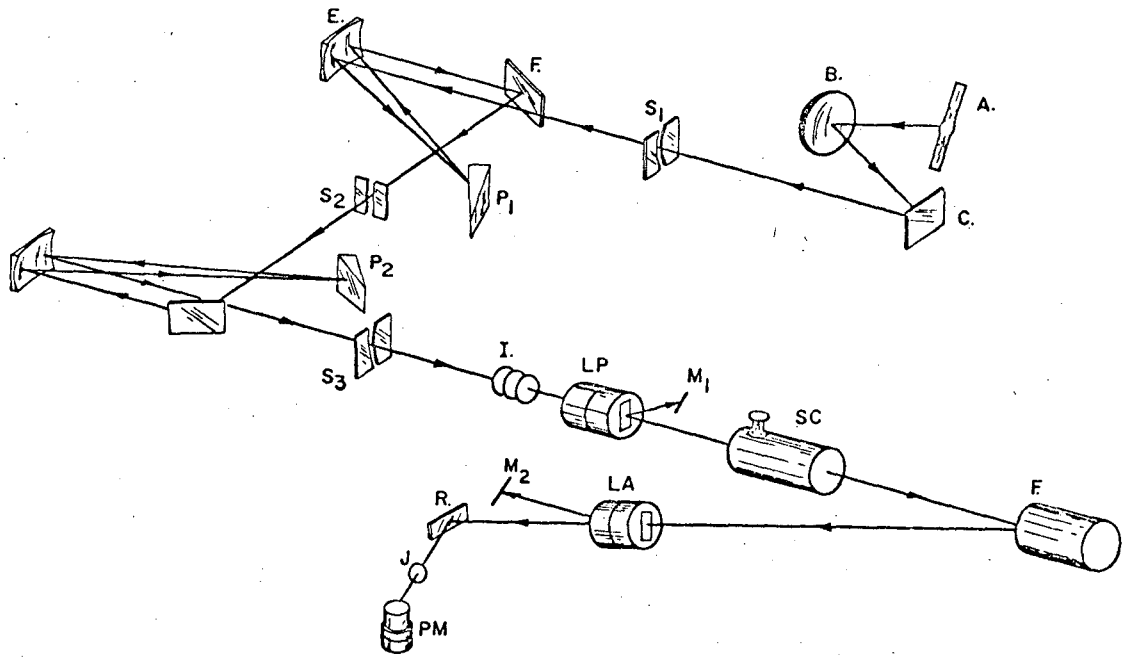

Fig. 16. Diagram of the optical system of the Cary 60 Spectropolarimeter taken from the operation manual for the instrument. The components and the operation of the instrument is discussed in the text.

It is well known that quartz and common solvents such as water, benzene, etc., all show a reasonably large magneto-optical rotation throughout the visible and ultra violet regions of the spectrum. This implies that the cell and solvent will produce a background rotation when the magnet system is used in an effort to obtain the MORD of a solute. The background is usually ten to one hundred times larger in magnitude than the solute rotation. Others[63] have simply subtracted the background MORD from the solution MORD, but this leads to poor accuracy for two

63. B. Briat, M. Billardon, and J. Badoz, Comptes Rendus 256, 3340 (1963).

reasons: (1) The solute rotation is a small difference obtained by subtracting one large number from another. Thus, a small percentage of error in either large number could lead to a large percentage error in the difference. (2) Both background and sample curves have considerable slope (especially in the ultra violet), so a minor wavelength shift of one curve with respect to the other can result in a great change in the magnitude of the solute rotation obtained from the curves.

This problem has most often been avoided in electromagnetic systems by using two magnets carrying the same current, but with the magnetic fields in opposite directions. The sample is placed in one magnet and an identical cell filled with solvent is placed in the other. The light beam passes sequencially through both, so that the background rotation produced in the sample cell is cancelled by that produced in the solvent cell where the magnetic field is oppositely directed.

This approach has proven successful when the temperature difference between the two cells can be kept sufficiently low (the Verdet constant has a slight dependence on temperature). Also, the magnetic fields must

remain equal. Applied Physics[58] uses this method in the attachment they have constructed for measuring MORD on the Cary 60.

58.J. J. Duffield, personal communication.

At this laboratory a solution with natural optical activity is placed in the light path beyond the sample and magnet. The background rotation is cancelled except for small rotations which the instrument adjustments (baseline multipots) can nullify. Thus, by choosing the proper concentration of the optically active material, and by minor instrument adjustments, one can achieve a stable, non-sloping baseline from which to measure small solute rotations. Spectra obtained in this manner can be reproduced to within 2×10^{-3} degrees (approximately the noise level of the instrument).

Another method used successfully here to cancel the solvent and cell MORD involves the use of two permanent magnets in the polarimeter cell compartment. One is positioned as usual; the other is placed in the light beam reflected from the Faraday modulator (Figure 109). This second magnet assembly contains a cell filled with solvent, which cancels the MORD of the cell and solvent in the first magnet. Since both magnets cannot easily be magnetized to the same extent, it is found necessary to equalize their fields by placing an iron bar across the strongest magnet of the pair. This bar extends from one leg of the horseshoe to the other. The more it is lowered toward the gap, the more flux it "short circuits", and the

weaker the gap field becomes. Magnets can be matched very precisely in this manner. Unfortunately, they are not exactly matched for all wavelengths at once because of changes in the light intensity distribution over the beam in the two gaps as wavelength varies. Again, the instrument multipots can compensate for this, and straight, stable baselines can be achieved.

B. Experimental Conditions

The conditions under which each experiment was run are listed in Appendix I. We will here describe the conditions and their implications in more detail than is found in the Appendix.

The temperature of the polarimeter is automatically controlled to within 0.2°C of a preset level (26.0°C for this work). The magnet and cell were placed in the polarimeter during the instrument warm-up, so their temperature was also 26°C. Only a small amount of sample was required to fill the short pathlength cells used, and it was assumed that the temperature of the sample was also 26°C 5 min after placing it in the polarimeter. Whenever the magnet and/or the sample was not at temperature equilibrium, the MOR could be observed to change with time due to the density of the sample changing as its temperature changed.

The MORD of the cell filled with solvent was measured over the appropriate wavelength range for each sample MORD spectrum taken. In most cases such a baseline was run both before and after each spectrum, and the baselines compared to be sure their differences were within experimental error.

The spectral slit width was 10 Å for many of the measurements, and never more than 20 Å except for spectra with very wide absorption bands. The spectral slit width was not recorded in some cases and is then listed as ca. 20 Å, although it was generally less than this.

The time constant of the instrument is described by the manufacturer in terms of the pen period (seconds required for the pen to travel 97% of the way back to the correct value after being displaced). The periods used were 1, 3, and 10 sec.

C. Chemicals

Practically all of the chemicals were obtained from K&K Laboratories or from Aldrich Chemicals, and all were used without further purification. A number of the smaller aromatic hydrocarbons were checked for impurities by vapor phase chromatography on an Aerograph 1520 with a 10-ft column. Table I lists the results in terms of chromatographic peak heights.

Solutions were used within 1 hr of the time they were made. The larger, less stable aromatic hydrocarbons were protected from light and oxygen as much as possible. Special care was taken with benzo[g,h,i]-fluoranthene which was found to exhibit spectral intensity changes very soon after exposure to light and air. In this case, the compound was dissolved in $CHCl_3$ under N_2 in the dark and the measurements made immediately after the solid was entirely dissolved.

D. Date Reduction

Many of the MORD and some of the absorption spectra of the compounds studied were digitized by means of a system constructed here. The instrument pen position was sensed potentiometrically and this information fed to a digital voltmeter. The voltage readings were then processed by a logic unit constructed here and the resulting information punched on cards by an IBM key punch. Many of the spectra were recorded before this digitizer became available, and it was found possible to digitize these spectra by mounting them in the polarimeter and using the instrument's electrical pen displacement control to follow the curve while the digitizer was operating. Once the spectra were on cards they could be converted to corrected molecular rotation by a computer.

Table I. Purity of chemicals used as indicated by vapor phase chromatography.

Compound	Source	Column	Temp °C	Ret Time[a]	Peak Height	Impurities Ret Time	Impurities Peak Height
Naphthalene	B&A	C[b]	280	2.25	360		0
		S[b]	350	1.2	450		0
		S	200	3.3	320		0
Azulene	K&K	C	200	3.25	130		0
		S	200	5.1	300	3.3	0.5 (naphthalene)
1,4-Dimethyl-naphthalene	K&K	C	200	3.6	47	2.75	12
						7.0	4
1,8-Dimethyl-naphthalene	K&K	C	200	4.3	284	2.0	0.5
2,7-Dimethyl-naphthalene	K&K	C	200	3.1	92		0
Acenaphthene	K&K	C	200	4.5	250		0
		S	200	8.2	132		0
Acenaphthylene[c] (Tech)	MCB	C	200	5.0	608	2.25	1.5
						2.9	3.0
						4.5	140.
		S	200	7.4	182	4.6	12.
						8.0	35
Pyrazine	Aldrich	S	350	>10	0		0
		S	200	>10	0		0
		A[b]	225	~4.5	167	>20	0
		A	120	~5.9	>20	>9.0	0
Anthracene	Eastman	C	200	>30	0		0
		S	350	2.1	200		0
		S	200	>10	0		0
Pyrene	Eastman	S	350	3.1	258	3.0	0.5
4,5-Dihydro-pyrene (=1,2-Dihydro-pyrene)	K&K	S		2.49	270	2.68	220
						3.1	82 (pyrene)
Phenanthrene	K&K	S	350	2.08	348		0
		S	200	22	100		0
Benzo(g,h,i) fluoranthine	K&K	S	350	4.6	162		0
Chloroform	B&A	A	120	1	2020.		0
Acetophenone (practical)		A	225	~7	151	~4.0	0.5
Benzaldehyde	Eastman	A	225	~5	180	~2.5	0.2

[a]Retention time relative to $CHCl_3$ (= 1 unit)
[b]A = 10 ft Apiezon 220°C, C = 10 ft Carbowax, S = 10 ft SE-30
[c]Acenaphthylene partly decomposes at its boiling point (265-275°C)

Molecular rotation is defined by the equation

$$[m] = \frac{[\alpha]\ MW}{100} = \frac{\alpha\ MW}{\ell c\ 100}$$

where α is the observed rotation in degrees, $[\alpha]$ the specific rotation, MW the molecular weight, ℓ the pathlength in decimeters, and c the concentration in grams per cc. In this work the MORD values are normalized to a magnetic field of one gauss. Others have used 10,000 gauss to make magnetic molecular rotations comparable in size to natural molecular rotations. A program called DATCON was written to handle the data. A listing of the main part of DATCON is given in Appendix II. Those parts not listed are standard library programs available at the Lawrence Radiation Laboratory Computer Center. This program not only converts observed rotation to molecular rotation normalized to one gauss, but also makes corrections for the MORD of the solvent displaced. Experimentally, the MORD of each of the solvents was found to follow an equation of the type

$$\alpha = \frac{AH}{\lambda^2 - \lambda_h^2}$$

where λ is the wavelength, H is the magnetic field strength, and A and λ_h are experimentally determined parameters. (This is known as a single term Drude equation.) λ_h for ethanol is 1414 Å, and A is 5.96×10^3 deg. Å^2/gauss. For $CHCl_3$, λ_h is 1559 Å, and A is 8.24×10^3 deg. Å^2/gauss. Of course, the observed rotation of a solvent is directly proportional to the cell pathlength as well.

The amount of solvent displaced by solute can be calculate from the density of the solution. The densities of some dilute solutions of

interest in this work are available in the International Critical Tables and other reference books; however, no information could be found for many of the larger aromatic hydrocarbons studied here. These were assumed to have the same density in chloroform as naphthalene does (where concentrations are compared on a weight percent basis). The corrections were usually 2 to 5 millidegrees (only a little above the experimental error). But for certain concentrated solutions the correction was as large as 250 millidegrees. When the MORD of the compounds is discussed, it will be noted if a large correction was required. It will also be noted if the correction was made from available density data. Otherwise, the reader may assume the correction was small (slightly larger than the noise level, which will be indicated). Of course, any common deviation from identity will not affect the MORD noticeably if the correction was small to begin with.

The data can be smoothed by the program if the operator desires. This is accomplished by fitting the data to a polynomial of the desired order and covering the desired number of points. (For example, a third order polynomial was commonly used and 2 points on each side of the point of interest were fit to the polynomial.) The computer plots these points as diamonds (see Figure 18). The coordinate axes are labeled in the computer's notation where E 03 means 10^3 and E-03 means 10^{-3}.

The program also punches cards in a format suitable for use in a least-squares fitting program (a combination of Lawrence Radiation Laboratory's programs LSQ and VARMIT). The user must specify the function to which he wants to fit the data in a subroutine called TABLE. The TABLE's used in this work are listed in Appendix II.

V. RESULTS AND DISCUSSION

A. Spectral Characteristics of Aromatic Hydrocarbons

The polynuclear aromatic hydrocarbons considered in this work fall into two categories, 1) cata-condensed if no carbon atom is a member of more than two rings, and 2) peri-condensed if one or more carbon atoms belong to three rings. Certain absorption patterns are observed in the molecules in the cata-condensed group, even though individual molecules differ widely in size and structure. These patterns are classified and summarized in Table II.

Several different names have been given to each of the electronic absorption bands listed in the table. Clar[64] investigated the spectra of a large number of aromatic hydrocarbons and applied the designations α, p, β, and β' to the four prominent electronic transitions he observed. Coulson[65] used the methods of LCAO molecular orbital theory to predict the frequencies of the symmetry allowed transitions of linear aromatic hydrocarbons. His V_2, V_1, and V_4 bands correspond to Clar's α, p, and β bands. Platt, et al.[66] used a free-electron model to calculate the energy levels of cata-condensed aromatic hydrocarbons and introduced the nomenclature listed in the "Platt" column in Table II. Even the symmetry forbidden bands are given names in this system. Platt's nomenclature appears to be more general than the others and seems to be gaining wider acceptance, so it will be used whenever possible throughout this work.

The oscillator strengths listed are figures which are derived from the integrated extinction coefficients of all the vibrational bands of the electronic transition listed. The formula used is

$$F = 4.31 \times 10^{-9} \int \varepsilon dv$$

Table II. Characteristics and classification of aromatic hydrocarbon absorption spectra

Notation			Relative energy of transition	Oscillator strength f	Polarization	Intensity (log ϵ_{max}	Fine structure (vibration bands)	Symmetry species	
Platt	Clar	Coulson						D_{6h}	D_{2h}
^1L_a	p	V_1	^1L ^1B	~ 0.1	trans	3.9-4.3	5 or 6 diffuse bands	B_{1u}	B_{2u}
^1L_b	α	V_2	^1L_a, ^1L_b vary	~ .005	long	2.3-3.5	5 or 6 sharp bands	B_{2u}	B_{1u}
^1C_a			Probably	0.3-0.8	major symm axis	4.2-4.7	none (?)	forbidden	forbidden
^1C_b			$B_b < C_b < B_a < C_a$	0.4-1.4	major symm axis	4.0-4.7			
^1B_a	β'		^1B_b ^1B_a	0.5-3.0	trans	3.9-4.5	1 strong, 2 or 3 weak bands. Increasingly sharp with length	E_{1u}	B_{2u}
^1B_b	β	V_4		0.5-3.0	long	4.7-5.5 proportional to length			B_{1u}

where ε is the molar extinction coefficient and ν is the frequency in cm^{-1}. Although there is some variation in the oscillator strength of a given type of band on going from one compound to another, Klevens and Platt[67] have noted that there are similarities in the intensities of the ^1L_a bands in a number of cata-condensed aromatics of widely different structure. The ^1L_b bands are also similar and have intensities roughly an order of magnitude greater than ^1L_a bands. The ^1B_a and ^1B_b bands are stronger yet, as can be seen from the table. These intensity relationships help in assigning an unknown band to the proper class.

Each allowed type of transition will show maximum absorption for light polarized in a certain direction but will absorb very little light having a polarization perpendicular to this. Group theory specifies what these directions are with respect to the symmetry of the molecule. These polarizations are listed in Table II as longitudinal (in the direction the molecule is longest), or transverse (the short direction) for molecules having the conjugated rings in line. The directions cannot be specified with such certainty for bent molecules like phenanthrene.

All of the molecules considered here fall into one of the point groups[68] D_{6h}, D_{2h}, D_{3h}, C_{2v} or C_S. Appendix III gives the character table of each of these groups. They show the symmetry operations are possible and list the irreducible representations for each group. For those unfamiliar with group theory, it is sufficient to note at this point that representations labeled A or B correspond to non-degenerate electronic states, and those labeled E are doubly degenerate.

It is rather easy to assign the p and β bands of the observed spectra of cata-condensed aromatic hydrocarbons. The α bands are weak and are

sometimes hidden by the stronger p bands. C bands are symmetry forbidden in centro-symmetric molecules.

Most of the characteristics given above apply to peri-condensed molecules, but not with as much regularity. The same nomenclature applies and the same point groups cover the peri-condensed systems. It seems best to describe their other features on an individual basis later.

B. Benzene

Garner, Nutt, and Labbauf[69] have measured the MORD of benzene between 3500 and 2500 Å. This included only the first band of the ^1L_b transition. Our measurements (Figure 18) extend to 2400 Å and include two other bands (practically all of the ^1L_b electronic transition). Our data agree with Garner, Nutt, and Labbauf's to within their experimental error, after their solvent rotation has been subtracted.

Several points should be made about Figure 18 and similar figures which are to follow. The graphs were made by a computer and the axes are labeled in its exponential notation (i.e., 2.70E+03 = 2.70×10^3 and 3.0E-02 = 3.0×10^{-3}). The absorption spectra on the bottom of the graphs are sketched in by hand from the strip chart record of the sample's optical density as measured on a Cary 14 spectrophotometer. The concentration and pathlength for the absorption measurement are the same as for the MORD, and are listed in Appendix II under the experiment number (193 for benzene). It seemed better to present the actual optical density of the sample rather than the extinction coefficient of the compound, so that the reader could evaluate for himself the meaningfulness of the MORD where absorption is high. Other authors have seldom done this, and the reliability of their results cannot be estimated in certain cases where the optical density appears to be far too high for accurate measurement

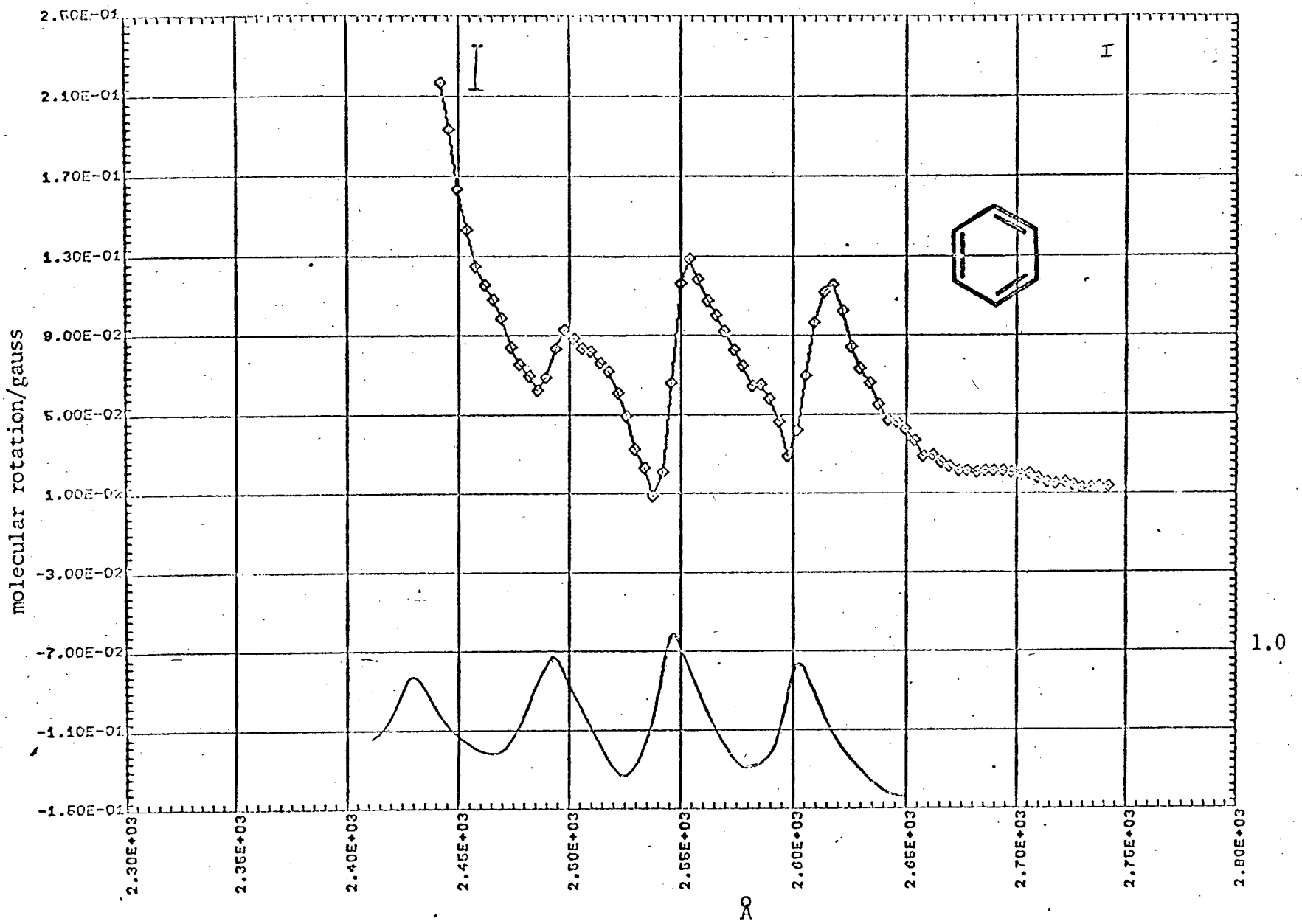

Fig. 18. MORD of benzene, top curve. Sample O.D., bottom curve.

of rotation. The MORD curve has been corrected for the MORD of displaced solvent and smoothed by the computer. The minimum and maximum RMS noise levels are indicated at the wavelength at which they occur. Figure 19 indicates what the noise for Figure 18 would look like before digitizing and smoothing.

The electronic transition in the 2500 Å region of the benzene spectrum is assigned as the ^1L_b transition on the basis of a very large amount of theoretical and experimental work.[70] The symmetry of the excited state is $^1B_{2u}$ so the transition is non-degenerate. It is symmetry forbidden but becomes partially allowed through vibrations of e_{1u} or a_{2u} symmetry. Each of the bands in the solution spectrum shown in Figure 18 is composed of at least 10 vibrational bands, which can be resolved more clearly in the vapor phase spectrum.[71] When the 10 bands are broadened so they merge (as in the solution spectrum) their sum has a rather asymmetric shape, as can be observed from Figure 18.

The next electronic transition is centered at about 2020 Å in solution and is approximately 50 times as intense as the previously discussed ^1L_b band. Both excited electronic states are non-degenerate, but the next higher one at 1830 Å is probably degenerate. It is about 350 times as intense as the ^1L_b band.

The quantum mechanical prediction is that the bands of a vibrational progression in a symmetry forbidden-vibronically allowed transition (such as the ^1L_b band of benzene) will be found to have MORD of each vibrational band with "the same shape . . . varying in magnitude in the same way as the components of the absorption band."[56] This does not apply rigorously to he ^1L_b band because it probably gets its intensity from more than one

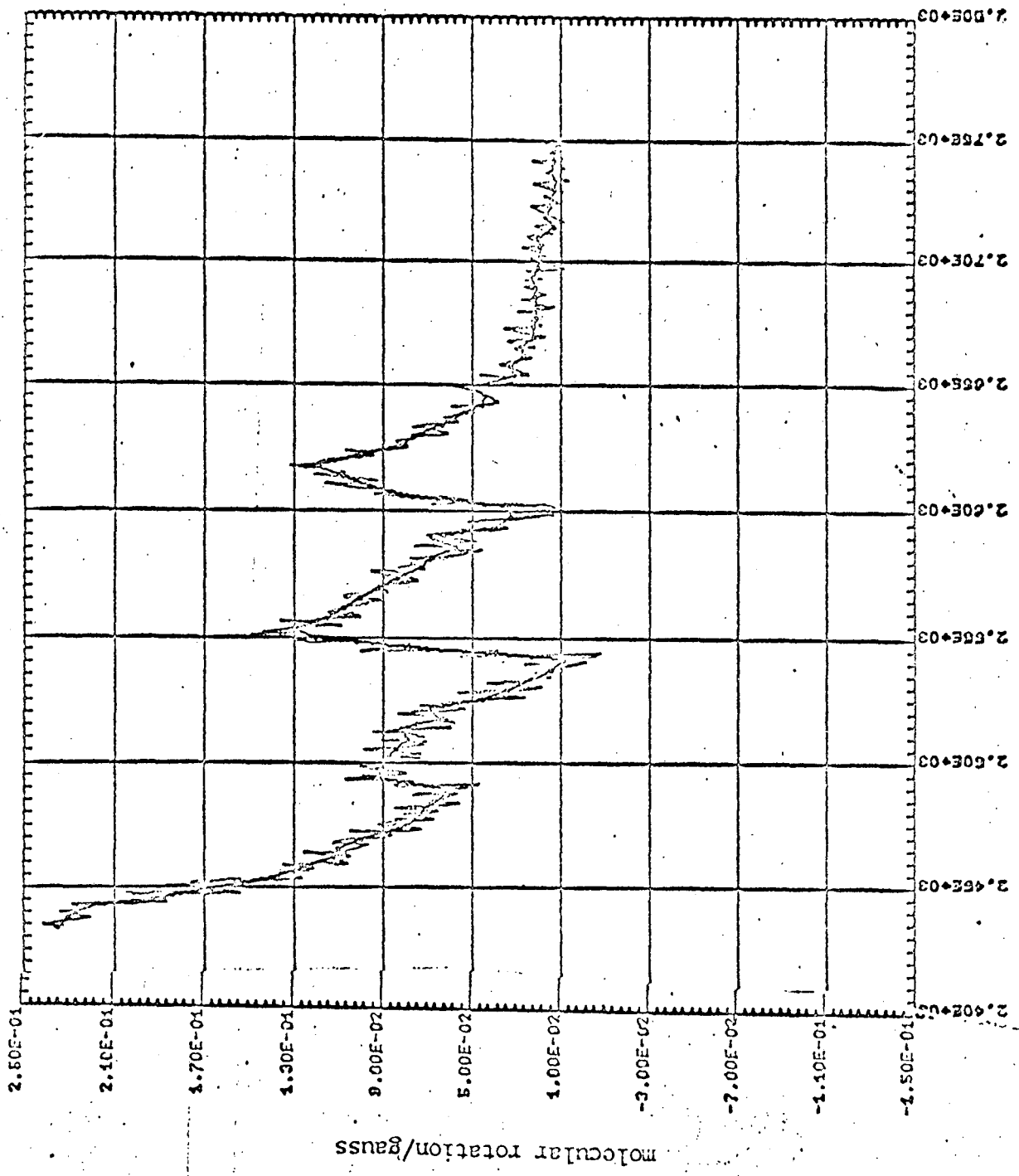

Fig. 19. MORD of benzene showing instrument noise level.

type of vibration. Nevertheless, it can be seen from Figure 18 that the size of the MORD anomalies are reasonably well proportioned to the intensities of their associated absorption bands. The anomalies also have the frequency dependence of the B term in the quantum theory, as they should if they are non-degenerate.

The two foregoing statements have been demonstrated by decomposing the curve from 2630 Å to 2500 Å into three overlapping parts. Each has the frequency dependence of a B term:

$$[m] = \frac{B_{oa}\omega^2(\omega_{oa}^2 - \omega^2)}{(\omega_{oa}^2 - \omega^2)^2 - \omega^2\Gamma_{oa}^2} \qquad (61)$$

with the following values for the parameters.

Table III. Parameters for fitting benzene MORD from 2630 Å to 2500 Å

ω_{oa} (cm^{-1})	λ_{oa} (Å)	Γ_{oa} (cm^{-1})	$B'_{oa} \times 10^4$
38370	2610	225	4.7
39273	2544	238	7.8
40176	2494	88	2.9
41143	2432	1003	87.

These values are the result of the least squares fitting computer program (Appendix II) applied to 18 evenly spaced points (wavelength) on the interval of interest. The last set of parameters (with ω_{oa} = 40107 cm^{-1}) was outside the interval and so does not truly indicate the size and shape of any one band. It functions solely to estimate the Drude tail resulting from all the other bands in the UV. 4 bands comprised of

The quality of the fit is indicated by $\Sigma\chi^2$ (the sum of the squares of the deviations) which is 5×10^{-4}. A more pictorial idea of the fit

is obtained from the computer "Y Graph", Figure 20.

Stephens[55] has calculated the expected MORD of the ^1L_b band of benzene and finds the value of the B term is less than 10% as large as the experimental values of this work and the work of Garner[63] indicate. A number of drastic assumptions must be made in calculating the MORD of forbidden bands, and the poor agreement should not be too discouraging.

C. Pyrene

We consider pyrene next because its characteristics lend themselves to a quantitative evaluation of the B_{oa} quantum mechanical term. The observed MOR in the 3700 Å region is approximately ten times as large as that of the 2500 Å benzene bands, but the extinction coefficient of pyrene is much less than that of benzene for the bands under consideration. This allows relatively concentrated solutions to be used, thus increasing the observed rotation. The corrections for solvent displacement are significant--about 0.025 deg. at 3500 Å. This is shown converted to molecular rotation/gauss in Figure 21.

The peak-to-trough MOR of pyrene is greater than of any other compound studied when samples are measured at equal optical densities. One possible quantum-mechanic explanation for this would be that the transition moments of nearby bands have perpendicular polarizations so the energy denominator is small. This has indeed been found to be the case in work independent of these studies. Bree and Vilkos[73] observed the polarized absorption and fluorescence of pyrene molecules substituted in a fluorene crystal lattice. They found the 3720 Å and 3670 Å bands to be polarized perpendicularly to all other transitions above 2800 Å. From their data it is not clear that any of the bands have purely one

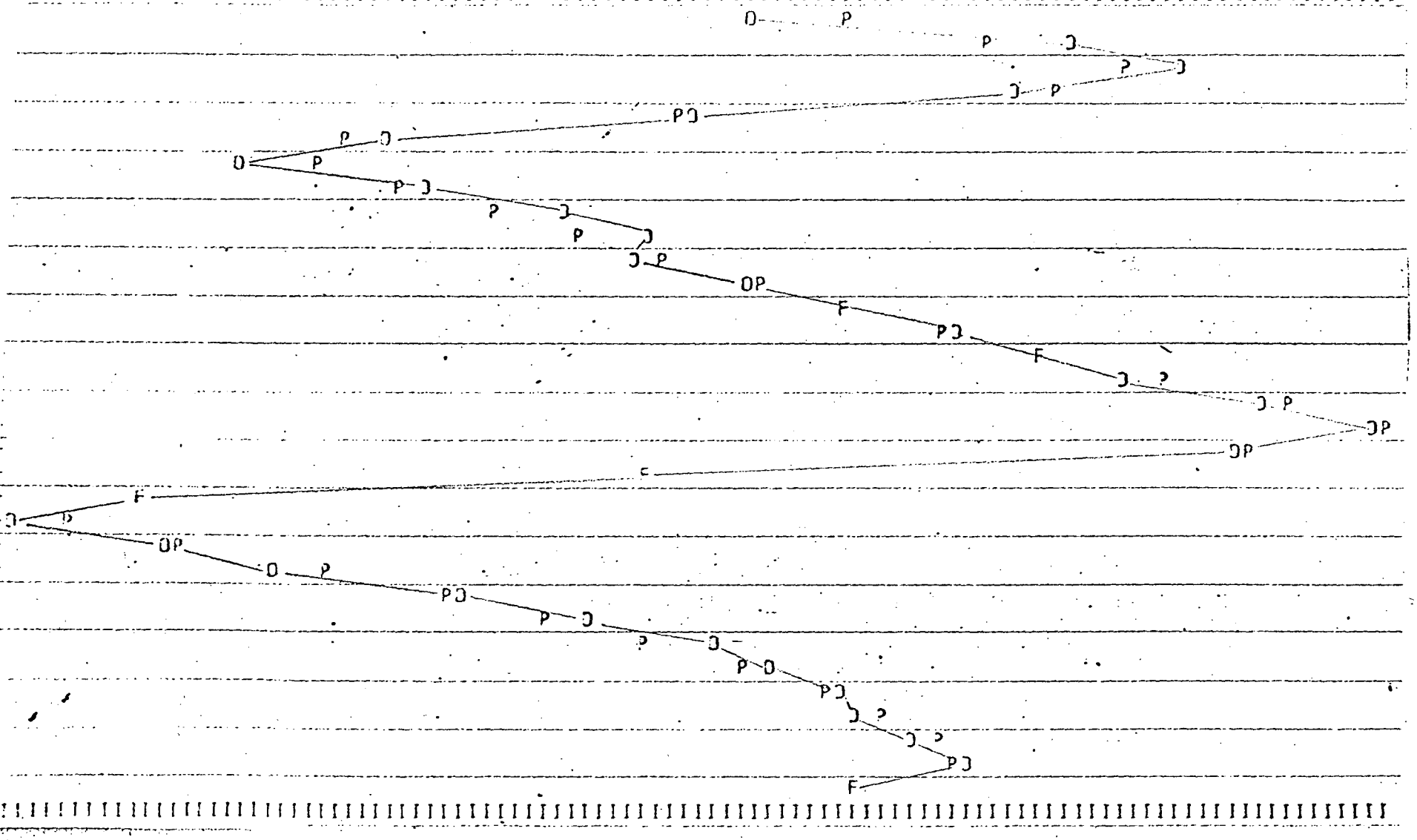

Fig. 20. Computer Y Graph for benzene. O = data point; P = computed point; F = coincidence of data and computed points.

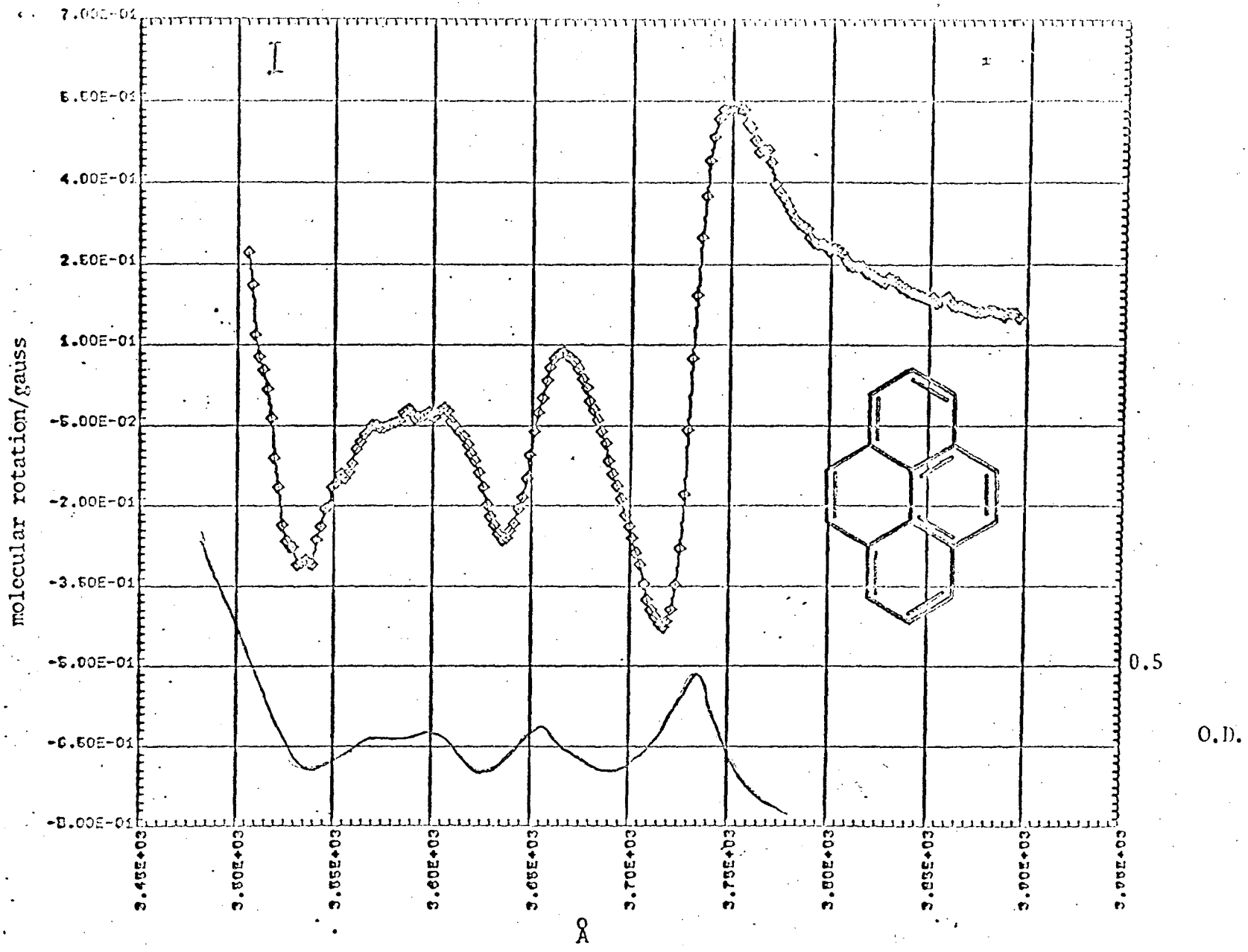

Fig. 21. MORD of pyrene, upper curve. Sample optical density, lower curve.

polarization--all seem to have 10 or 20% of the intensity in some other polarization. But it is possible from their curves and the oscillator strengths they give to estimate the transition moments of a given polarization for any of the long wavelength bands of pyrene (3800-3450 Å). These and other values needed to calculate B_{oa} for the 3720 Å band are listed in Table IV.

To calculate the expected MORD of pyrene we note that only the B_{oa} term will be non-zero in equations (36) - (38), because pyrene has D_{2h} symmetry. In order to calculate the value of B_{oa} the only spectral quantities we need in addition to the transition moments mentioned previously are the values of m_{ab}, the magnetic dipole transition moments between the excited states of interest. In pyrene these are all perpendicular to the plane of the molecule, but their value is somewhat hard to estimate. We now discuss Bree and Vilkos'[73] assignment of the long wavelength spectrum as background for the estimation of the magnetic transition moments.

The fluorescence and absorption of the 3720 Å band coincide, so it is assigned as a 0-0 band (0 vibrational level of the ground state to 0 vibrational level of the B_{2u} excited state). Succeeding bands correspond to higher vibrational excitations of the excited state, having both types of in-plane polarizations. Because of its greater intensity, the 3500 Å band is assigned as a transition to another excited electronic state, and its polarization was observed to be perpendicular to that of the 3720 Å band.

The part of the B_{oa} term with the small energy denominator gives rotation ϕ as:

$$\phi = \frac{4\pi}{hc} N_a^o \quad 1/3 \ \mathrm{Im}\left[\sum_b{}' \frac{\underline{\mu}_{oa} \cdot \underline{\mu}_{ob} \times \underline{m}_{ab}}{\omega_{ab}}\right] \frac{\omega^2(\omega_{oa}^2 - \omega^2)}{\omega_{oa}^2 - \omega^2)^2 + \omega^2 r_{oa}^2} \tag{64}$$

$$= B'_{oa} \frac{\omega^2(\omega_{oa}^2 - \omega^2)}{(\omega_{oa}^2 - \omega^2)^2 + \omega^2 r_{oa}^2} \tag{65}$$

where a is the first excited state (the one giving rise to the 3720 Å band in this case), b is another excited state (taken here as all of the states up to 3420 Å which are polarized perpendicularly to the 3720 Å band). N_a^o is the number of molecules per ml in the ground state, $\hbar$ is Plank's constant divided by 2π, and c is the velocity of light in vacuum.

Using the values in Table IV, we find that $B'_{oa} = 5.7 \times 10^{-3}$. Upon decomposing the MORD of pyrene into bands having the frequency dependence of equation (65), we obtain the value 9.9×10^{-3}. The agreement is very good, but of course we had considerable latitude in the choice of the magnetic dipole transition moments. They were selected on the basis that a fully allowed magnetic transition would be 1.0 Bohr magneton and that those of interest would be allowed only to the same extent as the associated vibrationally allowed electric dipole transitions.

The values of B'_{oa} calculated from the decomposition of the experimental MORD of pyrene are listed in Table V. The band with the second longest wavelength has the same polarization as the 3720 Å band, but about one-third the oscillator strength. We would expect B'_{oa} for this term to be $1/\sqrt{3}$ (i.e., 0.5) that of the 3720 Å band; in actuality, it is 0.55--again in very good agreement. The decomposition of such a complicated curve as Figure 21 is unfortunately not unique, so one must avoid placing too much confidence in the values given. The quality of the fit is indicated by the Y graph in Figure 22.

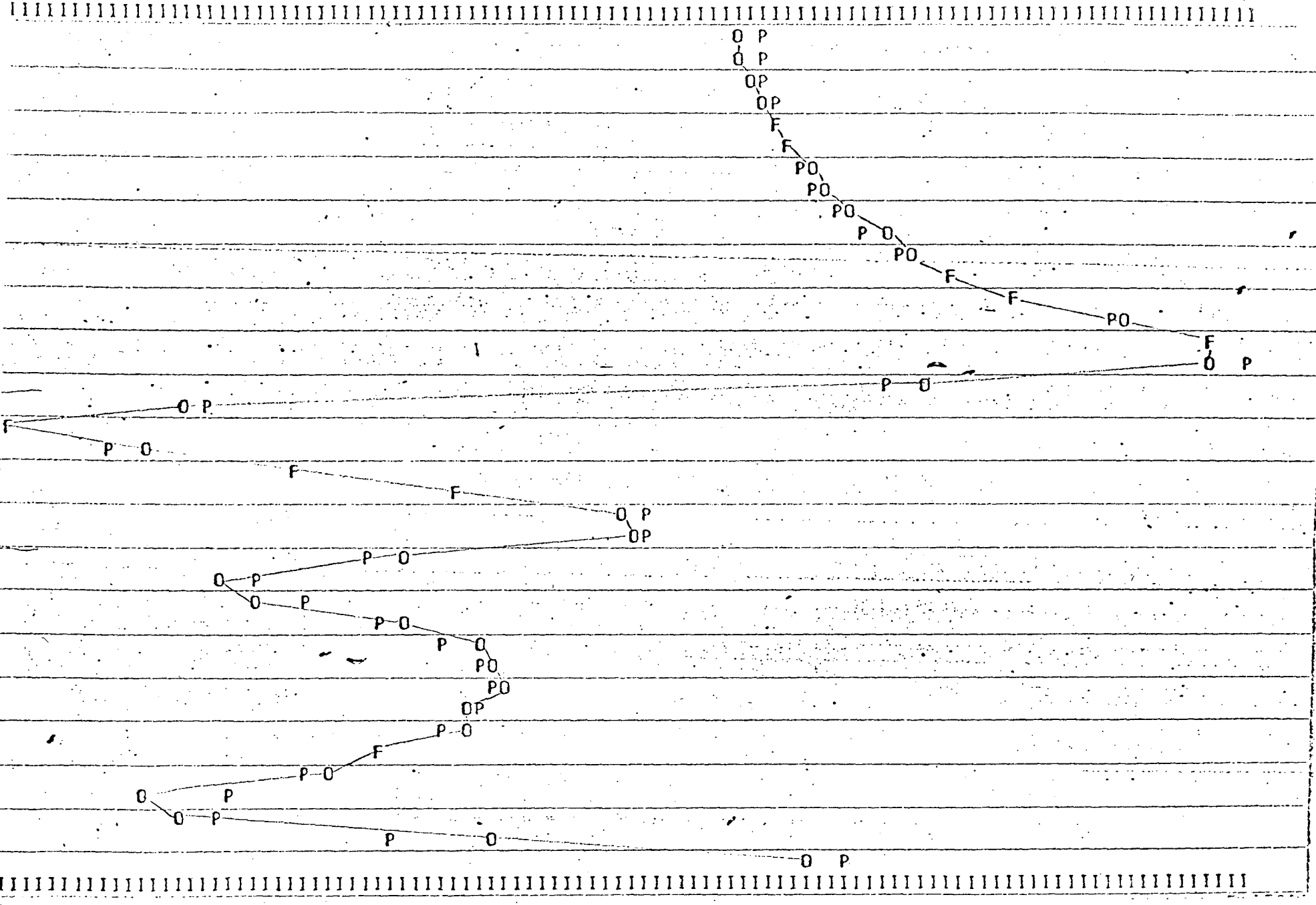

Fig. 22. Y Graph of pyrene MORD. O = data point; P = computed point; F = coincidence of data and computed points.

Although the foregoing calculations and comparisons do not "prove" the quantum mechanical theory to be correct, they certainly demonstrate one case where it explains MORD well in a quantitative sense. It appears that we are justified in placing confidence in predictions based on the B_{oa} term, and we will make repeated use of this in the discussion of the remaining aromatic hydrocarbons whose MORD has been measured.

Table IV. Parameters for calculation of B_{oa} for the 3720 Å transition of pyrene

ω_{ob} cm^{-1}	ω_{ab} cm^{-1}	$\lvert\mu_{ob}\rvert \times 10^{9}$ cm	$\frac{\lvert\mu_{oa}\rvert\lvert\mu_{ob}\rvert \times 10^{22}}{\omega_{ab}}$	m_{ab} (estimated) Bohr Magnetons
27300	550	.07	.32	.01
27500	750	.1	.33	.01
27880	1130	.14	.31	.01
28280	1530	.1	.16	.01
28690	1940	.83	1.05	.04
29100	2410	.62	.65	.04
29200	2450	.74	.75	.04

$\omega_{oa} = 26750\ cm^{-1}$ $\quad \lvert\mu_{oa}\rvert = .25 \times 10^{-9}$

D. Naphthalene and Derivatives

The ^1L_a, ^1L_b and ^1B_b bands are easily discernible in naphthalene. The energies and intensities of these transitions have been calculated.[67] MO and free electron calculations, including limited configuration interaction, predict experimental results rather well. The currently accepted assignments are given in Table VI. Longitudinal polarization is parallel to the long axis of the molecule; transverse is perpendicular to this but still in the plane of the carbon atoms.

Table VI. Absorption bands of naphthalene

Transition	Polarization	λ_{max}, Å	log ε_{max}
$^1L_b \leftarrow {}^1A$	Longit.	3120	2.40
$^1L_a \leftarrow {}^1A$	Trans.	2860	3.62
$^1B_b \leftarrow {}^1A$	Longit.	2210	4.98
$^1B_a \leftarrow {}^1A$	Trans.	1690	--
$^1C_b \leftarrow {}^1A$		1900	--

The MORD of naphthalene is somewhat more complicated than that of benzene because of the difference in the sizes of the vibrational bands. It can be seen from Figures 23 and 24 that the MORD bands appear to merge and it is very difficult to separate out the contribution of each of the bands observed in the solution absorption spectrum. Nevertheless, the MORD is decreasing rapidly at the wavelengths of maximum absorption for each band, which indicates the MORD arises from the quantum mechanical B'_{oa} term, and that this term is positive, as it was in benzene. This is

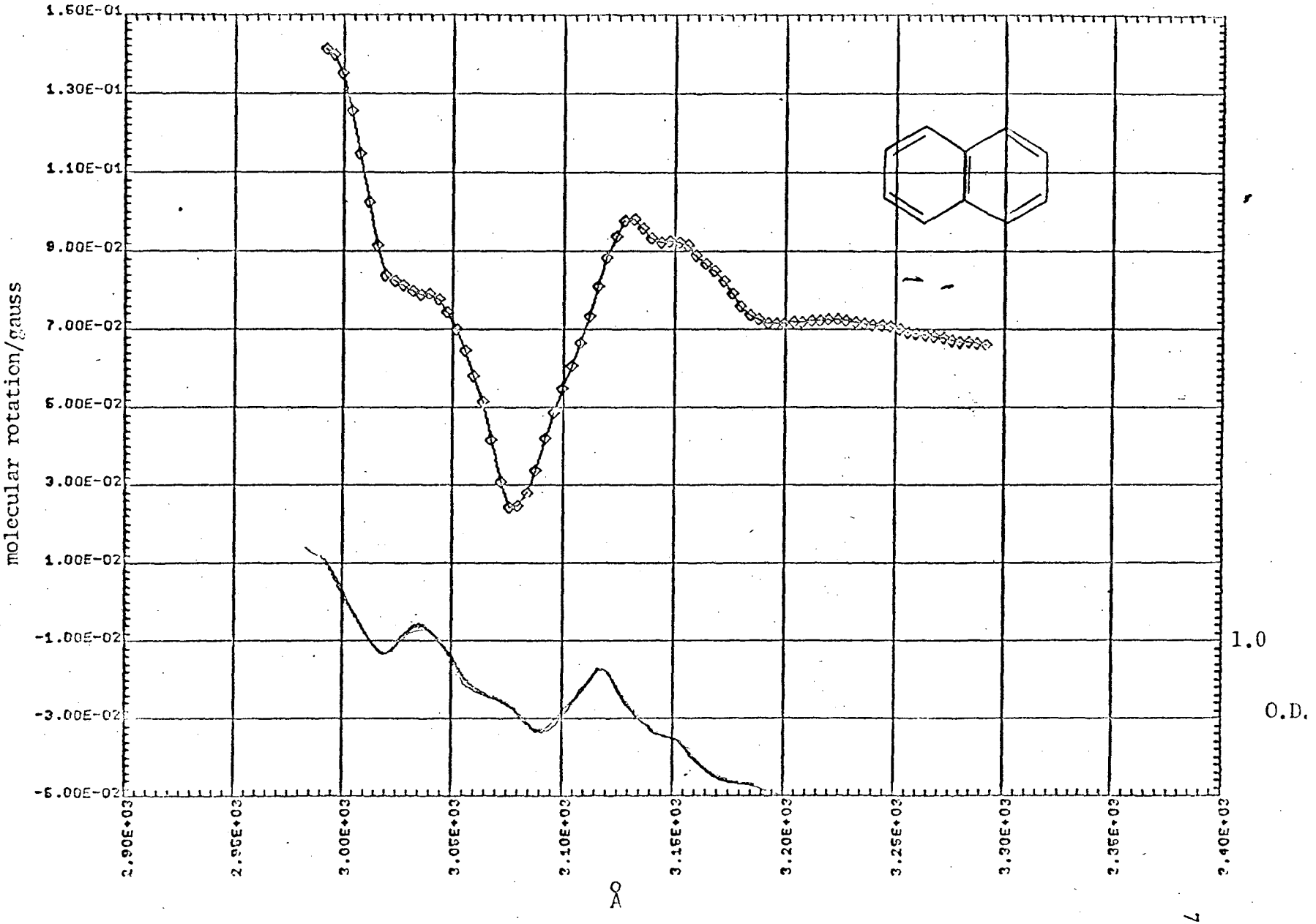

Fig. 23. MORD of Naphthalene, upper curve. Sample optical density, lower curve.

expected since no degeneracies are predicted for molecules such as naphthalene which have D_{2h} symmetry.

The MORD of several dimethyl derivatives of naphthalene (IX) was measured (see Figures 23 to 28) and all were found to have larger rotation than the parent hydrocarbon in the region of the ^1L_b band (3120 Å in naphthalene). This is not surprising because methyl substitution in positions

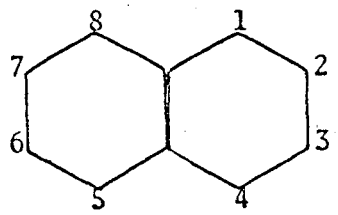

V

equivalent to 1 in the structure above, enhances the absorbance of the ^1L_a band and substitution in positions equivalent to 2 enhances absorption by the ^1L_b band.[73] The transition moments of each of these bands enter into the B_{oa} term for the MORD of the ^1L_a band, so as they increase, the observed MORD would be expected to increase.

It will be noticed that the MORD of the ^1L_b band of 2,7-dimethylnaphthalene is negative, while that of naphthalene and the other dimethylnaphthalenes is positive. This cannot be explained strictly on the basis of the destruction of the D_{2h} symmetry of naphthalene, becasue 1,8-dimethylnaphthalene lowers the symmetry in exactly the same way that 2,7-dimethylnaphthalene does, and the 1,8 compound can be seen to have rotation of the same sign as naphthalene. But the symmetry of the vibration giving rise to the long wavelength band in the 2,7 compound may be different from that in the other dimethylnaphthalenes shown.

The absorption spectrum of acenaphthene is very much like that of naphthalene except there is less vibrational structure and the extinction

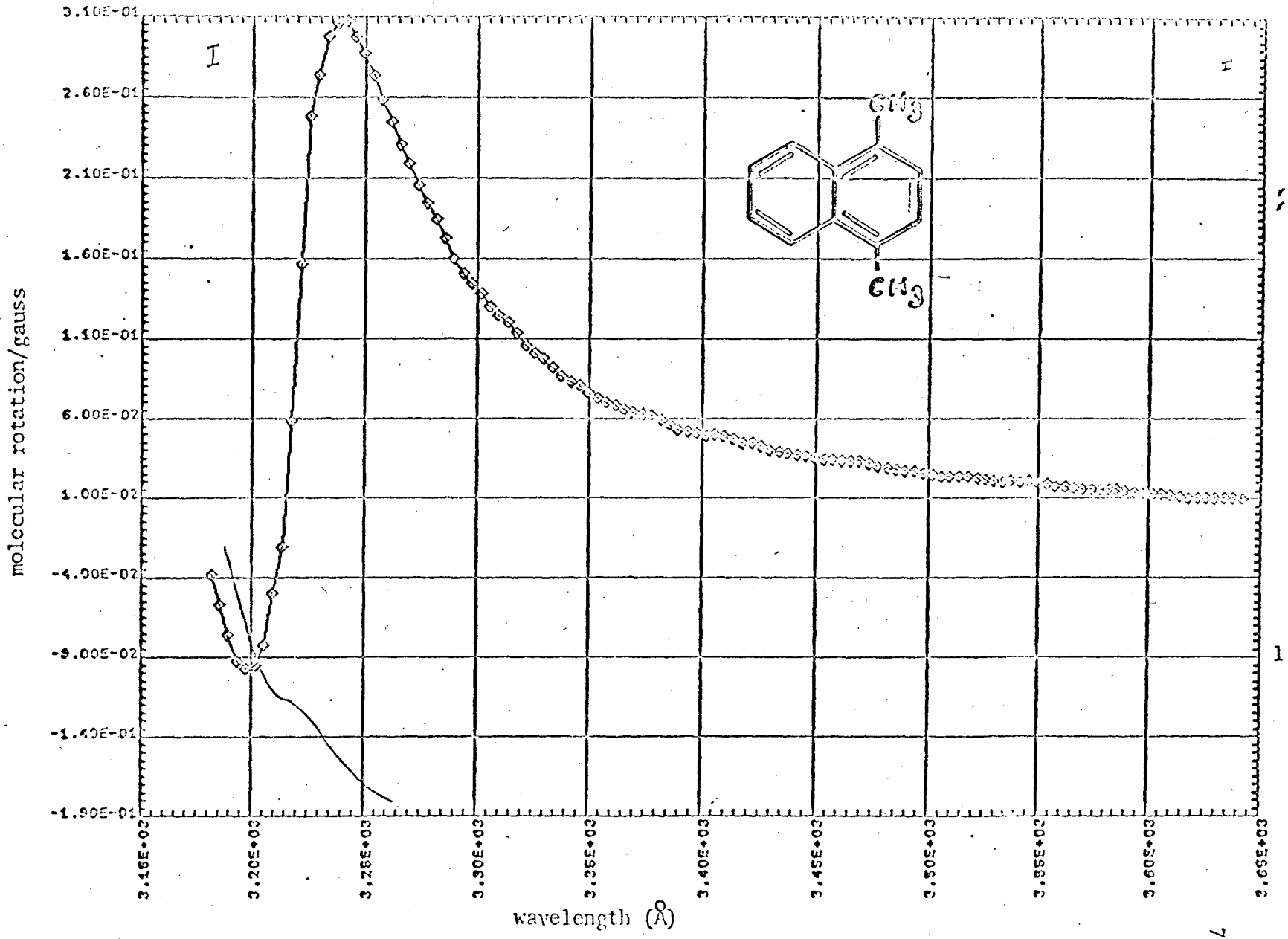

Fig. 25. ORD of 1,4-Dimethylnaphthalene, upper curve. Sample optical density, lower curve.

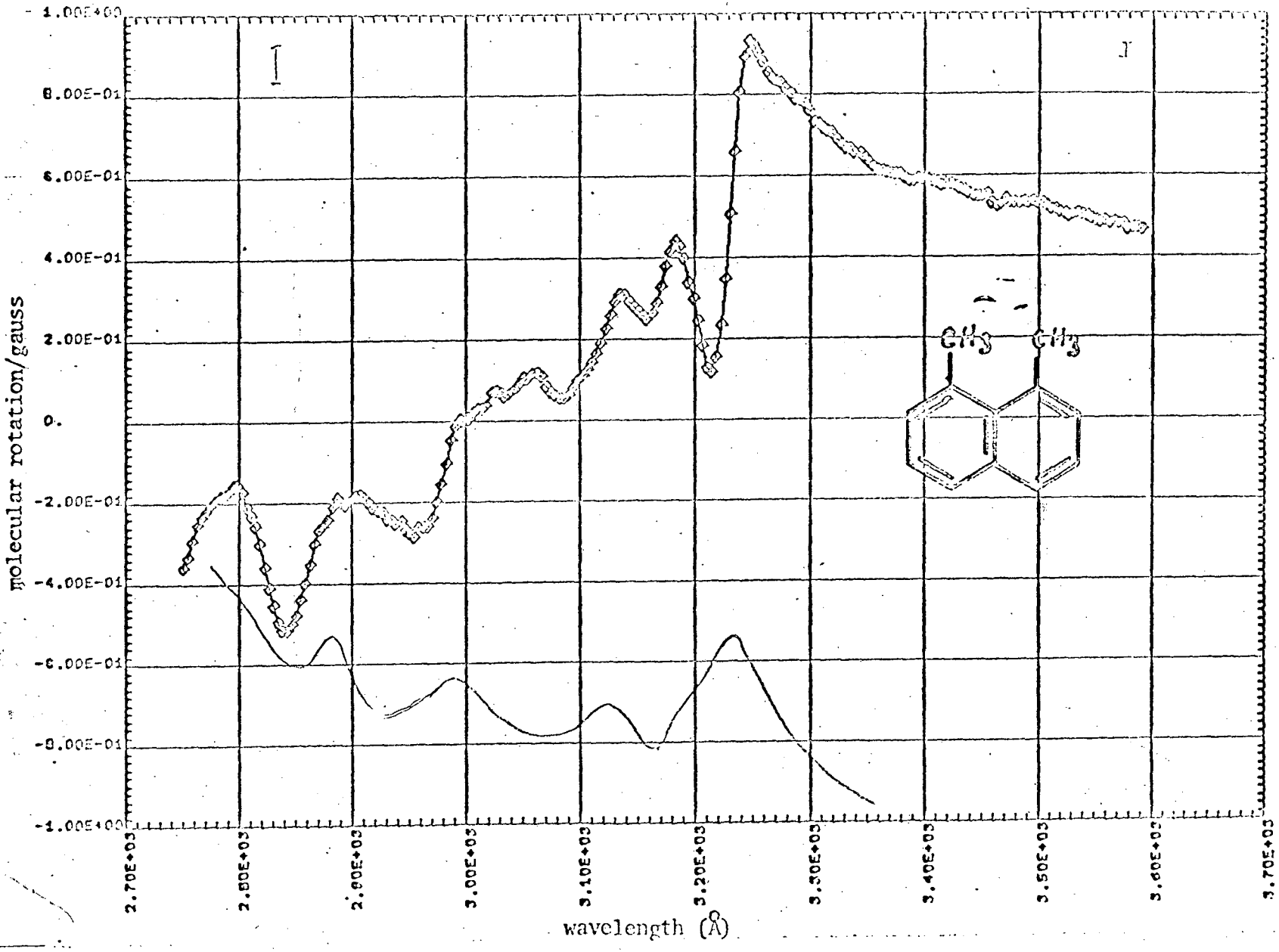

Fig. 26. MORD of 1,8-Dimethylnaphthalene, upper curve. Sample optical density, lower curve.

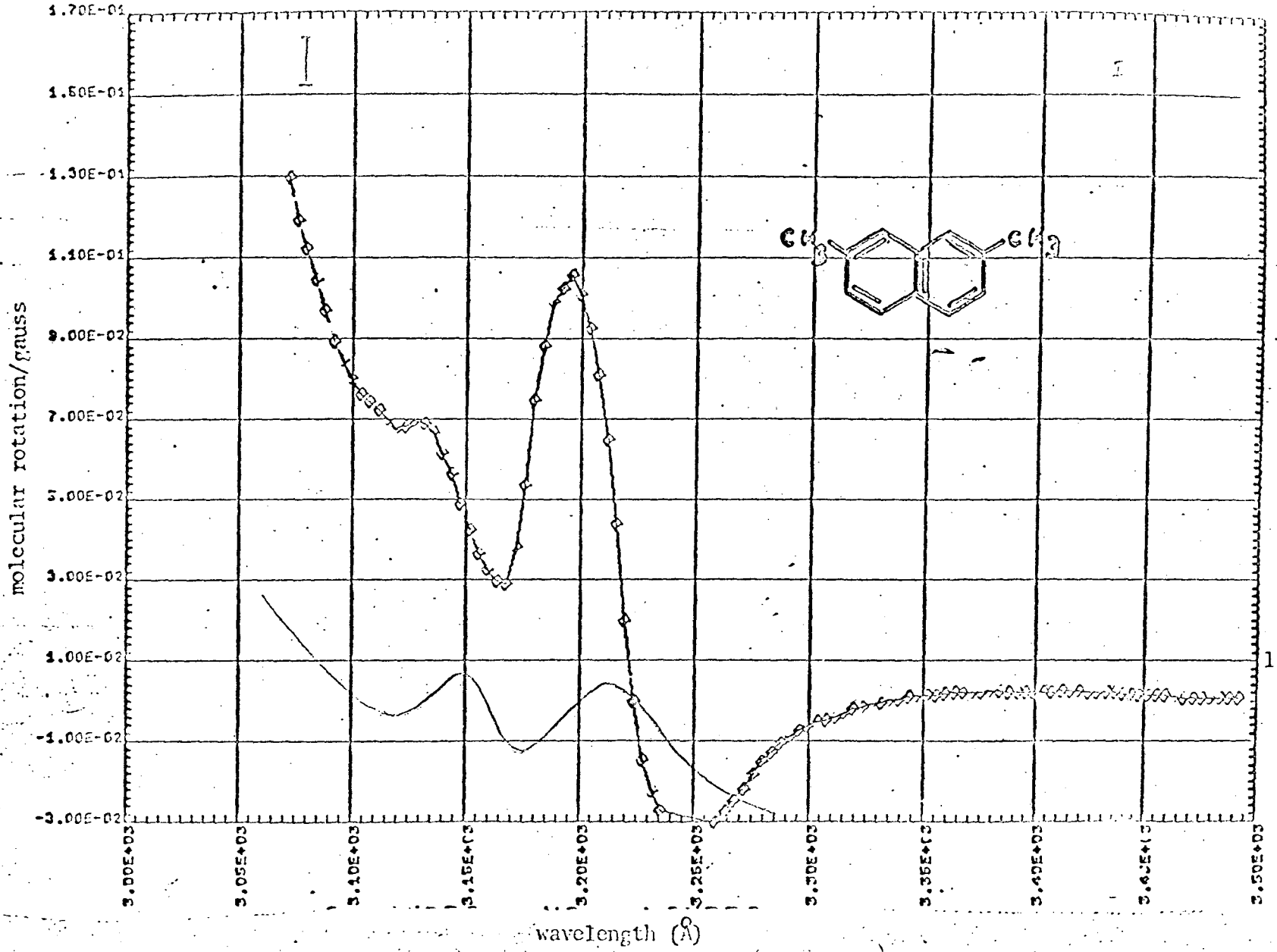

Fig. 27. MORD of 2,7-dimethylnaphthalene, upper curve. Sample optical density, lower curve.

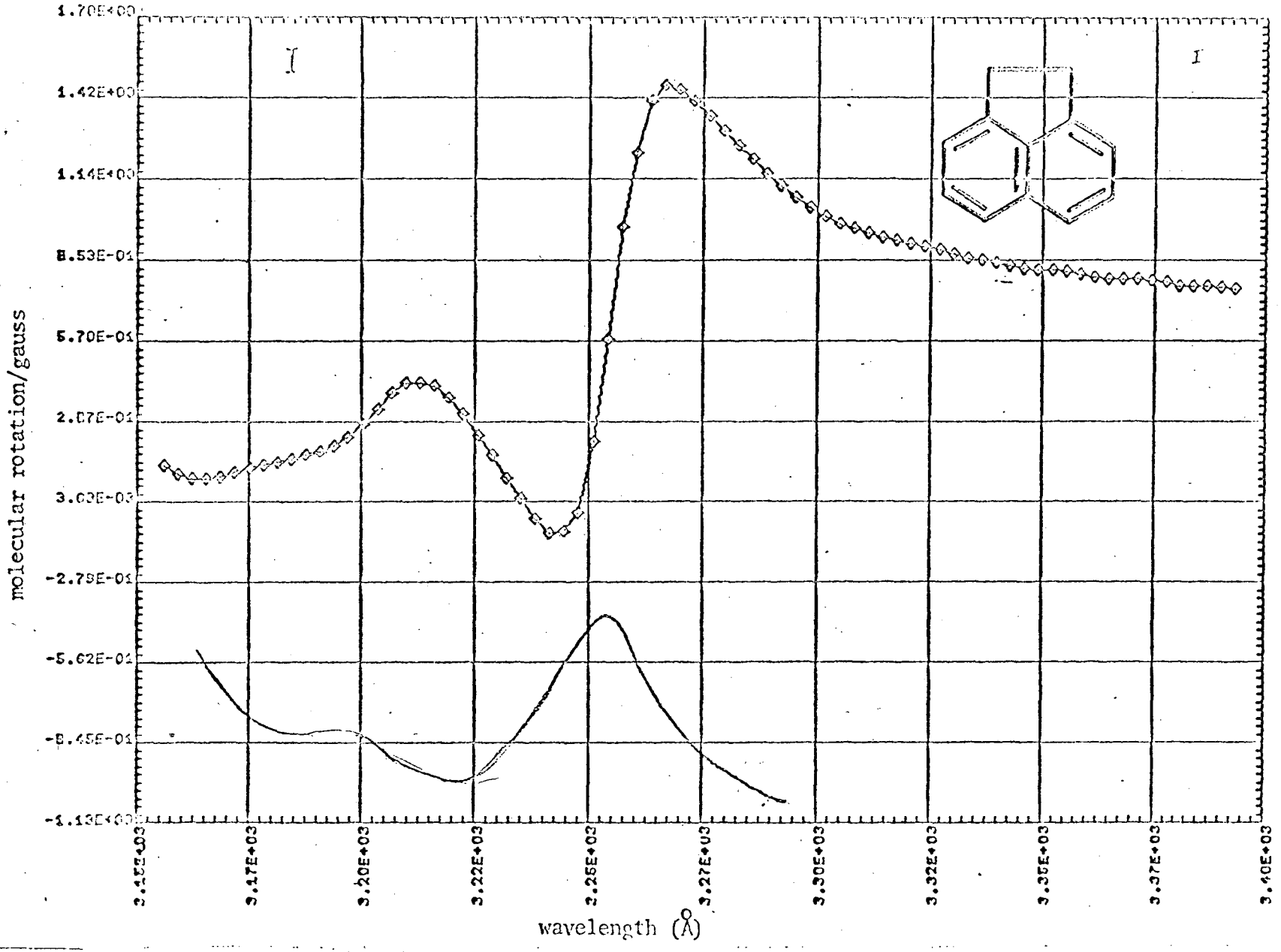

Fig. 28. MORD of Acenaphthene, upper curve. Sample optical density, lower cuver.

coefficient of the ^1L_b band is about ten times greater in acenaphthene. This band is also shifted to longer wavelengths by about 90 Å. The MORD (Figure 28) is somewhat larger but has the same general features as naphthalene through the first absorption band.

However, in acenaphthylene (Figure 29) the shape of the MORD curve is drastically different. The pi electron network here has true C_{2v} symmetry, and not the D_{2h} or perturbed D_{2h} of naphthalene and the derivatives previously discussed. No meaningful comparisons can be made--only note taken of the drastic change of MORD resulting from the addition of a pi bond to the acenaphthene framework.

It should also be mentioned that the large positive peak in the acenaphthylene MORD is characteristic of two closely spaced bands with nearly equal but opposite rotational strengths. The absorption spectrum indicates that the prominent band is single (with shoulders), but the MORD indicates that this band is composed of two closely spaced bands belonging to different vibrational modes or having different electronic excited states. The latter condition is necessary for the bands to have rotational strengths of opposite sign.

E. Anthracene

The set of five bands cetered at 3500 Å in the absorption spectrum of anthracene have been assigned as the ^1L_a electronic transition. The band whose maximum is at 2530 Å is taken to be the ^1B_b, but no one claims to have observed the ^1L_b bands seen in other linear polynuclear aromatic hydrocarbons. Theoretical calculations predict it to be in the neighborhood of 3400 Å.[74,75]

Foss and McCarville[76] claim to have found evidence of the ^1L_b band through the use of magnetic circular dichroism. All of the MCD bands

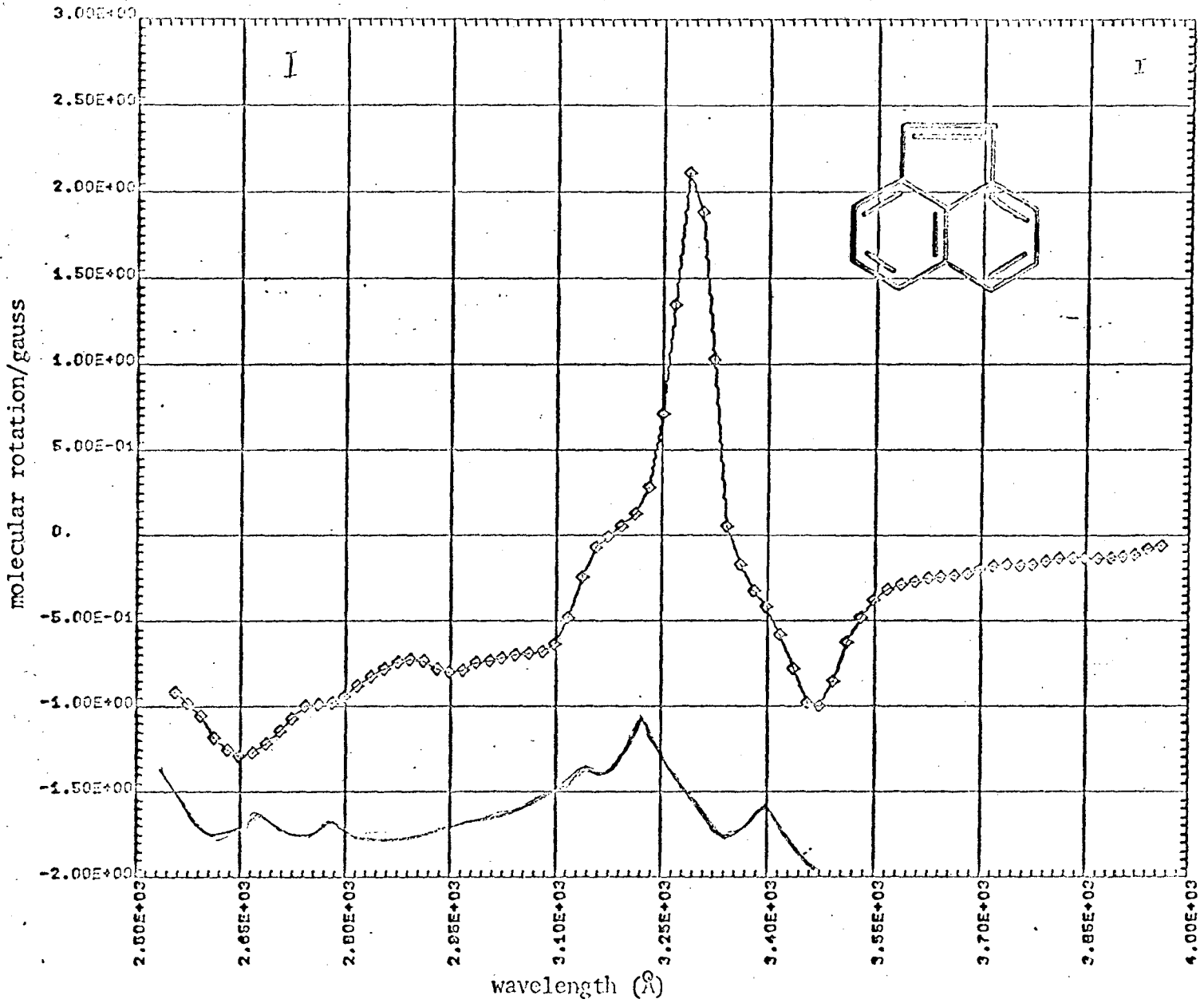

Fig. 29. MORD Acenaphthylene, upper curve. Sample optical density, lower curve.

but one between 4000 and 3000 Å have positive rotational strengths. The negative band is found at 28000 cm^{-1} (3570 Å) and is taken to be the ^1L_b band of anthracene. The MORD measured in this laboratory (Figure 30) qualitatively confirms the MCD measured by Foss and McCarville. The positive MORD peak at 3570 Å can be decomposed into two curves having the frequency dependence of the quantum mechanical B_{oa} term. The parameters for this are given in Table VII, and the Y graph in Figure 31. The results do not correspond exactly to those of Foss and McCarville, whose negative dichroism appears to have larger magnitude than the positive. In addition, the separation between their bands is indicated to be at least 150 cm^{-1}, while that obtained from decomposition of the MORD is about 30 cm^{-1}.

If the MORD peak at 3570 Å really has the frequency dependence of a pair of B_{oa} terms and not that of an A_{oa} term (with similar shape), it should be possible to separate the B_{oa} type components if the bands can be made sufficiently narrow, whereas an A_{oa} term would maintain its same general shape for very narrow bands. The bands of aromatic hydrocarbons are known to become more narrow at lower temperatures, so the MORD of anthracene in ethanol was measured at -60°C. The peak was observed to broaden slightly as if it would split at yet lower temperatures. The troughs on each side of the peak did not change position and the magnitude of the rotation did not increase by a factor of 1.3 as it would for a C_{oa} term. (The magnitude of C_{oa} terms is proportional to 1/T.) This supports the notion that the 3570 Å MORD peak results from a pair of adjacent B_{oa} type curves.

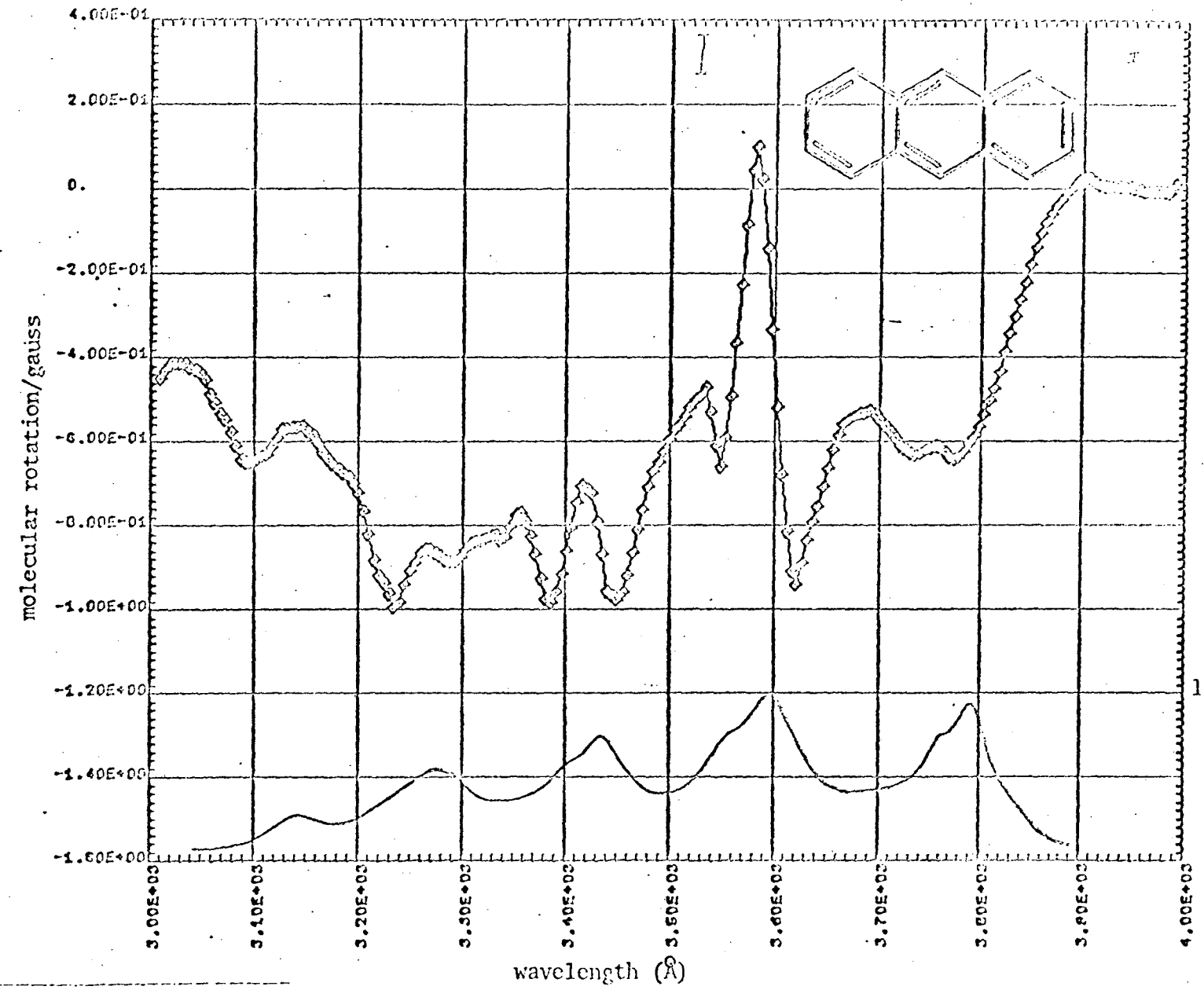

Fig. 30. MORD of anthracene, upper curve. Sample optical density, lower curve.

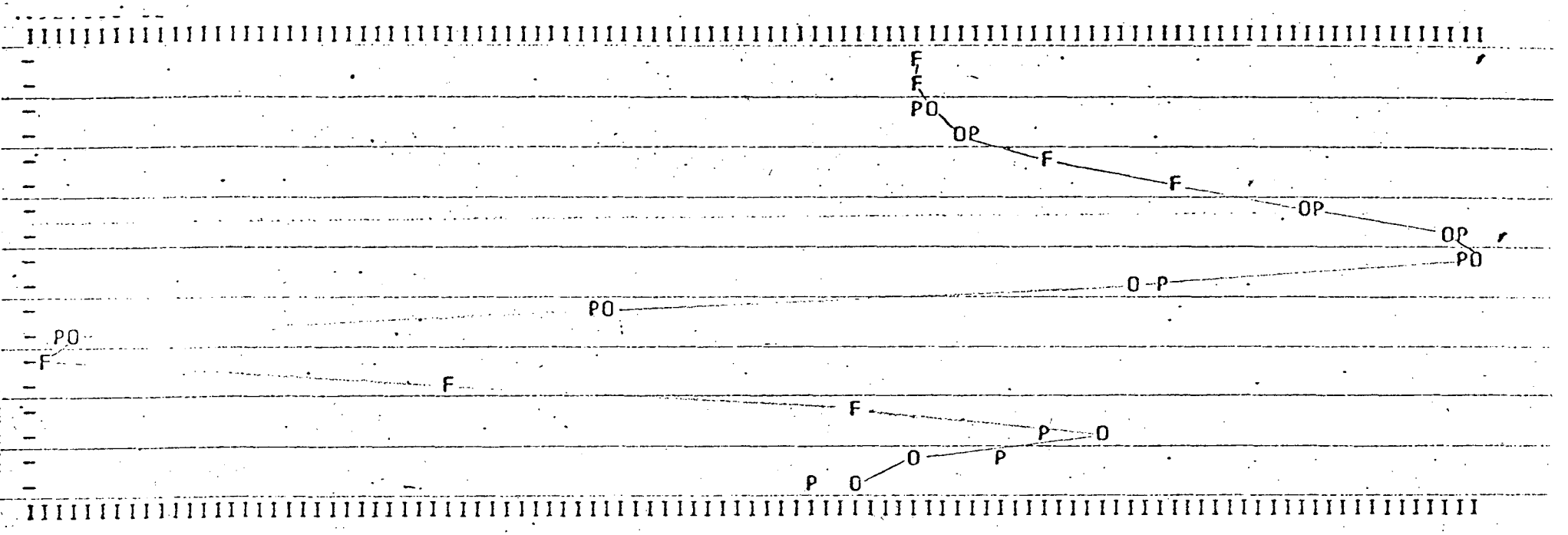

Fig. 31. Anthracene Y Graph. O = data point; P = calculated point; F = coincidence.

For an allowed transition such as the ^1L_a (major transition in the 3000-4000 Å region), the excited vibrations to which transitions are allowed all are completely symmetric and would give MORD curves of the same sign. Therefore, the negative rotational strength of the 3595 Å band must arise from an excited electronic state other than the ^1L_a. On the basis of the foregoing evidence the obvious choice for this band is the ^1L_b. This demonstrates how MORD and MCD can be useful in revealing absorption bands hidden by intense absorption from nearby transitions if the two transitions have different excited electronic states.

Table VII. Parameters for fitting 3570 Å MORD peak of anthracene

ω_{oa} cm^{-1}	λ_{oa} Å	Γ_{oa} cm^{-1}	B'_{oa} deg
27036	3699	58.4	$+5.3 \times 10^{-4}$
27816	3595	596	-1.95×10^{-1}
27848	3590	727	$+2.62 \times 10^{-1}$
28205	3545	1506	-1.38×10^{-1}

F. Singlet-Triplet Transitions

Shashoua[77] stimulated considerable interest in the Faraday effect by reporting results that indicated the MORD of singlet-triplet transitions was large and easily observable. Much of his work bearing on singlet-triplet transitions proved to be erroneous, however. In this study we attempt to reevaluate the Faraday effect as an aid in the study of a few well documented singlet-triplet transitions.

An excellent review covering singlet-triplet transitions recently appeared in Chem. Rev.[78] and the reader is referred to it for information on the nature and implications of singlet-triplet transitions.

In this study MORD was measured in a 0.5 cm cell at 5320 gauss. The spectral slit width was less than 20 Å. Table VIII gives further pertinent data on the samples. It will be noticed that only pyrazine shows any inflection in the region of the S → T assignment. (An inflection is here defined as a deviation from the sloping tail of the MORD of transitions at shorter wavelengths.) Inflections smaller than about 0.010° would not have been seen in the benzaldehyde and acetophenone spectra, but .002° would have been detected in the p-benzoquinone and .004° in the glyoxal. These results indicate that the singlet-triplet MORD is nonexistent or very small for all the compounds except pyrazine in Table VIII.

Snowden and Eberhardt[79] have observed the magnetic rotation spectrum of pyrazine in the same wavelength region as that observed here. In their experiment, polychromatic light is passed successively through a polarizer, a 70 cm cell filled with pyrazine vapor in a longitudinal magnetic field, a polarizer oriented at 90° to the first, and then into a spectrograph. The light is stopped by the second polarizer unless it has been rotated by the sample. When rotation occurs the spectrograph plate shows darkening at the position corresponding to the appropriate frequency. By slightly changing the angular orientation of one of the polarizers and performing the experiment again, it is possible to determine from the resulting spectrograph record in which direction the magnetic rotation

Table VIII. MOR of some singlet-triplet transitions

Compound	Concentration	Solvent	Approx. % total impurities	Wavelength range of observation	MORD
Benzaldehyde E.K. chlorine free	undiluted liquid	none	<0.5%*	3800-4100 Å	large† positive rotation no inflections
Acetophenone E.K.	undiluted liquid	none	<0.5%*	3700-3950 Å	large† positive rotation no inflections
Pyrazine Aldrich lot 073031	3 M	$CHCl_3$	<0.05%*	3450-4000 Å	large† positive rotation (maximum = 0.45° at 3700 Å)
	saturated	5:1 methylcyclohexane-isopentane	<0.05%*	3400-4000 Å	moderate positive rotation (maximum = 0.054° at 3660 Å)
p-Benzoquinone twice recrystallized from EtOH	.07 M	5:1 methylcyclohexane-isopentane		6000-4000 Å	small positive rotation no inflections
Glyoxal E.K. Tech	30%	H_2O		6000-4000 Å	small positive rotation no inflections

*By comparison of areas of VPC trace (10 ft. Apiezon column).

†A few tenths of a degree.

has occurred. But the "intensity-direction of rotation" information thus obtained is much more difficult to interpret than analogous information from MORD which gives directly the amount of rotation. At any rate, Snowden and Eberhardt see magnetic rotation at the wavelengths of the established singlet-triplet transition of pyrazine (3600-3750 Å).[80]

The absorption bands are greatly broadened in going from the vapor phase into solution. This greatly decreases the amplitude of the observed rotation, as can be seen from the amplitude factors in Figure 8, where Γ is the band width. It is thus not surprising that effects seen clearly in the vapor phase magnetic rotation are not at all obvious in the MORD of solutions.

None of the theories of the Faraday effect indicate that a singlet-triplet transition should have especially large or distinctive MORD. They do predict that the MORD will be proportional to the singlet-triplet transition moment, which is usually very small. It is not, therefore, surprising that little, if any, rotation due to singlet-triplet transitions was observed in the compounds studied here. More success might be achieved in an MORD apparatus where large magnetic fields could be maintained over pathlengths long enough to achieve optical densities near one in the wavelength region of the weak singlet-triplet transitions. But at present it appears that MORD instrumentation is not developed highly enough to permit successful study of singlet-triplet transitions.

G. Aggregated Dyes

Sauer[81] has found that solutions containing chlorophyll dimers have ORD that is much larger and qualitatively different from chlorophyll monomer solutions. It seemed possible that aggregates of non-optically active dyes would have different MORD than dye monomers, and that the MORD may provide information about the geometry and/or degree of association of dye molecules.

Two dyes were studied in detail. They were methylene blue and proflavin. Both are known to aggregate in water solution as the dye concentration is increased. These two were chosen because they show large changes in the fraction of dye aggregated through concentration ranges where accurate MORD measurements can be made with the cell pathlengths available.

The maximum molar extinction coefficient is 4000 for the 4700 Å band of a 9.55×10^{-4} percent solution, but only 2700 for a 7.96×10^{-2} percent solution.[82] These values are for solutions at 25°C. From the value of the equilibrium constant[82] (500 ℓ./m) it can be seen that the dilute solution contains practically no dimer, but in the concentrated solution over 90% of the proflavin is dimerized.

Solutions of the above concentrations were made up in .05 M, pH 4, acetate buffer, and their MORD measured. The dilute solution was run in a 1.0 cm cell at 2200 gauss, from 7000 to 3300 Å. The MORD was less than the experimental noise level (0.001 deg.). No rotation was observed for the concentrated solution either (after the MORD of the displaced solvent was subtracted). This solution was run in a 0.1 mm cell at 8300 guass over the same wavelength range. A sample of intermediate

concentration (7.96×10^{-3} percent) was also run in an 0.1 mm cell at 8300 gauss. Again, no rotation was observed.

In another experiment the MORD of methylene blue in water was measured. The concentrations (in terms of monomer before aggregation) were 2×10^{-5} M and 10^{-3} M. The absorption spectra of the two solutions were markedly different, indicating aggregation. The first solution had a 0.63 OD peak at 6620 Å and a 0.34 OD shoulder at 6120 Å (in a 1 cm cell). The second solution had only a shoulder at 6620 Å (0.3 OD) and the main peak was at 6070 Å (0.5 OD). No MORD was observed for this solution; however, the dilute solution showed about +0.002 deg. rotation at 6100 Å which decreased to zero at both 7000 Å and 5000 Å.

No other dye with extinction coefficient and dimerization equilibrium constant suitable for MORD study was found. From these measurements MORD does not appear to be of value in studying aggregation. It should be noted, however, that neither of the monomers studied had measureable MORD. This in itself is unusual. Perhaps for compounds showing monomer MORD, the Faraday effect will be useful in studying aggregation.

H. Charge-transfer Complexes

The MORD of several charge-transfer complexes was investigated in hopes that MORD would yield information on one of the following properties of the complexes:

1) The nature of the charge transfer electronic transition
2) The geometry and degree of the association between donor and acceptor
3) The perturbation of the electronic states of the components as a result of the association

A description of the MORD of five liquid charge-transfer systems is listed in Table IX along with the experimental conditions. It can be seen from the table that the observed rotations were very small. It therefore seemed unprofitable to include the curves in this work. Only the pyrene-iodine complex can be said unequivocally to show a Faraday effect in a charge-transfer band. The observed rotation in the first three systems could be attributed to the MORD of the displaced solvent. The DMSO-TCNE system has a small rotation, but it is in the opposite direction from the displaced solvent correction, so it is probably real. The freshly formed complex has an appreciably populated triplet state (as evidenced by EPR[83]) which decreases to less than 10% of its original population in 20 min. The MORD was measured 1 and 20 min after preparation of the complex, and no difference in rotation was detected.

Of the components listed in the table, only pyrene and iodine have MORD different from a gentle, monotonic curve in the wavelength intervals investigated. The MORD of the pyrene was not changed in the solutions investigated, but that of the iodine may have been. The charge-transfer band in the pyrene-iodine-CCl_4 system is near the iodine absorption, and it is difficult to tell if the changed MORD is from the charge-transfer band or the perturbed iodine absorption.

It should be noted that the optical density of the first two samples was low. The combination of low solubilities, limited optical pathlengths, and low extinction coefficients for these charge-transfer bands precluded the use of higher optical densities, where more sensitivity could be attained. Solubility is seldom a problem in complexes where the donor or acceptor is also the solvent, as in the third and fourth

Table IX. MORD of Charge-transfer Complexes

Donor	Acceptor	Solvent	K(ℓ/m)	λ_o	Sample OD	Magnetic field (kilogauss)	Wavelength range covered	Amplitude of MORD	Ref
Hexamethyl-benzene VII sat.	TCNQ VIII sat.	Acetonitrile	26.3		0.15	5.3	4350-6500 Å	Too small to be measured	84
Pyrene XI 8×10^{-4}	Chloranil X sat.	$CHCl_3$	2.24	6100 Å	0.15	7.2	4500-6800 Å	.013° to .050° 6800-4500 Å	85
Mesitylene	TCNQ[a] VIII	Mesitylene			~1.0	8.0	4000-6000 Å	Too small to be measured	86
DMSO[b]	TCNE[c] VIII sat.	DMSO[b]	95.4	3720 Å	~1.5	7.2	2800-5100 Å	.005° broad negative peak at ~4100 Å. No rotation above 4400 Å or below 3600 Å.	83
Pyrene XI	Iodine	CCl_4		~5100 Å	>2.0	8.1	6500-3550 Å	Negative Cotton effect at ~5600 Å. Peak to peak amplitude ~.010.	84

[a]TCNQ = 7,7,8,8-tetracyanoquinonedimethan

[b]DMSO = dimethyl sulfoxide

[c]TCNE = tetracyanoethylene

systems listed. In theory, it should be possible to go one step further and measure the MORD of charge-transfer crystals. This was attempted, but results were not reproducible. For most complexes, the crystals are so dark that even rather finely ground crystallites transmit too little light for accurate MORD measurements. It may be possible, however, to obtain accurate measurements of suspended crystallites if one chooses the right complexes and suspending media.

Symmetry arguments show that the Faraday effect is not forbidden in the charge transfer complexes studied, if one assumes the charge-transfer transition moment is directed between the centers of the two component molecules, as Mulliken's theory indicates. This is demonstrated in the following way for the HMB-TCNQ complex:

Assume the plane of the HMB (VII) is parallel to that of the TCNQ (VIII) and that one molecule is directly over the other. Taken

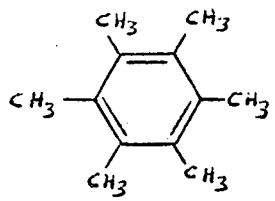

VII

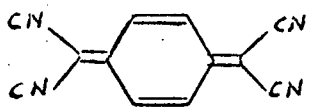

VIII

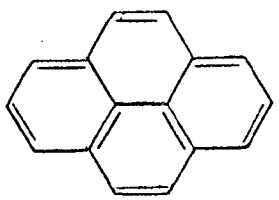

IX

together, the pair has C_{2v} symmetry, and of the quantum mechanical terms for the Faraday effect, only the B_{oa} term could be non-zero. We will use symmetry arguments to show that under certain conditions B_{oa} can be non-zero if a is the charge transfer excited state.

According to Mulliken's formulation,[87] μ_{oa}, the transition moment of the charge-transfer absorption band, will be directed from the center of one component molecule to the center of the other. Call this the x direction. The allowed electronic transitions in each individual

component molecule are polarized either in the y or z direction. Let their exicted states be labeled by b's. From the character table for C_{2v} (Appendix III), it can be seen that each μ_{ob} must have either B_1 or B_2 symmetry, whereas μ_{oa} will have A_1 symmetry. If we take the ground state of the molecule to be totally symmetric the excited states will have the same symmetry as their corresponding transition moments. We can now see from the symmetry of the a and b excited states that m_{ab} will belong to the same irreducible representation as μ_{ob}. From the character table it can be seen that if μ_{ob} is z polarized, m_{ab} will be y polarized, and conversely. Thus, the three transition moments in the first part of the B_{oa} term (equation (37)) will be perpendicular to one another, so they will not vanish on symmetry grounds. Similar arguments show the same to be true for the second part of the B_{oa} term. Extension of the argument to D_{2h} and C_2 symmetry yields the same result. This means that the Faraday effect in the charge-transfer bands of the complexes studied is not predicted to be zero on symmetry grounds. It should be noted that the DMSO-TCNE complex is not as likely to fit the symmetry groups mentioned as the other complexes are. Also, it has been assumed that the iodine is in the plane of the pyrene molecule. The pyrene-iodine complex can still be classified as having either D_{2h} or C_{2v} regardless of which ring or how many rings are filled by iodine.

A factor likely to make the B term smaller for charge-transfer bands than for the normal absorption bands of aromatic hydrocarbons is the energy denominator, ω_{ab}. The charge-transfer bands are usually separated further in energy from adjacent bands than are normal transitions. ω_{ab} would be proportionately larger and the B term smaller.

The large band width, Γ, of charge-transfer bands also adds to the difficulty of observing their MORD. The maximum amplitude of the MORD is proportional to $1/\Gamma$ (see Figure 8) and this factor is at least ten times smaller for CT bands than for similar bands in most uncomplexed aromatic hydrocarbons.

Although the observed MORD of charge-transfer bands was too small to measure or interpret with accuracy, it seems possible on theoretical grounds that success in this area can be attained as better instrumentation for MORD and MCD is developed.

VI. CONCLUSIONS

The present high level of spectropolarimetric instrumentation can be utilized in connection with permanent magnets to measure the Faraday rotation of solutions. In this work, it was possible to make measurements from 2400 Å to 7000 Å, but with a little more effort it should be possible to extend the short wavelength limit to that of the instrument (1850 Å). The measurements can be made to ±0.001 degrees under favorable conditions. Magnetic field strengths up to 12,500 gauss have been attained for solution path lengths of 1.0 mm. It appears impossible to achieve fields of greater than 15,000 guass with permanent magnets, but, of course, super-conducting magnets promise many times this field strength. With the permanent magnets used here the sample can be cooled to approximately -140°C, or, in principle, warmed to the point where the permanent magnet loses its magnetism.

The MORD of the near UV transitions of several aromatic hydrocarbons is presented and shown to be in harmony qualitatively with what recent quantum mechanical theories predict for such compounds. It is possible to get reasonable qualitative agreement between theory and experiment for pyrene where certain necessary experimental parameters can be found in the literature. Considerably more experimental work must be done to adequately verify other parts of the theory, particularly those applying to molecules of high symmetry. The methods developed in this work should adequately handle the experimental part of verification, as should those developed for magnetic circular dichroism. But the expected MORD of other molecules must be calculated, and this may prove the most difficult part of the verification.

On the basis of the MORD of a few chemical systems it is shown that the Faraday effect will probably be of limited value in the study of molecular aggregation, singlet-triplet transitions, and charge-transfer complexes. The availability of more sensitive instruments and/or considerably higher magnetic fields may reverse this outlook, since on theoretical grounds it has not been shown that any of the systems may show significant Faraday rotation. In fact, it is shown that many charge-transfer complexes should have Faraday activity on the basis of group theory and Mulliken's model of the charge-transfer complex. The nature of the complexes makes MORD hard to measure, however.

It appears that the primary use of the Faraday effect in the study of aromatic hydrocarbons will be in revealing electronic transitions which are hidden in absorption spectra by other stronger, nearby electronic transitions, and in making spectroscopic assignments. As more confidence is gained in the quantum mechanical theory, it may be possible to study magnetic dipole transition moments by means of the Faraday effect.

A strictly empirical approach to the interpretation of the observed MORD of aromatic hydrocarbons does not appear profitable. The MORD of similar compounds show such drastic differences that comparisons can be misleading. Theory must be invoked to make experimental results meaningful. On the other hand, theorists have complained of a lack of experimental data for use in the guidance of their efforts. It is hoped that close cooperation between theorists and experimentalists will soon bring the Faraday effect to its full usefulness in chemistry.

Note: AA and XLAMO are used in making the correction for the MORD of the displaced solvent. See the program DATCON in Appendix II for the way it enters into the calculation.

EXP. NO. 174 COMPOUND PYRENEINSTCHECK
SOLVENT CHCL3 TYPE OF MEASUREMENT MORD TEMP +26C
SPEC. SLIT WIDTH 20A TIME CONSTANT 1
MAG. SET 2 DATE 10/9/66 EXPERIMENTER JMT

THE 2 CURVES WERE ADDED WITH SIGNS OF
-1 1
AND THE NUMBERS OF THE EXPERIMENTS WERE, RESPECTIVELY -
174 179
4944O VOLTS ON CARD = FULL SCALE PEN DEFLECTION
1.62E+00 = FACTOR FOR OBS ROT TO MOLEC ROT
1.05000E+02 1.55900E+03 = AA AND XLAMO
.1000 CM PATH,12370 GAUSS, 5.00000E-02 MOLES/LITER

EXP. NO. 185 COMPOUND ANTHRACENE
SOLVENT CHCL3 TYPE OF MEASUREMENT MORD TEMP 26C
SPEC. SLIT WIDTH 12A TIME CONSTANT 3
MAG. SET 4 DATE 8/13/66 EXPERIMENTER JMT

THE 2 CURVES WERE ADDED WITH SIGNS OF
1 -1
AND THE NUMBERS OF THE EXPERIMENTS WERE, RESPECTIVELY -
185 -0
4944O VOLTS ON CARD = FULL SCALE PEN DEFLECTION
8.24E+01 = FACTOR FOR OBS ROT TO MOLEC ROT
1.06000E+00 1.55900E+03 = AA AND XLAMO
.1000 CM PATH,12140 GAUSS, 1.00000E-03 MOLES/LITER

EXP. NO. 193 COMPOUND BENZENE
SOLVENT ETOH TYPE OF MEASUREMENT MORD TEMP 126C
SPEC. SLIT WIDTH 0A20A TIME CONSTANT 1
MAG. SET 1 DATE 65 EXPERIMENTER J THORNE

THE 2 CURVES WERE ADDED WITH SIGNS OF
-1 1
AND THE NUMBERS OF THE EXPERIMENTS WERE, RESPECTIVELY -
19300 -0
4944O VOLTS ON CARD = FULL SCALE PEN DEFLECTION
9.09E+00 = FACTOR FOR OBS ROT TO MOLEC ROT
2.31000E+00 1.41400E+03 = AA AND XLAMO
1.0000 CM PATH, 2200 GAUSS, 5.00000E-03 MOLES/LITER

EXP. NO. 201 COMPOUND ACENAPHTHENE 340
SOLVENT CHLC TYPE OF MEASUREMENT TEMP MOI
SPEC. SLIT WIDTH +26CC TIME CONSTANT A2
MAG. SET OA DATE 1 210/o/6 EXPERIMENTER 5

THE 2 CURVES WERE ADDED WITH SIGNS OF
-1 1
AND THE NUMBERS OF THE EXPERIMENTS WERE, RESPECTIVELY -
201 -C
49440 VOLTS ON CARD = FULL SCALE PEN DEFLECTION
1.22E+01 = FACTOR FOR OBS ROT TO MOLEC ROT
1.3CCCCE+CC 1.559CCE+03 = AA AND XLAMO
.10CC CM PATH, 8190 GAUSS, 1.0C0C0E-02 MOLES/LITER

EXP. NO. 205 COMPOUND NAPHTHALENE 3400
SOLVENT CHL3 TYPE OF MEASUREMENT TEMP MORD
SPEC. SLIT WIDTH +26CC TIME CONSTANT A2
MAG. SET OA DATE 10/26/65 EXPERIMENTER JMT

THE 2 CURVES WERE ADDED WITH SIGNS OF
-1 1
AND THE NUMBERS OF THE EXPERIMENTS WERE, RESPECTIVELY -
205 -0
49440 VOLTS ON CARD = FULL SCALE PEN DEFLECTION
2.05E+00 = FACTOR FOR OBS ROT TO MOLEC ROT
6.35000E+01 1.55900E+03 = AA AND XLAMO
.1000 CM PATH, 8120 GAUSS, 6.00000E-02 MOLES/LITER

EXP. NO. 225 COMPOUND 1,8DIMETHNAPHTHALEN
SOLVENT ETCH TYPE OF MEASUREMENT TEMP MORD
SPEC. SLIT WIDTH +26CC TIME CONSTANT A2
MAG. SET DATE 10/6/6 EXPERIMENTER 5 JMT

THE 2 CURVES WERE ADDED WITH SIGNS OF
-1 1
AND THE NUMBERS OF THE EXPERIMENTS WERE, RESPECTIVELY -
225 -0
49440 VOLTS ON CARD = FULL SCALE PEN DEFLECTION
1.22E+02 = FACTOR FOR OBS ROT TO MOLEC ROT
1.27CCCE+CC 1.414C0E+03 = AA AND XLAMO
.10CC CM PATH, 8190 GAUSS, 1.00000E-03 MOLES/LITER

EXP. NO. 227 COMPOUND 1,4DIMETHNAPHTHALEN
SOLVENT CHCL3 TYPE OF MEASUREMENT TEMP MORD
SPEC. SLIT WIDTH +26CC TIME CONSTANT A2
MAG. SET DATE 12/1/656 EXPERIMENTER 5 JMT

THE 2 CURVES WERE ADDED WITH SIGNS OF
-1 1
AND THE NUMBERS OF THE EXPERIMENTS WERE, RESPECTIVELY -
227 -0
49440 VOLTS ON CARD = FULL SCALE PEN DEFLECTION
2.08E+00 = FACTOR FOR OBS ROT TO MOLEC ROT
8.25500E-01 1.55900E+03 = AA AND XLAMO
.1000 CM PATH, 8030 GAUSS, 6.00000E-02 MOLES/LITER

EXP. NO. 231 COMPOUND 2,7DIMETHNAPHTHALEN
SOLVENT CHCL3 TYPE OF MEASUREMENT TEMP MORD
SPEC. SLIT WIDTH +26CC TIME CONSTANT A2
MAG. SET DATE 12/1/656 EXPERIMENTER 5 JMT

THE 2 CURVES WERE ADDED WITH SIGNS OF
-1 1
AND THE NUMBERS OF THE EXPERIMENTS WERE, RESPECTIVELY -
231 -0
49440 VOLTS ON CARD = FULL SCALE PEN DEFLECTION
5.19E+01 = FACTOR FOR OBS ROT TO MOLEC ROT
1.60000E-01 1.55900E+03 = AA AND XLAMO
.1000 CM PATH, 8030 GAUSS, 2.40000E-03 MOLES/LITER

EXP. NO. 275 COMPOUND ACENAPHTHYLENE
SOLVENT CHCL3 TYPE OF MEASUREMENT MORD TEMP 25
SPEC. SLIT WIDTH 10A TIME CONSTANT 1
MAG. SET 2 DATE 7/27/56 EXPERIMENTER JMT

THE 2 CURVES WERE ADDED WITH SIGNS OF
-1 1
AND THE NUMBERS OF THE EXPERIMENTS WERE, RESPECTIVELY -
275 274
49440 VOLTS ON CARD = FULL SCALE PEN DEFLECTION
7.14E+01 = FACTOR FOR OBS ROT TO MOLEC ROT
1.25000E+00 1.55900E+03 = AA AND XLAMO
.2000 CM PATH, 7000 GAUSS, 1.00000E-03 MOLES/LITER

Appendix II

Program for MORD Data Reduction

```
      PROGRAM DATCON( INPUT, OUTPUT, TAPE2=INPUT, TAPE3=OUTPUT, TAPE14,
     1TAPE98, TAPE99)
      DIMENSION V(300), IS(300), IPEN(300), DEG(300), ROT(300), XL(300)
      DIMENSION CORROT(300,20), SIGN(20), F(300), IV(300), VV(300)
      DIMENSION A(20,10), B(20), YS(300), CO(10), IEX(20)
      DIMENSION OM(300)
      COMMON/CCPOOL/XMIN, XMAX, YMIN, YMAX, CCXMIN,CCXMAX,CCYMIN,CCYMAX
      COMMON/CCFACT/FACTOR
      EQUIVALENCE(VV, IV)
      DATA IGO/0/
      CALL CCBGN
   24 J = 0
      IF( IGO .EQ. 0) GO TO 41
      CALL CCNEXT
   41 IGO = 1
      READ(2,1) IX, COM1, COM2, S, TYPE, TEMP, SSW, TIME, MAG, DATE, EXP
    1 FORMAT( I3, 3A10, 2A4, A5, 2A2, 2A10 )
      IF( ENDFILE 2) 25, 26
   26 WRITE(3,2) IX, COM1, COM2, S, TYPE, TEMP, SSW, TIME, MAG, DATE,EXP
    2 FORMAT(1H1, 5X, 9H EXP. NO., I4, 3X, 10H COMPOUND , 2A10, /6X,9H S
     1OLVENT , A10, 3X, 21H TYPE OF MEASUREMENT , A4, 3X, 6H TEMP , A4,/
     25X, 18H SPEC. SLIT WIDTH , A5, 3X, 15H TIME CONSTANT , A2,/6X,
     310H MAG. SET , A2, 3X, 6H DATE , A10, 3X, 14H EXPERIMENTER ,A10//)
      CCYMAX = 630.
      READ(2,32) IFIT, IPTS, IORD, IP1, IP2, CCXMAX, N
   32 FORMAT(5I5, F10.2, I5)
C
C        IFIT = 1     WILL SMOOTH F(LAMBDA)
C        IFIT = 0     WILL NOT SMOOTH F(LAMBDA)
C        IPTS         NUMBER OF POINTS TO BE CONSIDERED ON EACH SIDE OF
C                     POINT THAT IS TO BE SMOOTHED
C        IORD         ORDER OF POLYNOMIAL THAT IS TO BE FIT TO
C                     2*IPTS+1 POINTS
C        IP1 = 1      PUNCH SMOOTHED F(LAMBDA) IN LSQVMT FORMAT
C        IP1 = 0      DO NOT PUNCH
C        IP2 = 1      PUNCH SMOOTHED F(LAMBDA) ACCORDING TO 10F8.6
C        IP2 = 0      DO NOT PUNCH
C        CCXMAX       LENGTH OF THE GRAPH IN PAPER COORDINATES
C                     CCXMAX = 1070. = 10 INCHES
C                     CCXMAX = 2070. = 20 INCHES
C
      READ(2,5) (SIGN(I), I=1,N)
    5 FORMAT(16F5.2)
      READ(2,49) (IEX(I), I=1,N)
   49 FORMAT(16I5)
```

```
      READ (2,439) AXMX, AXMN, AYMX, AYMN
  439 FORMAT (4E15.4)
      WRITE(3,23) N, (SIGN(I), I=1,N)
   23 FORMAT(5X, 4H THE, I3, 32H CURVES WERE ADDED WITH SIGNS OF,/
     1(10X, 20F5.0))
      WRITE(3,50) (IEX(I), I=1,N)
   50 FORMAT(5X, 56H AND THE NUMBERS OF THE EXPERIMENTS WERE, RESPECTIVE
     1LY =, /(10X, 20I5))
    9 J = J+1
      READ(2,3) P, H, C
    3 FORMAT ( 2F10.5,  E15.4)
      READ(2,4) XLIM, DE_L, XLAMO, AA
    4 FORMAT ( 3F10.4,  E15.4)
      I = 1
    7 I1 = I+4
      READ(2,6) (IPEN(K), IS(K), IV(K), K=I,I1)
    6 FORMAT( 4X, 5(I1, I2, I7, 5X))
      IF( IPEN(I) .EQ. 0) GO TO 8
      I = I1+1
      GO TO 7
    8 CONTINUE
      NN = I-1
      SC = 100./(C*H*P)
      D = 50900.-1460.
      WRITE(3,423) D
  423 FORMAT (6X,F6.0, 42H VOLTS ON CARD = FULL SCALE PEN DEFLECTION)
      WRITE(3,424) SC
  424 FORMAT (6X E10.2, 34H = FACTOR FOR OBS ROT TO MOLEC ROT)
      WRITE (3,434) AA, XLAMO
  434 FORMAT (2E15.5, 15H = AA AND XLAMO)
      DO18 I=1,NN
      VV(I) = IV(I)
      V(I) =VV(I)-.25*(FLOAT(IPEN(I))-1.0)*D - 1230.
C          ZERO ON CHART IS 1230 VOLTS ON CARD
      ISI = IS(I)
      GO TO (10, 11, 12, 13, 14, 15, 16), ISI
   10 DEG(I) = V(I)*.02/D
      GO TO 17
   11 DEG(I) = V(I)*.04/D
      GO TO 17
   12 DEG(I) = V(I)*.10/D
      GO TO 17
   13 DEG(I) = V(I)*.20/D
      GO TO 17
   14 DEG(I) = V(I)*.40/D
      GO TO 17
   15 DEG(I) = V(I)/D
```

```
      IF (AXMX .EQ. 0.0) GO TO 310
      XMAX = AXMX
      XMIN = AXMN
  310 CONTINUE
      CALL CCGRID( 10, 10, 6HLABELS, 10, 10 )
      CALL CCLTR( 200., 10., 0, 2, 23H                    )
      CALL CCLTR(900., 10., 0, 2, 29H A COMPOSITE OF EXPERIMENTS -)
      WRITE(98, 202) (IEX(I), I=1,N)
  202 FORMAT( 2016 )
      CALL CCLTR(1400., 10., 0, 2)
      CALL CCPLOT( XL, F, NN, 4HJOIN, 1, 1 )
      IF( IFIT .EQ. 0 ) GO TO 24
      I1 = 2*IPTS
      I2 = IORD+1
      I11 = 2*IPTS+1
      WRITE(3,48) IORD, I11
   48 FORMAT(1HL, 5X, 61H THE CURVE WILL BE SMOOTHED BY FITTING A POLYNO
     1MIAL OF DEGREE, I2, 4H TO , I2, 8H POINTS.)
      DO33 I=1,I1
      B(I) = F(I)
      DO33 K=1,I2
      K1 = K-1
   33 A(I,K) = XL(I)**K1
      I3 = IPTS+1
      I4 = NN-IPTS
      DO34 I=I3,I4
      I5 = I+IPTS
      DO35 K=1,I2
      K1 = K-1
   35 A(I11,K) = XL(I5)**K1
      B(I11) = F(I5)
C
C          LSQS SOLVES THE OVERDETERMINED SYSTEM OF EQUATIONS A*CO=B
C          IF KERR = 99, THE SYSTEM IS SINGULAR
C          I11 = NO. OF ROWS IN A
C          I2 = NO. OF COLUMNS IN A
C
      CALL LSQS(A, CO, B, I11, I2, 1, KERR, 9)
      YS(I) = 0.0
      DO36 K=1,I2
      K1 = K-1
   36 YS(I) = YS(I) + CO(K)*XL(I)**K1
      DO37 K=1,I1
      B(K) = B(K+1)
      DO37 L=1,I2
   37 A(K,L) = A(K+1,L)
   34 CONTINUE
```

```
      WRITE(3,45)
   45 FORMAT(//, 20X, 29H POINTS ON THE SMOOTHED CURVE/)
      WRITE (3,404)
      DO39 I=I3,I4
      WRITE (3,401) I, XL(I), YS(I), OM(I)
   39 CONTINUE
      I6 = I4-I3+1
      CALL CCNEXT
      CALL CCGRID(10, 10, 6HLABELS, 10, 10)
      CALL CCLTR( 200., 10., 0, 2, 23H                    )
      CALL CCLTR(900., 10., 0, 2, 29H A COMPOSITE OF EXPERIMENTS -)
      WRITE(98, 202) (IEX(I), I=1,N)
      CALL CCLTR(1400., 10., 0, 2)
      CALL CCPLOT(XL(I3), YS(I3), I6, 4HJOIN, 6, 1)
      IF( IP1 .EQ. 0) GO TO 42
      WRITE (14,40)  (YS(I), OM(I), I= I3,I4)
   40 FORMAT( 2E10.3)
   42 IF( IP2 .EQ. 0) GO TO 24
      I = I3
   46 I2 = I+3
      OMI = OM(I)
      MI = OMI
      WRITE(14,44) MI, (YS(J), J=I,I2)
   44 FORMAT( I6, 4E16.7)
      I = I2+1
      IF( I2 .GE. I6) GO TO 24
      GO TO 46
   25 CONTINUE
      CALL CCEND
      ENDFILE 14
      STOP
      END
```

```
      SUBROUTINE LSQS(A,X,B,M,N,LP,KERR,ITER)
C  LSQS SOLVES THE OVERDETERMINED SYSTEM OF EQUATIONS AX=B
C    M= NUMBER OF ROWS IN A
C     N=NUMBER OF COLUMNS IN A
C    LP=NUMBER OF COLUMNS IN B
C     KERR IS SET TO 99 IF THE SYSTEM IS SINGULAR
C    ITER IS THE MAXIMIM NUMBER OF ITERATIONS TO IMPROVE THE SOLUTION
      DIMENSION A(20,10), X(10,1), B(20,1), QR(20,10), R(20)
      DIMENSION Y(10), KPIVOT(10), ALFA(10), BETA(10), SUM(10), Z(10)
      DATA FRCT/.0625/
      LA = 20
      KERR = 0
      DO 1 I = 1,M
      DO 1 J = 1,N
    1 QR(I,J) = A(I,J)
      DO 20 J = 1,N
      KPIVOT(J) = J
      CALL IP (1,M,QR(1,J),1,QR(1,J),1,0.,SUM(J),DUM)
   20 CONTINUE
      DO 21 K = 1,N
      SIGMA = SUM(K)
      JBAR = K
      KP = K+1
           IF(KP.GT.N)GOTO27
      DO 22 J = KP,N
           IF(SIGMA.GE.SUM(J))GOTO22
      SIGMA = SUM(J)
      JBAR = J
   22 CONTINUE
           IF(JBAR.EQ.K)GOTO27
      I = KPIVOT(K)
      KPIVOT(K)= KPIVOT(JBAR)
      KPIVOT(JBAR) = I
      SUM(JBAR) = SUM(K)
      SUM(K) = SIGMA
      DO 26 I =1,M
      SIGMA = QR(I,K)
      QR(I,K) = QR(I,JBAR)
   26 QR(I,JBAR) = SIGMA
   27 CALL IP (K,M,QR(K,K),1,QR(K,K),1,0.,SIGMA,DUM)
           IF(SIGMA.EQ.0.0)GOTO99
      QRKK=QR(K,K)
           ALFAK=SQRT(SIGMA)
           IF(QRKK.GT.0.0)ALFAK=-ALFAK
```

```
      ALFA(K)=ALFAK
      QR(K,K) = QRKK-ALFAK
      BTA=1.0/(SIGMA-QRK(*ALFAK)
      BETA(K)=BTA
              IF(KP.GT.N)GOTO21
            . DO33J=KP,N
              CALLIP(K,M,QR(K,K),1,QR(K,J),1,0.0,ANS,DJM)
      BTA1=BTA*ANS
      DO 34 I=K,M
   34 QR(I,J)=QR(I,J)-QR(I,K)*BTA1
   33 SUM(J)=SUM(J)-QR(K,J)**2
   21         CONTINUE
      NM=N-1
      DO2K=1,LP
      ITR=ITER
              DO3I=1,M
    3 R(I)=B(I,K)
      KK=1
C   SOLVE SECTION
   50         DO40J=1,N
              CALLIP(J,M,QR(J,J),1,R(J),1,0.0,ANS,DUM)
      GAMMA=ANS*BETA(J)
              DO40I=J,M
   40 R(I)=R(I)-GAMMA*QR(I,J)
      Z(N)=R(N)/ALFA(N)
              DO41L=1,NM
      I=N-L
      IS=I+1
      DUM=-R(I)
              CALLIP(IS,N,QR(I,IS),LA,Z(IS),1,DUM,ANS,DJM)
   41 Z(I)=-ANS/ALFA(I)
              GOTO(43,44),<K
   43         DO42I=1,N
      L=KPIVOT(I)
   42 Y(L)=Z(I)
              IF(ITR.EQ.0)GOTO10
      KK=2
      VNRM1=0.0
              DO9I=1,N
    9 VNRM1=VNRM1+Z(I)**2
   60         DO4I=1,M
      DUM=-B(I,K)
              CALLIP(1,N,A(I,1),LA,Y(1),1,DJM,ANS,DUM)
    4 R(I)=-ANS
              GOTO50
```

Appendix III

Selected Character Tables

C_s	I	σ^{xy}		
A'	1	1	T_x, T_y; R_z	α_{xx}, α_{yy}, α_{zz}, α_{xy}
A''	1	-1	T_z; R_x, R_y	α_{yz}, α_{xz}

C_2	I	C_2^z		
A	1	1	T_z; R_z	α_{xx}, α_{yy}, α_{zz}, α_{xy}
B	1	-1	T_x, T_y; R_x, R_y	α_{yz}, α_{xz}

C_{2v}	I	C_2^z	σ_v^{xz}	σ_v^{yz}		
A_1	1	1	1	1	T_z	α_{xx}, α_{yy}, α_{zz}
A_2	1	1	-1	-1	R_z	α_{xy}
B_1	1	-1	1	-1	T_x; R_y	α_{xz}
B_2	1	-1	-1	1	T_y; R_x	α_{yz}

For planar C_{2v} molecules the x axis should be chosen perpendicular to the plane.

D_{2h}	I	C_2^z	C_2^y	C_2^x	i	xy	xy	yz		
A_g	1	1	1	1	1	1	1	1		α_{xx}, α_{yy}, α_{zz}
A_u	1	1	1	1	-1	-1	-1	-1		
B_{1g}	1	1	-1	-1	1	1	-1	-1	R_z	α_{xy}
B_{1u}	1	1	-1	-1	-1	-1	1	1	T_z	
B_{2g}	1	-1	1	-1	1	-1	1	-1	R_y	α_{xz}
B_{2u}	1	-1	1	-1	-1	1	-1	1	T_y	
B_{3g}	1	-1	-1	1	1	-1	-1	1	R_x	α_{yz}
B_{3u}	1	-1	-1	1	-1	1	1	-1	T_x	

This group is sometimes called V_h. For planar D_{2h} molecules the x axis should be taken perpendicular to the plane. The z axis should pass through the largest possible number of atoms, or, if this is not decisive, through the largest possible number of bonds.

D_{6h}	I	$2C_6^z$	$2C_3$	C_2^z	$3C_2$	$3C_2'$	i	$2S_3$	$2S_6$	σ_h	$3\sigma_d$	$3\sigma_v$		
A_{1g}	1	1	1	1	1	1	1	1	1	1	1	1		$\alpha_{xx} + \alpha_{yy}$, α_{zz}
A_{1u}	1	1	1	1	1	1	-1	-1	-1	-1	-1	-1		
A_{2g}	1	1	1	1	-1	-1	1	1	1	1	-1	-1	R_z	
A_{2u}	1	1	1	1	-1	-1	-1	-1	-1	-1	1	1	T_z	
B_{1g}	1	-1	1	-1	1	-1	1	-1	1	-1	1	-1		
B_{1u}	1	-1	1	-1	1	-1	-1	1	-1	1	-1	1		
B_{2g}	1	-1	1	-1	-1	1	1	-1	1	-1	-1	1		
B_{2u}	1	-1	1	-1	-1	1	-1	1	-1	1	1	-1		
E_{1g}	2	1	-1	-2	0	0	2	1	-1	-2	0	0	(R_x, R_y)	$(\alpha_{yz}, \alpha_{xz})$
E_{1u}	2	1	-1	-2	0	0	-2	-1	1	2	0	0	(T_x, T_y)	
E_{2g}	2	-1	-1	2	0	0	2	-1	-1	2	0	0		$(\alpha_{xx} - \alpha_{yy}$, $\alpha_{xy})$
E_{2u}	2	-1	-1	2	0	0	-2	1	1	-2	0	0		

REFERENCES

1. M. Faraday, Phil. Mag. 28, 294 (1846).
2. R. R. Rau, M. E. Caspari, Phys. Rev. 100, 632 (1955).
3. T. S. Moss and A. K. Walton, Proc. Intern'l. Conf. on Semiconductor Physics, Prague, 1960 (Academic Press, N. Y., 1961).
4. Borel, Compt. Rend. 128, 1095 (1889).
5. P. Gabiano, Ann. phys. 20, 68 (1933).
6. W. Heller and D. Fitts, Polarimetry in A. Weissberger's Technique of Organic Chem., Vol. I, part III, p. 2147 (Interscience, N. Y., 1960).
7. T. M. Lowry and I. J. Falkner, J. 127, 2883 (1925).
8. K. Djerassi, Optical Rotation (McGraw-Hill, N. Y., 1960).
9. A. E. Martell and M. Calvin, Chemistry of the Metal Chelate Compounds (Prentice-Hall, N. Y., 1952).
10. C. Tanford, Physical Chem. of Macromolecules (John Wiley & Sons, N. Y., 1961).
11. C. Reid, Excited States in Chemistry and Biology (Butterworth, London, 1957).
12. A. J. Fresnel, Ann. chim. 28, 147 (1825).
13. Brace, Wied Ann. 26, 576 (1885).
14. Brace, Phil. Mag. 6, 464 (1901).
15. R. W. Wood, Physical Optics, 2nd Edition (Macmillan, N. Y., 1911).
16. J. Mills, Phys. Rev. 95, 65 (1904).
17. A. Verdet, Ann. chim. 52, 129 (1858).
18. O. Schonrock, Z. Phys. 46, 314 (1928) and 78, 757 (1932).
19. B. N. Chuckerbutti, Indian J. Phys. 8, 387 (1932).

20. Shuner, J. de Phys. 3, 45S (1932).

21. De la Rive, Phil. Mag. 40 (1870).

22. De la Rive, Ann. chim. 15, 57 (1871).

23. G. G. Stokes, Burnett Lectures on Light (Macmillan Co., London, 1882).

24. W. H. Perkin, Sr., J. Chem. Soc. 41, 330 (1882). (For a more complete list of his works, see Partington, J. R., An Advanced Treatise on Physical Chemistry, Vol. 4, p. 599, Longmans, Green, 1953.)

25. W. H. Perkin, ibid. 81, 177 (1902).

26. F. W. Kay and W. H. Perkin, Jr., ibid. 89, 26 (1906).

27. F. Gallais, J. Chim. Phys. 61, 717 (1964).

28. A. Labbauf, C. W. Nutt, and F. H. Garner, J. Inst. Pet. 41, 336 (1955).

29. Lord Rayleigh, Phil. Trans. 176, 343 (1885).

30. W. Voigt, Magneto-und Electrooptik, Druck und Verlag von B. G. Teubner, Leipzig (1908).

31. E. D. Palik, J. R. Stevenson, and J. Webster, J. Appl. Phys. 37, 1982 (1966).

32. Rodger and Watson, Phil. Trans. 186, 621 (1895) and Z. Phys. Chem. 19, 322 (1896).

33. Hirsch, Phil. Mag. 8, 177 (1836).

34. Borel, Compt. Rend. 128, 1095 (1889); Arch. Sci. Phys. Nat. 16, 24 and 157 (1903).

35. F. Bates and F. P. Phelps, Phys. Rev. 10, 90 (1917).

36. De la Rive, Ann. chim. 22, 5 (1871).

37. John Tyndall, Six Lectures on Light (Longmans, Green, London, 1873), p. 147.

38. A. J. Fresnel, Ann. chim. 28, 147 (1825).

39. P. J. Stephens, Ph.D. Thesis, Oxford, 1964.

40. M. Sharnof, Am. J. of Phys. 32, 40 (1964).

41. R. W. Ditchburn, Light, 2nd Ed. (Interscience, N. Y., 1963).

42. A. H. Kramers, Congr. Intern. Risci Como 2, 545 (1922).

43. de L. Kronig, J. Opt. Soc. Am. 12, 547 (1926).

44. W. Moffitt and A. Moscowitz, J. Chem. Phys. 30, 648 (1959).

45. K. Sauer, Proc. Nat. Acad. Sci. 53, 716 (1965).

46. E. A. Dratz, Ph.D. Thesis, Univ. of Calif., Berkeley, in press.

47. J. M. Thiery, personal communication.

48. P. Drude, Theory of Optics, translated by C. R. Mann and R. A. Millikan, Dover, N.Y., 1959.

49. (a) R. Wood, Phil. Mag., Oct. 1905, July 1907, or Physical Optics (Macmillan Co., London, 1934); (b) A. Cotton and M. Scherer, Compt. Rend. 195, 915 (1932).

50. L. Rosenfeld, Z. Phys. 57, 835 (1929).

51. H. A. Kramers, Proc. Acad. Sci., Amsterdam, 33, 959 (1930).

52. R. Serber, Phys. Rev. 41, 489 (1932).

53. I. Tinoco and C. A. Bush, Biopolymers Symp. No. 1 (Wiley, N. Y., 1964).

54. M. P. Groenewege, Molec. Phys. 5, 541 (1962).

55. P. J. Stephens, Ph.D. Thesis, Oxford, 1964.

56. A. D. Buckingham and P. J. Stephens, Ann. Rev. Phys. Chem. (in press).

57. H. Eyring, J. Walter, and G. E. Kimall, Quantum Chemistry (Wiley, N. Y., 1944).

58. J. J. Duffield, personal communication.

59. Permanent Magnet Handbook, Crucible Steel Co. (1957).

60. D. Bruce Montgomery, High Magnetic Fields, ed. H. Kolm (Wiley, N. Y., 1962).

61. H. Cary, et al., Applied Optics 3, 329 (1964).

62. J. J. Duffield, personal communication.

63. B. Briat, M. B. Hardon, and J. Badoz, Compt. Rend. 256, 3340 (1963).

64. E. Clar, Aromatische Kohlenwasserstoffe, Berlin, 1941; J. Chem. Phys. 17, 741 (1949); and Ber. 82, 495 (1949).

65. C. A. Coulson, Proc. Phys. Soc. 60, 257 (1948).

66. J. R. Platt, et al., Free Electron Theory of Conjugated Molecules (Wiley, N. Y., 1964).

67. H. B. Klevens and J. R. Platt, J. Chem. Phys. 17, 470 (1949).

68. F. A. Cotton, Chemical Applications of Group Theory (Wiley, N. Y., 1963).

69. F. H. Garner, C. Nutt, and A. Labbauf, J. Inst. Pet. 41, 329 (1955) (see also Ref. 28).

70. M.J.S. Dewar and H. C. Longuet-Higgins, Proc. Phys. Soc. A67, 795 (1954).

71. R. A. Friedel and M. Orchin, U.V. Spectra of Aromatic Compounds (Wiley, N. Y., 1951).

72. J. R. Platt, J. Chem. Phys. 18, 1168 (1950).

73. A. Bree and V.V.B. Vilkos, J. Chem. Phys. 40, 3125 (1964).

74. W. Moffitt, J. Chem. Phys. 22, 320 (1954).

75. R. Pariser, J. Chem. PHys. 24, 250 (1956).

76. J. G. Foss and M. R. McCarville, J. Chem. Phys. 45, 4350 (1966).

77. V. E. Shashoua, J. Am. Chem. Soc. 82, 5505 (1960).

78. S. K. Lower and M. A. El-Sayet, Chem. Rev. 66, 199 (1966).

79. B. S. Snowden and W. H. Eberhardt, J. Molec. Spect. 18, 372 (1965).

80. L. Goodman, J. Molec. Spect. 6, 109 (1961).

81. K. Sauer, Proc. Nat. Acad. Soc. 53, 716 (1965).

82. G. R. Haugen and W. H. Melhuish, Trans. Faraday Soc. 66, 386 (1964).

83. F. E. Stewart, M. Eisner, and W. R. Carper, J. Chem. Phys. 44, 2866 (1966).

84. L. J. Andrews and R. M. Keefer, Molecular Complexes in Organic Chemistry (Holden-Day, Inc., San Francisco, 1964).

85. S. K. Chakrabarti and S. Basu, Trans. Faraday Soc. 495, 465 (1964).

86. D. Ilten, Ph.D. Thesis, Univ. of Calif., Berkeley, 1964.

87. R. S. Mulliken, J. Am. Chem. Soc. 72, 500 (1950); ibid. 74, 811 (1952); J. Chem. Phys. 19, 514 (1951); and J. Phys. Chem. 56, 801 (1952).

PART II. CONFORMATION OF CELLULOSE TRIACETATE

A. Introduction

Membranes made of cellulose triacetate (CTA) have been used successfully for desalination of water by the process of reverse osmosis.[1] Salt water is put under pressure on one side of the membrane and relatively pure water is collected on the other side. Flow due to osmosis, in contrast, would transport pure water to the salt water side of the membrane--thus the name "reverse osmosis". This process is also called "molecular ultrafiltration".

Very little is known about the detailed structure of the CTA, which allows water to pass but retards ions. Blunk[2] has shown that ions will pass through the membrane only if they are univalent and capable of hydrogen bonding (e.g., ammonium hydroxide). Certain small, non-ionic molecules will also pass through the membrane if they will form hydrogen bonds with the CTA (e.g., butanol). It has been postulated that the membrane contains a positive charge[2] and that it has pores of about 10 Å radius. It may be that the structurally organized clusters of water, which exist in the liquid state, are disorganized in passing through the membrane. But it is energetically unfavorable to disorganize the water molecules around an ion unless the ion can form hydrogen bonds in the CTA. Thus the membrane discriminates against non-hydrogen bonding ions.

This selective permeability is shown by CTA membranes only after they have undergone certain treatments. They are cast from a mixture of approximately equal weights of CTA, acetone and formamide, of about 25% CTA, 45% acetone, and about 30% formamide (or other aldehyde as

plasticizer). After a short period of drying, they are quenched in ice water for about 30 min. Although there are a few other methods for making CTA films for desalinzation, large deviations from the procedure and materials listed usually result in membranes having poor selective permeability.

Membranes showing selective permeability are also important in areas other than water purification. Their function in biological systems has long been known, but is still not well understood. Even the transmission of nerve impulses involves membrane semi-permeability. (The electrical signal propagates because changes in the ion permeability permit certain inorganic ions to flow through the axon membrane.)

It has been suggested that the conformations of the structural molecules in membranes play a vital role in their selective permeability. The following work gives evidence that this is indeed the case for CTA films, and presents methods which may be used for the study of molecular conformation in other membranes.

B. Optical Rotation of CTA Membranes

Samples of CTA (cellulose triacetate) membranes are mounted in a Cary 60 polarimeter and the optical rotation recorded. It is observed that the optical rotation is a function of the azimuthal angle, θ, measured in the plane perpendicular to the instrument light beam. A cell was constructed which permits observation of the optical rotation of a membrane at any value of θ (Figure 1). The sample is held between two teflon washers by a small amount of stopcock grease applied around

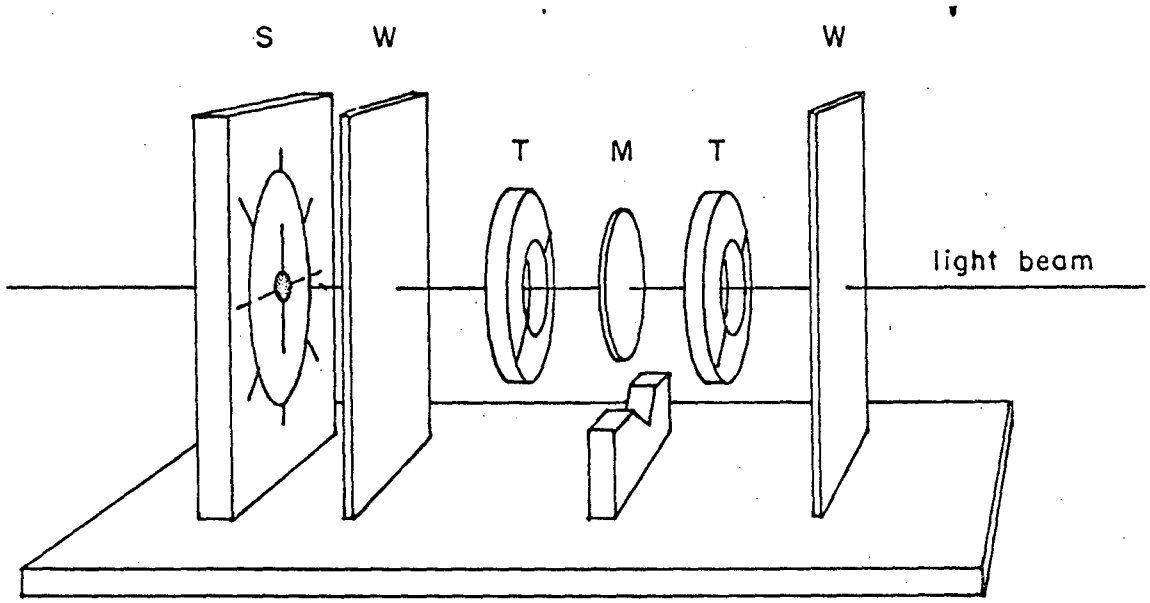

MUB 11450

Fig. 1. Exploded view of cell and holder used in the measurement of the ORD of CTA. S is a removable divided circle for measuring the asimuth of the Teflon holder rings, T. M is the CTA membrane and W a quartz window.

the edges of the membrane. This assembly is then lowered into a quartz cell that can be filled with a solution that will approximate the index of refraction of the film. (This prevents reflection from the slightly irregular surface of the membrane which may result in spurious optical rotation.) The washer assembly can be rotated without removing it from the cell or disturbing the membrane. Figure 2 shows the observed rotation of a CTA membrane as a function of θ as measured at 2600 Å. It is seen that the function is not symmetrical, but that it repeats itself approximately every 180°, as do trigonometric functions of 2θ. For some films at visible wavelengths, the optical rotation was very nearly

$$\phi = A \cos 2\theta$$

where ϕ is the observed rotation and A a constant.

Variation of optical rotation with the azimuthal angle is characteristic of linear retarders (materials having different indices of refraction for light polarized along the x or y axis when the beam is traveling in the z direction). For example, a thin sheet of mica shows different indices of refraction for light polarized along different crystal axes. This leads to the observed optical rotation shown in Figure 3. It will be noted that the apparent optical rotation, ϕ, is well described by sin 4θ. But the optical rotation of the CTA film is some function of 2θ, showing that a linear retarder is not a good model for the membrane.

The θ dependence does not arise from the orientation or ordering of the CTA molecules in the field (assuming no linear dichroism). If the molecules were randomly oriented there would obviously be no change in the optical rotation as the film is turned in the plane perpendicular

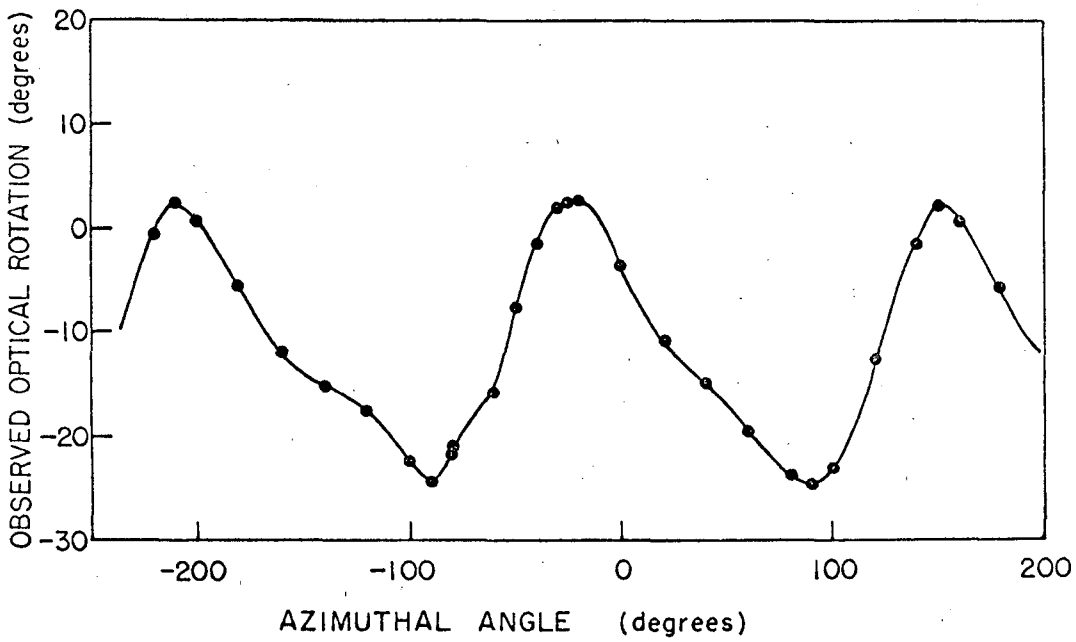

Fig. 2. Optical rotation of a CTA membrane as a function of its angle of rotation about the axis of the light beam.

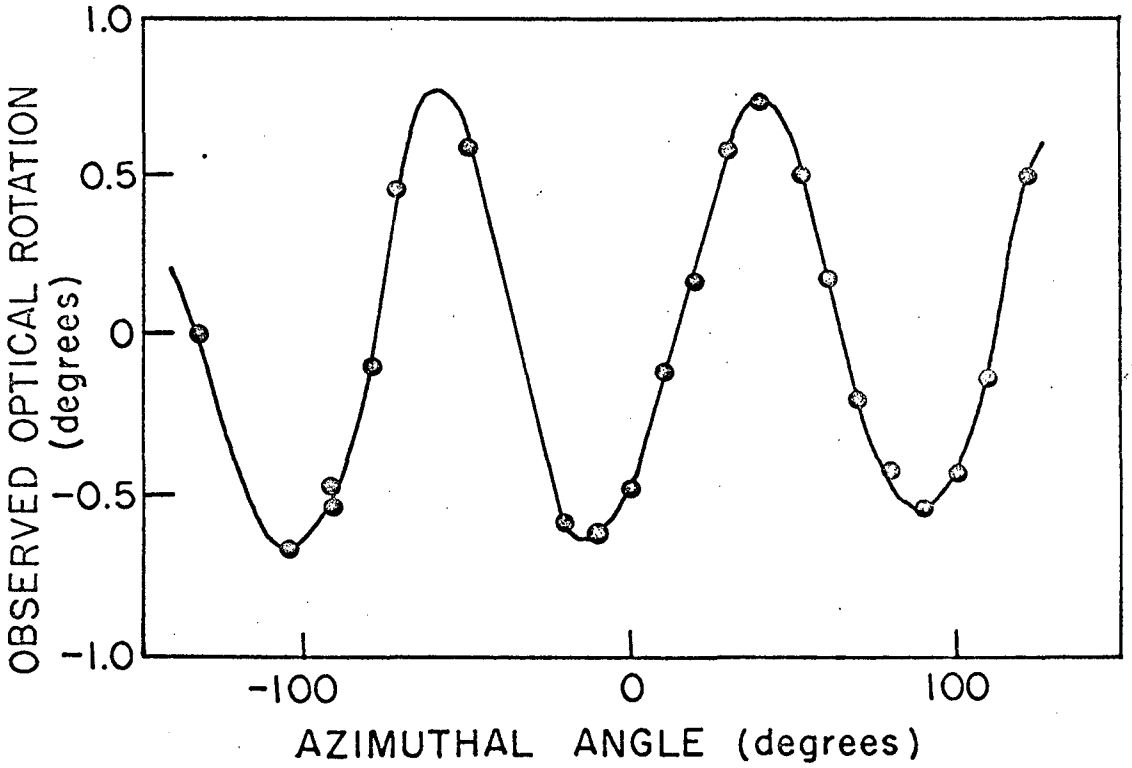

MUB 11455

Fig. 3. Optical rotation of a sheet of mica as a function of its angle of rotation about the axis of the light beam.

to the light beam. If the molecules were oriented there would still be no change so long as the film is turned only in the xy plane and the light beam travels along the z axis. This is seen from the symmetry of the equation for the optical rotation of oriented systems.[2a]

$$\phi_z \propto [\underline{j} \cdot \underline{\mu}\,\underline{k} \cdot (\underline{rp}) \cdot \underline{i}] - [\underline{i} \cdot \underline{\mu}\,\underline{k} \cdot (\underline{rp}) \cdot \underline{j}]$$

where ϕ_z is the observed optical rotation, $\underline{i}$, $\underline{j}$, and $\underline{k}$ are unit vectors along the x, y, and z axes respectively, and $\underline{\mu}$ and $(\underline{rp})$ are the electric and magnetic dipole transition moments of the molecule. The angle between $\underline{\mu}$ and $(\underline{rp})$ is constant and is determined by the molecular structure. The angle they make with $\underline{k}$ does not change in the experimental apparatus described, so the above equation reduces to scaler products. By remembering that $\underline{A} \cdot \underline{B} = AB \cos \theta_{AB}$, where θ_{AB} is the angle between the vectors, it is easily shown that ϕ_z depends only on the angle between $\underline{\mu}$ and $(\underline{rp})$ and not their orientation in the xy plane.

There are mathematical methods of assessing the polarization and intensity of a light beam which has passed through one or more optical elements.[3] One such method is the Mueller Calculus,[4] which correctly predicts the sin 4θ dependence of the optical rotation of a linear retarder. However, it does not predict a sin 2θ dependence for any optical element which the CTA film might approximate, with the exception of a dichroic plate (or scattering plate with the scattering different for polarizations in perpendicular directions). Even when one considers the two polarizers and Faraday modulator in the optical train of the polarimeter and solves for minimum intensity at the photomultiplier, one cannot get a 2θ dependence except for dichroic or scattering devices.

CTA has no absorption at visible wavelengths, but the films scatter. Dichroism and scattering are mathematically equivalent in the following

equations. The effect of scattering can be put in quantitative form by assuming that $S_{\parallel}^2$ is the fraction of the incident light intensity transmitted when the electric vector of the light is parallel to the molecular axis, and $S_{\perp}^2$ is the fraction transmitted when they are perpendicular. The observed rotation will then be:

$$\phi_S = \tan^{-1}\left[\frac{\tan\theta - \frac{S_{\parallel}}{S_{\perp}}\tan\theta}{1 + (\tan^2\theta)\frac{S_{\parallel}}{S_{\perp}}}\right] \qquad (1)$$

where is the azimuthal angle in the xy plane. If S is nearly equal to S , this equation becomes:

$$\phi_S \approx 1/2\left(\frac{S_{\parallel}}{S_{\perp}} - 1\right)\sin 2\theta \qquad (2)$$

Equation (1) is most easily obtained by considering vectors representing the amplitude of the components of the electric vector of the light in the x and y directions and observing how their resultant rotates as one is shortened by scattering more than the other. It must be remembered that the intensity of the light is proportional to the square of the length of the electric vector.

Equation (1) would account for the observed behavior in the visible region of the spectrum. It would have to be assumed that S has a much different value than S in the UV in order to account for the deviation from the sine function.

The origin of this anisotropy is probably the unidirectional smoothing of the film when it is cast. A bar or scraper called a casting knife is drawn across a puddle of the CTA solution at a constant height in order to achieve a uniform film thickness. It is observed that the amplitude of the variation of optical rotation as a function of θ is roughly

proportional to the speed with which the knife is drawn across the CTA solution. The amplitude varies over a factor of 5 or more. The rotation is not significantly affected by annealing, that is, by holding the film above its glass transition temperature (80°C) for about 30 min. This relieves mechanical strains and allows the molecules to reorient themselves to some extent. It appears, therefore, that mechanical strain in the film is not the origin of the anisotropy. The degree of crystallization (concentration of CTA microcrystals in the film) has little influence on the amplitude of the θ dependence. Microcrystals may still be the scatterers, however, since to the first approximation it is the ratio $S_{\parallel}/S_{\perp}$ that determines the amplitude, and this depends on the degree of orientation and not the concentration of scatterers.

It is not possible from the data to determine whether the scatterers have a larger index of refraction than the matrix (as microcrystals would) or whether they have smaller indices of refraction (as pockets of water would). One can only say that more light is scattered when the polarization of the light is parallel to the direction the casting knife is pulled than when it is perpendicular.

The θ dependence of the optical rotation would not be expected to give information about the conformation of the CTA molecules in the film. Equation (2) indicates that at $\theta = n\pi/2$ where $n = 0, 1, 2, \ldots$ the observed rotation will be due only to the molecules in the film and not to the scatterers. Experimentally most of the films studied have been set at $\theta = 45°$ because in the UV the slope of ϕ versus θ is more gentle there than at $\theta = 0°$ and multiples of 90°. Reproducible results are achieved in this case for sections cut from the same film, although there is a

slight variation due to the uneven thickness of any particular film. Variations between similarly cast films can be fairly large.

The experimental results for films presented in the remainder of this work are for $\theta = 45°$ unless otherwise noted. The optical rotation is normalized so that the residue rotation of the film is given. Residue rotation is defined here as it is in the ORD of polypeptides, and the molecular weight of the anhydroglucose unit is taken to be 162, as is customary. It should be noted, however, that about 10% of the -OH groups in the CTA used for these films were not acylated. The residue rotations of the films are directly comparable to the residue rotations of the solutions to be presented later.

Figure 4 shows the residue rotation of a pair of films, one cast with four times as much plasticizer as CTA in the casting mixture, the other without plasticizer. The films were treated identically otherwise, but the non-plasticized film was more dense and contained less water after the usual quenching process than the plasticized film. The selective permeability properties shown by desalinization membranes would be expected in the non-plasticized film, but its thickness prevents much water flow. It should be a good sample for the study of the optical properties of the state of CTA that exhibits reverse osmosis. The plasticized film is permeable to all small ions and molecules. Working desalinization membranes are composed of a thin (0.25 μ) layer of the dense material and a thicker (100 μ) substrate of the permeable CTA.[5] All plasticizer was leached from the films studied.

As can be seen from Figure 4, the dense, non-plasticized film showed a somewhat larger optical rotation than the plasticized membrane. This may be due to the conformation of the CTA being different in the

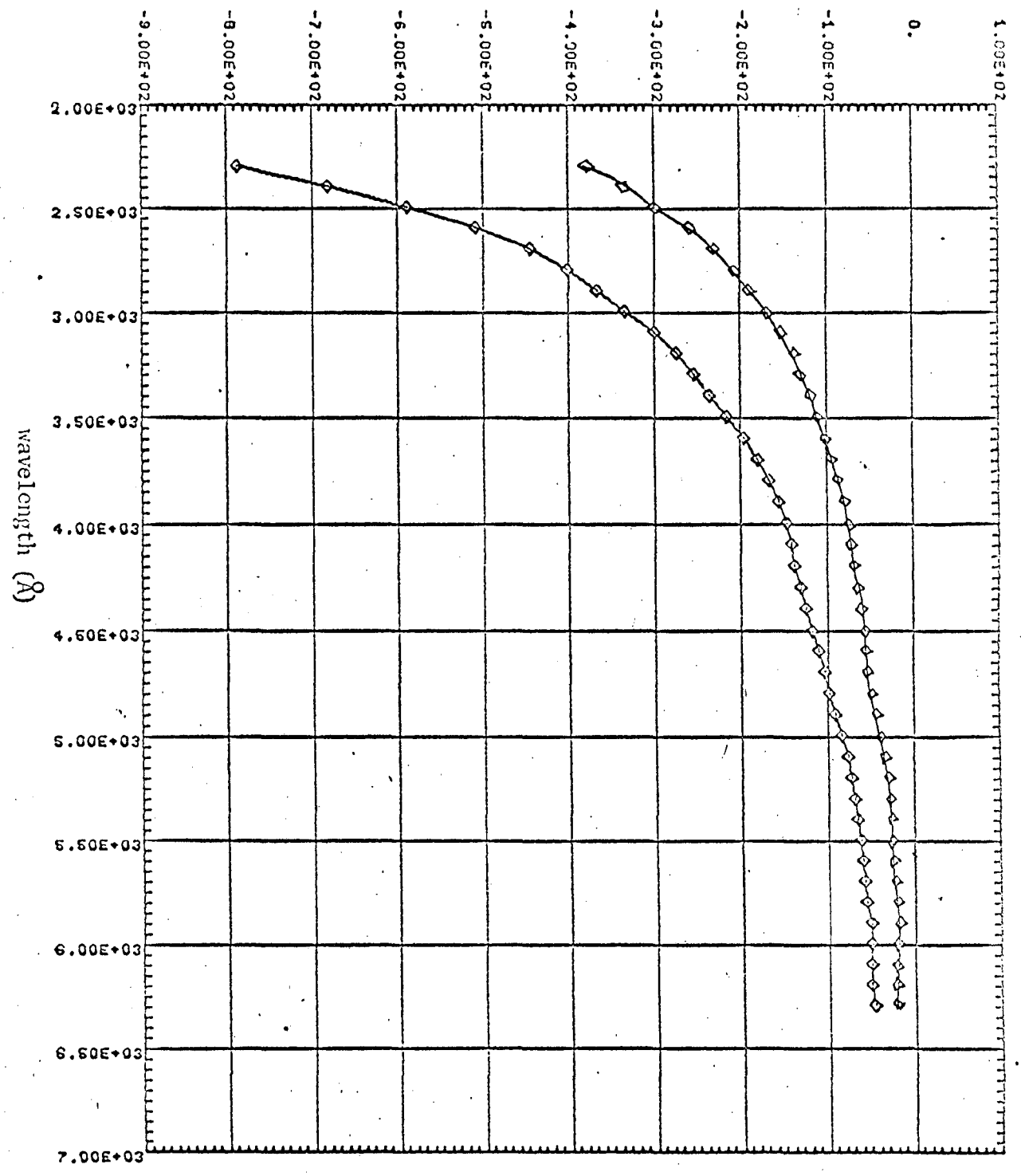

Fig. 4. Optical rotatory dispersion of CTA films. Film cast without plasticizer, lower curve. Film cast with plasticizer, upper curve,

two films. It is well established that changes in conformation of proteins and nucleic acids have a profound effect on the ORD of these molecules. But variation of the ORD does not in itself indicate with certainty that a conformation change has taken place.

Optical rotation is greatly influenced by the local environment of the molecule being studied. The two factors which one would expect to dominate the local environment are the crystallinity of the CTA and the interaction of the CTA with the water in the membrane. The crystallinity can be rejected as a possible cause of the difference in rotation shown in Figure 4 because there is very little difference in the crystallinity of the two samples and when films that do differ greatly in crystallinity have been studied, the difference in the optical rotation observed was rather small. The water content, however, could have more influence on the ORD since it was only 7.3% in the non-plasticized film and 24.3% in the plasticized film. There is an index of refraction correction to optical rotation $\frac{(n^2 + 1)}{3}$ which is negligible in this case. (The films have indices of refraction 1.435 and 1.440 for the plasticized and non-plasticized samples respectively, which amounts to less than 0.5% difference in the correction factors at the Na D line. The difference would become larger in the UV but would still not account for the observed rotation.)

The plasticized film can be thought of as a more dilute solution of CTA, but the ORD in Figure 4 is normalized for concentration, so this would make no difference unless there are interactions between the CTA molecules in the dense film that give rise to ORD. In conclusion, it appears that the difference in ORD observed in the plasticized and

non-plasticized films is due to differences in conformation or interaction between the CTA molecules, which is not the same interaction that leads to crystallinity.

C. Possible Conformation of Cellulose Triacetate

It is usually assumed[6] that in solution, cellulose has the same conformation as it does in the crystalline state. The anhydroglucose units are in the chair form and the chain is rather rigid (see Figure 5). In fact, it is assumed that any changes in the molecular shape are due to changes in bond angles and internal rotation around the β-1,4-linkages joining one ring to another, and not to kinks in the chain such as occur in vinyl polymers. One would expect this behavior from CTA also. A molecular model of CTA built with atomic models, confirms this notion. Figures 6 and 7 show such a model consisting of six anhydroglucose units. This ribbon-like molecule has a surprisingly rectangular cross section with dimensions about 5.6 Å x 12 Å. The carbonyl groups are fairly free to rotate about the C-O-C bonds (ester linkage) connecting them to the polymer backbone. It is thought that hydrogen bonding along the edges of the ribbons occurs in aggregated states of cellulose. The ribbons then form sheets which are attracted to one another by Van der Waal's forces. In this manner a large crystal may be formed, or a small crystallite involving a small part of each of many chains may be formed in an otherwise amorphous matrix of cellulose. This may be true of CTA also.

Models of CTA show that it can take on conformations other than the ribbon shown in Figures 6 and 7. One of the most interesting is a tightly wound right-handed helix (Figures 8 and 9). It appears from the model to have an inside diameter of about 4.8 Å and about a 14 Å outside diameter. There are six saccharide residues per turn, as is

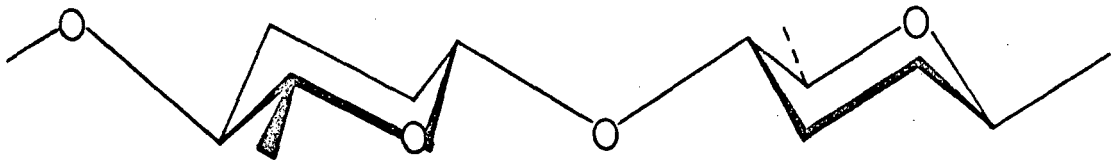

MUB 11632

Fig. 5. Conformation of cellulose in the crystalline state.

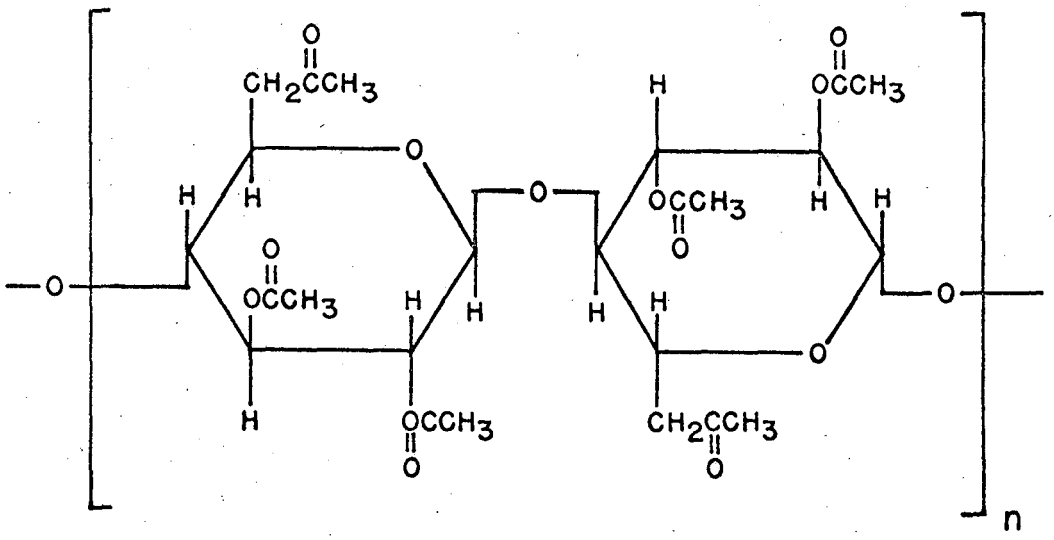

Fig. 5a. Structure of CTA showing two anhydroglucose units.

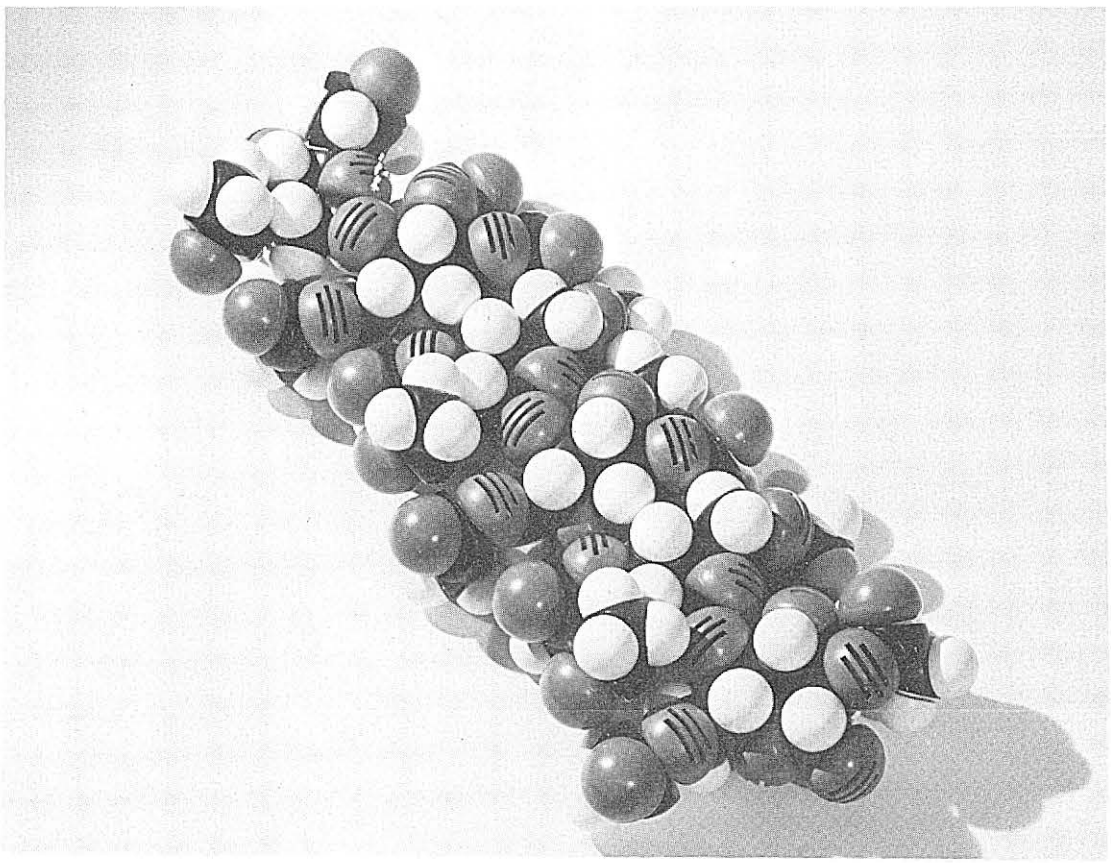

ZN-5768

Fig. 6. Ribbon-like conformation of cellulose triacetate (highly oxygenated side up). White = H, black = C, gray (slotted = -O-, gray (solid) = $\overset{O}{\underset{\|}{}}$ (carbonyl oxygen).

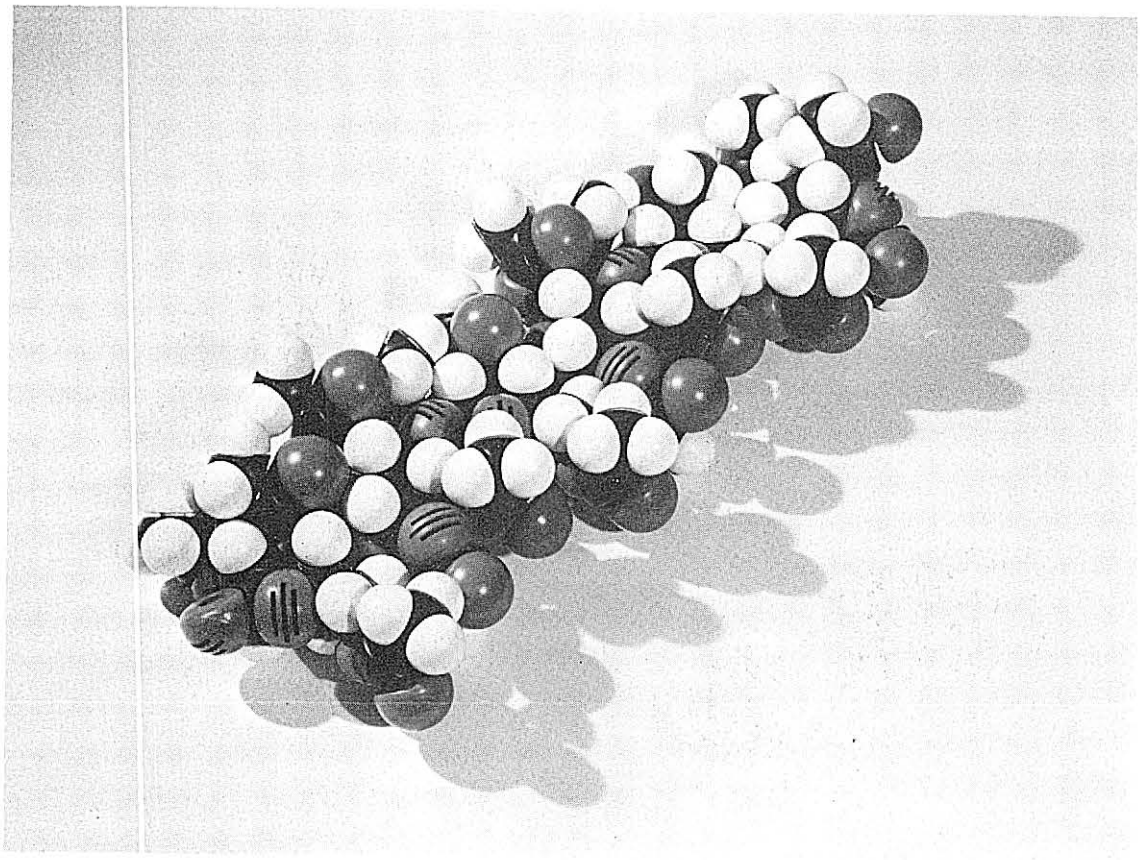

ZN-5770

Fig. 7. Ribbon-like conformation of cellulose triacetate (hydrocarbon side up).

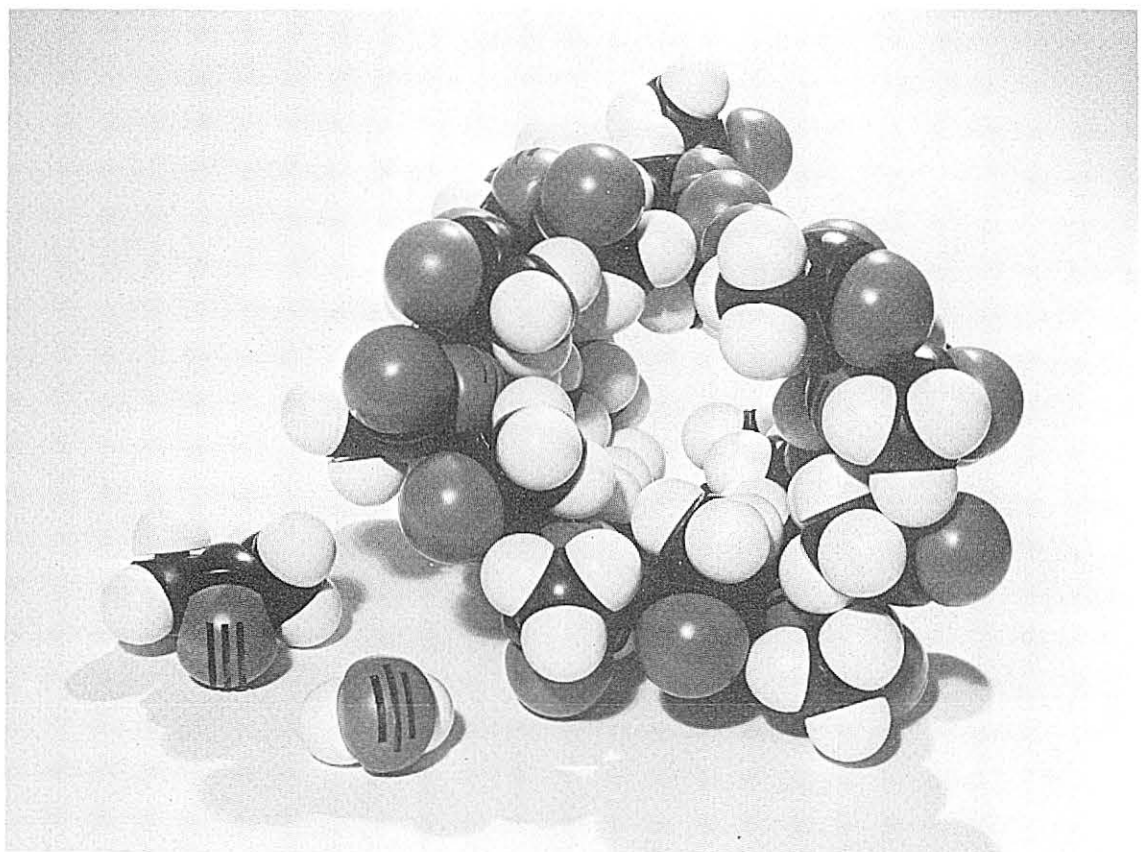

ZN-5769

Fig. 8. Tightly wound cellulose triacetate helix (end view shows cavity along helix axis). Molecules in the lower left corner are acetone and water for size comparison.

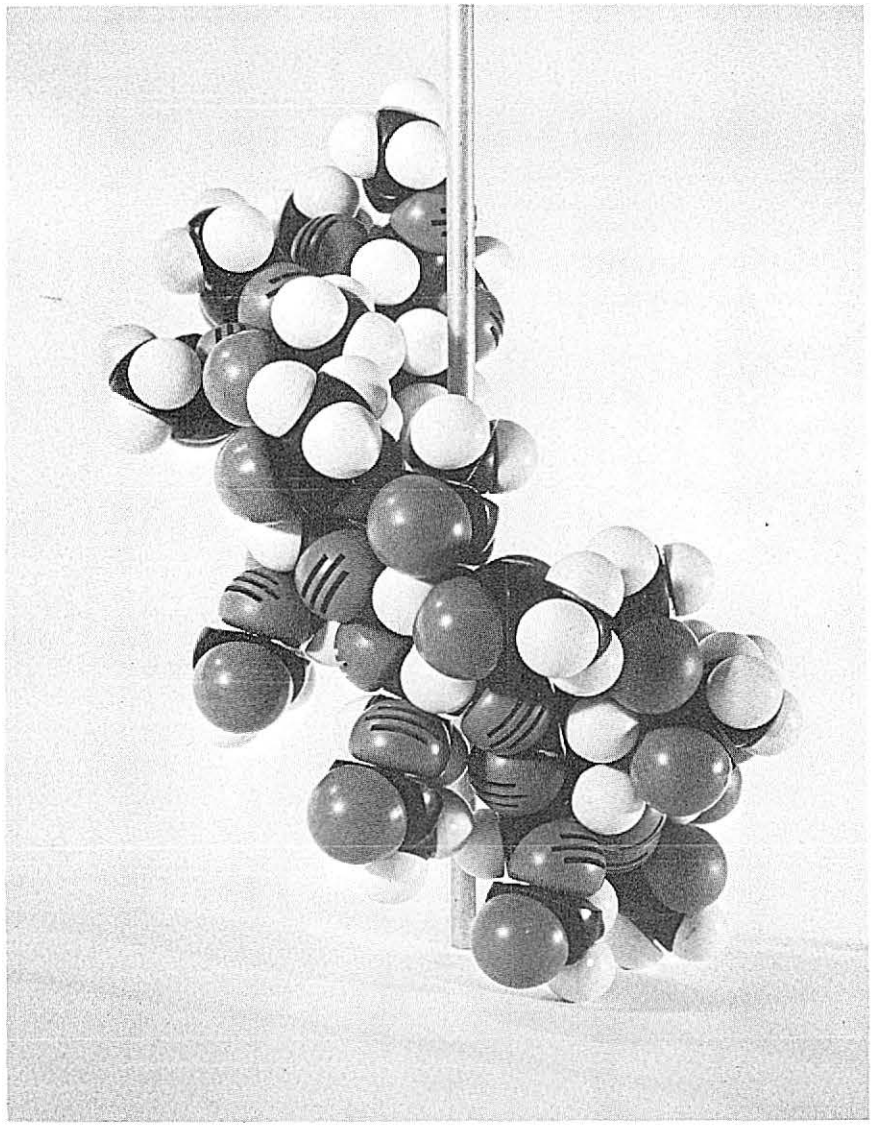

ZN-5771

Fig. 9. Tightly wound helix, side view. 4.5 Å inside diameter. Rod indicates helix axis.

presumed for the amylose helix.[6a] The carbonyl groups are not held in a fixed orientation as they are in polypeptides, although there is a possibility that intramolecular hydrogen bonds would form between the oxygen of one carbonyl and a hydrogen on another carbonyl carbon.[7] Two points should be made regarding this helix: 1) its entire inner lining is made up of C-H groups, and 2) acetone is about the largest molecule that can be accommodated inside the cavity (except for long molecules with diameters smaller than about 4.5 Å). A hydrated ion would not pass through. Water itself would not be likely to enter such a hydrocarbon lined cavity.

Figures 10 and 11 show a medium diameter helix (8 Å inside). This helix can have hydrocarbons and ether linkage oxygens inside, or it can turn some of the carbonyl oxygens inside without changing the backbone of the helix. Thus the inside of the helix could be made somewhat hydrophylic. This helix can be put into a conformation which has a smaller pitch, where the inside diameter can be made as large as 15 Å. The estimated pore size of good desalinization membranes is estimated[2] to be about 10 Å, which is within the range of the inside diameters of the last helix mentioned.

D. Optical Rotation of Solutions of CTA

The search for various conformations of CTA is ideally conducted on solutions because they eliminate the possibility of spurious rotation induced by sample strain or directionally dependent scattering. But CTA is not soluble in water and has very limited solubility in most organic solvents. Table II lists the few common solvents that will dissolve more than 3% CTA, along with comments regarding the method of solubilization.

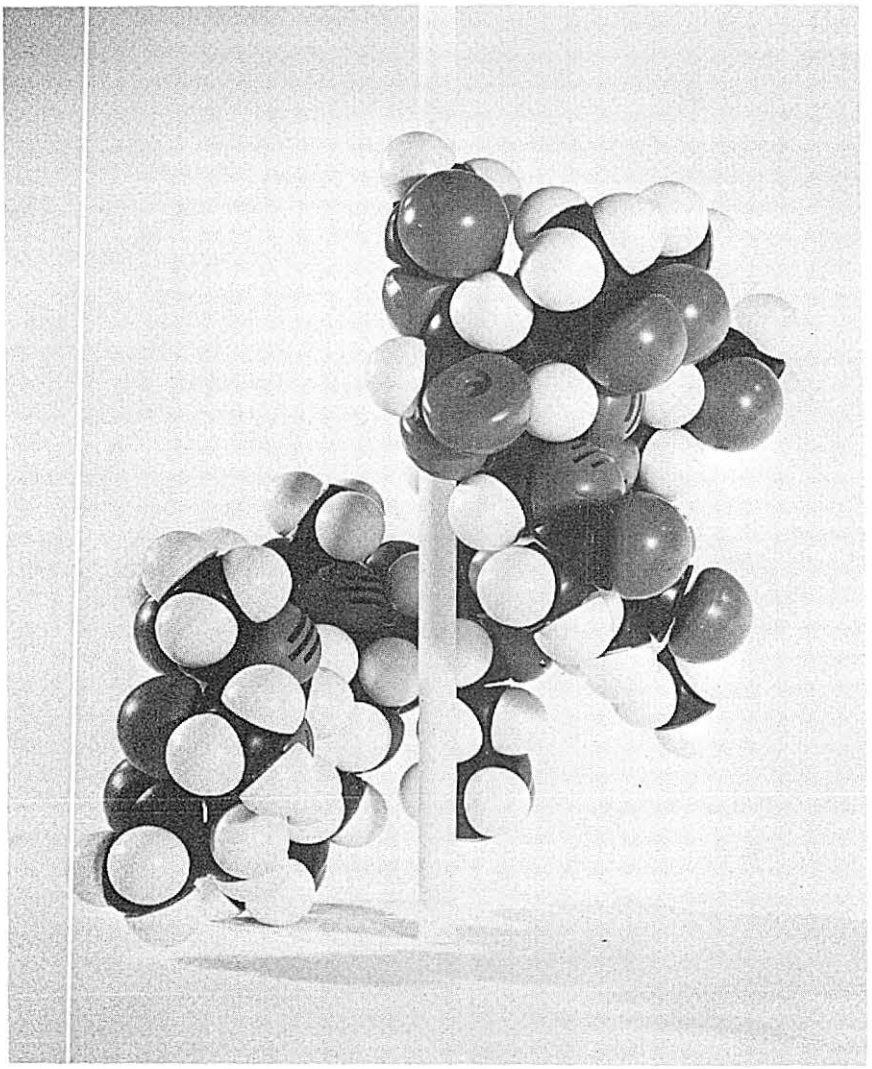

ZN-5773

Fig. 10. Medium diameter cellulose triacetate helix (rod shows helix axis.

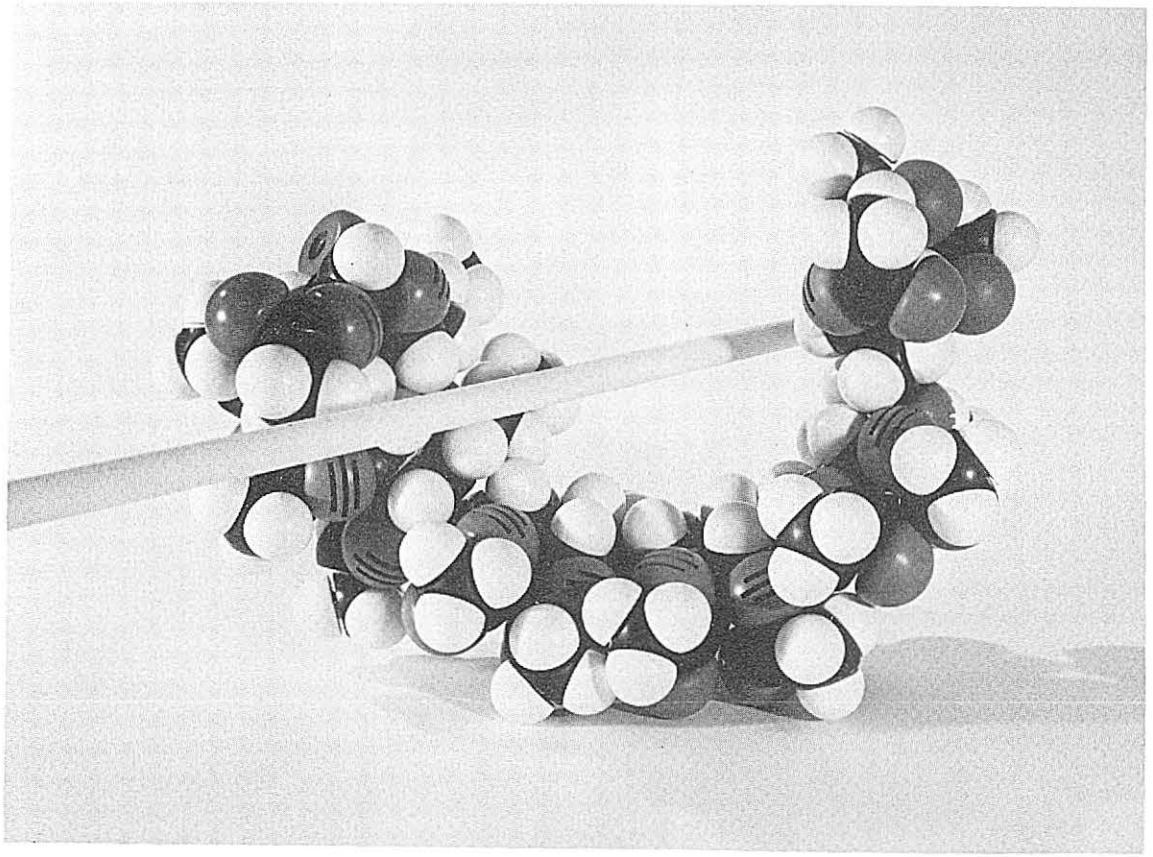

ZN-5772

Fig. 11. Medium diameter cellulose triacetate helix (rod shows helix axis).

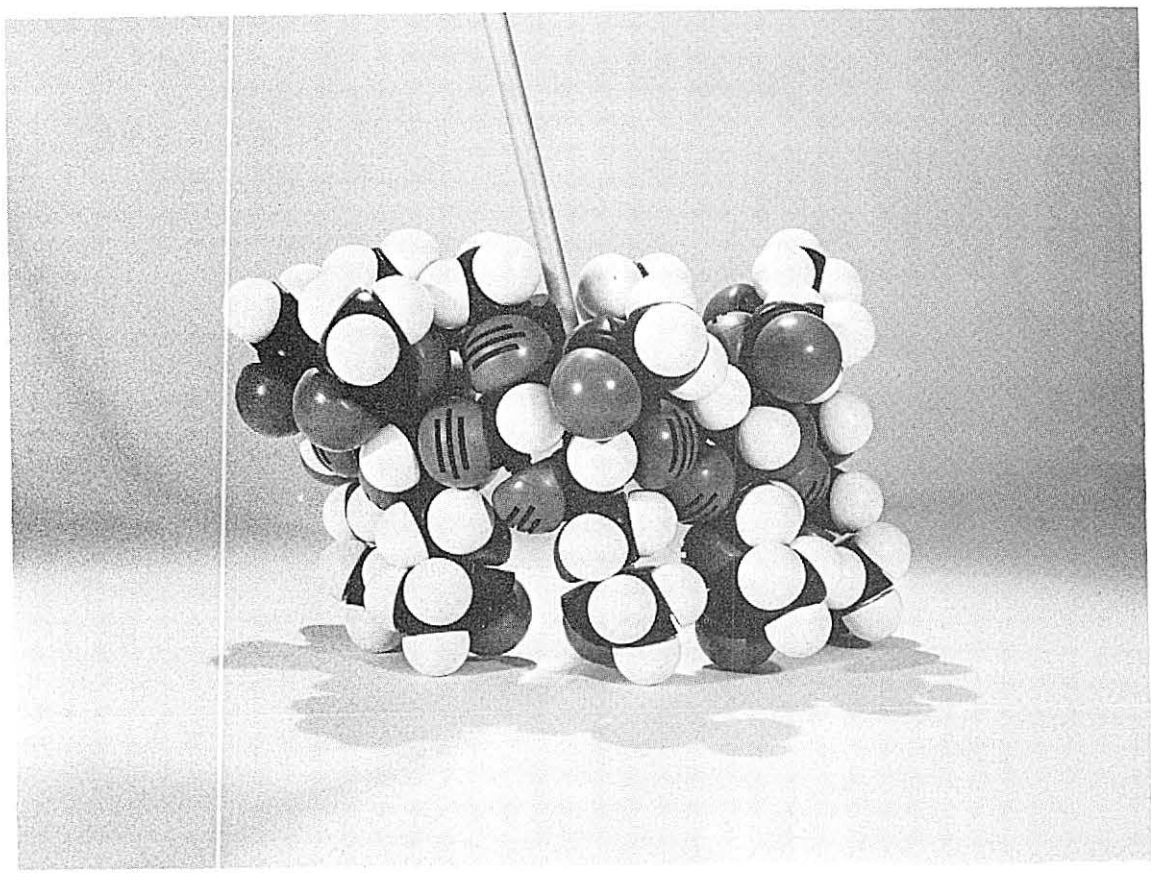

ZN-5765

Fig. 12. CTA helix with inside diameter greater than 12 Å. Outside view. Approximately 12 anhydroglucose units per turn. Five anhydroglucose units shown. Rod indicates helix axis.

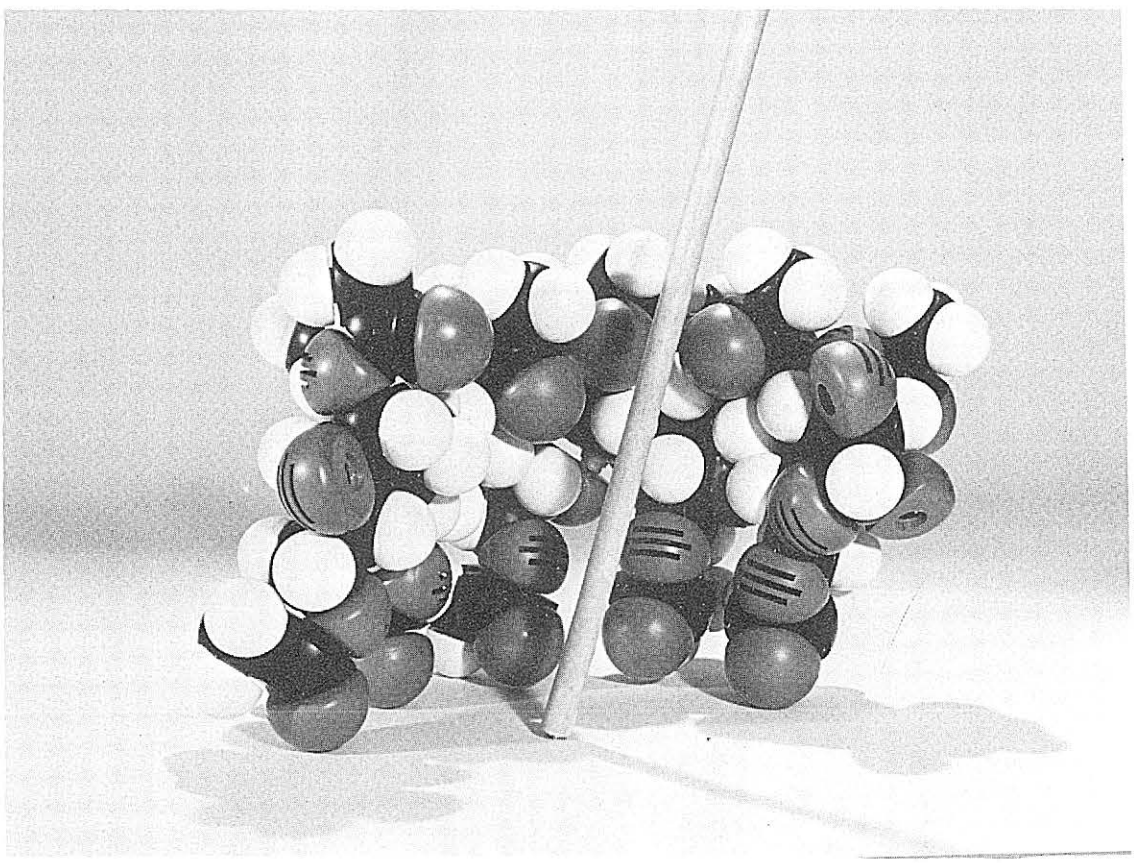

ZN-5766

Fig. 13. CTA helix with inside diameter greater than 12 Å. Inside view. Approximately 12 anhydroglucose units per turn. Five anhydroglucose units shown. Rod indicates helix axis.

Table II. Solubility of CTA

Solvent	Solubilization
Methylene chloride (dichloromethane)	By stirring at room temp
Ethylene chloride	" " " " "
Chloroform	" " " " "
1,4-Dioxane	" " " " "
Methylene chloride and alcohol (4:1)	" " " " "
Dimethylsulfoxide	" " " " "
Nitromethane	By heating (may form a gel on cooling
Acetone	By prolonged stirring at -40 to -50°C
Methylacetate	" " " "

It is difficult to dissolve CTA, even in cold acetone, probably because water tends to freeze out on the CTA powder, thus shielding it from the solvent. A clear solution can be obtained by raising the temperature several times during the process to melt the ice and then cooling to -50°C once again. The solution remains clear for about an hour at room temperature and then starts to become turbid, possibly because of absorption of water from the air.

The difference in the solubility properties of CTA in various solvents is the only guide available for choosing a pair of solvents where the CTA will exist in different conformations. The solvent properties which govern conformational changes in other polymers do not apply to CTA, that is, pH and ionic strength would not be expected to affect directly the conformation of CTA since it is not ionized and, in fact, is not soluble in liquids where ions are commonly found. Further, there

is no possibility of strong hydrogen bonding between parts of CTA molecules except for the few -OH groups that remain unacetylated. The hydrogen bonding ability of a solvent would not, therefore, be expected to play an important role in the conformation of CTA.

The molecular models show that the only microscopic property of CTA that changes very much as conformation is changed is the polarity of certain areas of the molecule. The outside surface can be moderately to highly polar in the helical form, while the inside is moderately polar to non-polar. In the ribbon-like form the whole surface appears to be moderately polar.

It was therefore decided to measure the ORD of CTA in methylene chloride (fairly non-polar) and in acetone (fairly polar). The ORD of the two solutions proved to have roughly the same form but differed in magnitude by a factor of about two. Figure 14 shows the ORD of a clear 0.125% solution of CTA in acetone. The optical rotation did not change during the 30 min the sample was left in the polarimeter. Ten ml of the solution was then evaporated to dryness by passing a stream of dry nitrogen over it and then redissolved in methylene chloride. The second curve in Figure 14 shows the ORD of this solution. The difference in magnitudes of the two curves is obvious. It is obvious that the curvature would be different if one curve were normalized so its rotation was equal to the other at a given wavelength.

It is customary to describe these two characteristics of an ORD curve by the values of the parameters k_h and λ_h in the Drude Equation:

$$[m] = \Sigma_h \frac{k_h}{\lambda^2 - \lambda_h^2}$$

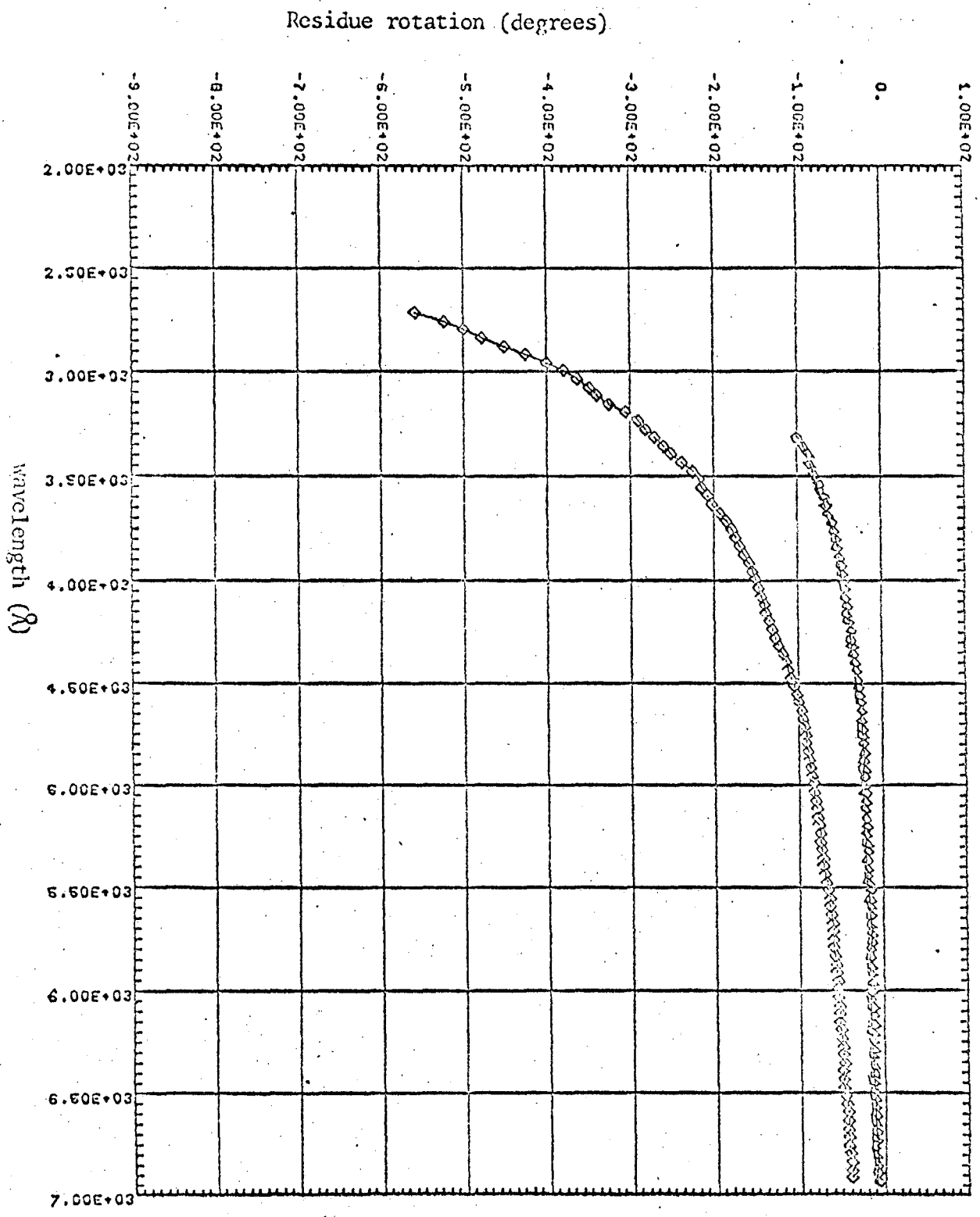

Fig. 14. Optical rotatory dispersion of CTA in acetone (upper curve), and the same CTA redissolved in an equal volume of methylene chloride.

where λ is the wavelength and [m] is the mean residue rotation given by

$$[m] = \frac{M_o\ [\alpha]}{100}$$

where M_o is the mean molecular weight of the units of the polymer (162 for CTA) and $[\alpha]$ is the specific rotation defined in the usual way. Table III lists the parameters k_h and λ_h for the CTA solutions studied.

Table III. Drude parameters for CTA solutions and films

Sample	λ_h (Å)	k_h (Å^2 deg)
CTA in methylene chloride	2261	-16.0×10^8
CTA in acetone	3022	-3.5×10^8
Film C2-1 (not plasticized)	1671	-20.0×10^8
Film C2-2 (plasticized)	1647	-10.2×10^8

It can be seen from the table that CTA in acetone or treated with the plasticizer (usually an aldehyde or amide) has a longer λ_h and smaller k_h than CTA not exposed to plasticizer or acetone. The significance of this can be appreciated when it is realized that similar (but usually smaller) differences in λ_h and k_h occur between solutions of helical protein and of the same protein in a random coil conformation. The same can be said of DNA and coiled and uncoiled forms. The author is not aware of any conditions other than conformation or configuration changes that result in such large differences in the observed ORD as expressed by the Drude parameters. It seems safe to assume the configuration of the CTA did not change in going from the acetonesolution to the methylene chloride solution, so we must conclude that the conformation of the CTA

is different in acetone than in methylene chloride. In addition, it appears that the conformation in the plasticized film is somewhat similar to that in acetone, and in the non-plasticized film to that in methylene chloride.

Even though studying models of CTA indicates the different conformations possible, it is not possible on the basis of the present information to determine which conformation corresponds to CTA in acetone and which in methylene chloride. Theoretical predictions of the rotation of various conformations is made difficult by the relatively free rotation of the carbonyl chromophores. Calculations for proteins are simplified because the amide chromophore is assumed planar and always has the same position with respect to the helix. Likewise, the positions of bases in DNA have a certain fixed relationship to the helix. But it does not appear that such a relationship can be reasonably assumed for the carbonyls in CTA. We must therefore be satisfied with the conclusion that CTA has different conformations in acetone and methylene chloride, as it does in plasticized and non-plasticized films, and that conformation is very likely to play an important role in the permeability properties of CTA films.

REFERENCES

1. Research and Development Report #83, Office of Saline Water, Department of the Interior, 1963.
2. R. Blunk, A Study of Criteria for Semipermeability of Cellulose Acetate Membranes to Aqueous Solutions, Report No. 60-60, Department of Engineering, UCLA, 1964.
3. W. A. Shurcliff, Polarized Light (Harvard University Press, Cambridge, Mass., 1962).
4. H. Mueller, J. Opt. Soc. Am. 38, 661 (1948).
5. R. Riley, J. O. Gardner, and U. Merten, Science 143, 801 (1964).
6. H. Morawetz, Macromolecules in Solution (Interscience, N. Y., 1965), p. 111.

6a. C. S. Hanes, New Phytologist 36, 101, 189 (1937); K. Freudenberg, E. Schauf, G. Dampert, and T. Ploetz, Naturwissenschaften 27, 850 (1939).

7. G. C. Pimentel and A. L. McClellan, The Hydrogen Bond (W. H. Freeman & Co., San Francisco, 1960).